

DESIGN AND FABRICATION OF SALICYLIC ACID-BASED POLYANHYDRIDE
DEVICES FOR WOUND HEALING AND TISSUE REGENERATION

by

SABRINA SACHIKO SNYDER

A Dissertation submitted to the

Graduate School-New Brunswick

Rutgers, The State University of New Jersey

and

The Graduate School of Biomedical Sciences

University of Medicine and Dentistry of New Jersey

in partial fulfillment of the requirements

for the degree of

Doctor of Philosophy

Graduate Program in Biomedical Engineering

written under the direction of

Professor Kathryn E. Uhrich

and approved by

New Brunswick, New Jersey

May, 2013

ABSTRACT OF THE DISSERTATION

Design and Fabrication of Salicylic Acid-based Polyanhydride Devices for Wound
Healing and Tissue Regeneration

By SABRINA SACHIKO SNYDER

Dissertation Director:

Professor Kathryn E. Uhrich

Wound healing and tissue regeneration after injury is regulated by inflammatory response degree and duration. Localized, controlled release of anti-inflammatory drugs at the injury site can modulate inflammation, thereby, controlling the wound healing process. This research uses salicylic acid-based poly(anhydride-esters) (SAPAEs) to release salicylic acid (SA), an anti-inflammatory drug, in a controlled manner for wound healing and tissue regeneration applications.

In the first studies, SAPAE-containing bone regeneration devices were developed. SAPAEs were melt-cast as guided bone regeneration (GBR) caps onto osteoconductive scaffolds, then *in vitro* drug release was quantified. *In vivo* inflammation and bone regeneration capacity were evaluated. The SAPAE caps suppressed inflammation and had no effect on bone formation in a rabbit cranial trephine defect model.

Second, SAPAEs were blended with polycaprolactone (PCL) and electrospun to create flexible GBR mats. Electrospun mat structure, mechanical

properties, and *in vitro* drug release were determined. Mats were assessed *in vivo* for their ability to prevent heterotopic ossification (HO) in a rat femoral defect model. Initial studies indicate that the SAPAE:PCL blends prevent HO, but also inhibit bone regeneration in the defect site.

Third, SAPAE:poly(ethylene glycol) (PEG) copolymers at various ratios were developed for fibrous adhesion prevention. These, copolymers behave as viscous liquids at room temperature. Rheological properties, *in vitro* drug release profiles, cytotoxicity, and anti-inflammatory activity were assessed. Shear viscosities are comparable with FDA-approved fibrous adhesion barriers and have the additional benefit of drug release to modulate the excessive inflammation that causes adhesion formation.

Fourthly, SAPAEs exhibit an initial lag period in drug release, which could be unfavorable in applications where immediate SA release is desired. By varying the amounts of small molecules incorporated into an SAPAE matrix with an 11-day lag period, immediate and constant SA release profiles were achieved.

Overall, SAPAEs were utilized to create bone scaffolds and wraps to direct bone growth, as injectable adhesion barrier devices, and to control early SA release. All these approaches were focused on controlling the wound healing process with biodegradable SAPAEs.

PREFACE

*“Choose my instruction instead of silver,
knowledge rather than choice gold.
for wisdom is more precious than rubies,
and nothing you desire can compare with her.”*

Proverbs 8:10-11

DEDICATION

This work is dedicated to God and to my family, especially to my wonderful husband, Matthew Snyder, whose steadfast love and support have helped me throughout this experience. Also, to my parents, David Engler and Risë Matsunami, who instilled in me a love for science and provided me with two amazing role models, not just as scientists, but in every aspect of life.

ACKNOWLEDGEMENTS

I would like to express my sincere gratitude to all those whose guidance and support helped make this dissertation possible.

Special thanks to:

Dr. Kathryn Uhrich, Dr. J. Patrick O'Connor, Dr. David Shreiber, Dr. Pallassana Narayanan, Dr. John Ricci, Dr. Charles Roth, Dr. Ashley Howell, Dr. Jeremy Griffin, Dr. Roselin Rosario-Meléndez, Dr. Sarah Sparks, Dr. Alex Harmon, Dr. Roberto Delgado-Rivera, Dr. Sarah Hehir, Dr. Dawanne Poree, Dr. Dalia Abdelhamid, Dr. Kristin Fischer, Dr. Jessica Cottrell, Dr. Jeffrey Barminko, Dr. Bryan Langowski, Michelle Ouimet, Yong Soo Lee, Connie Yu, Nick Stebbins, Li Gu, Allison Faig, Joanna Zhang, Dave Orban, Sammy Gulrajani, Hana Hamdi, Ashley Mitchell, Sangeeta Subramanian, Renata Fogaça, Ian Gaudet, Sagar Singh, Kathryn Drzewiecki, Kristina Wetter, and the Foundation of UMDNJ Society of Research Scholars.

Please forgive me if your name does not appear in this list, it is by no means complete. I am truly blessed to have had so many people help me through the years, thank you.

TABLE OF CONTENTS

ABSTRACT OF THE DISSERTATION.....	ii
PREFACE.....	iv
DEDICATION.....	v
ACKNOWLEDGEMENTS.....	vi
TABLE OF CONTENTS.....	vii
LIST OF TABLES	xiv
LIST OF FIGURES	xv
ABBREVIATIONS, SYMBOLS, AND UNITS	xxii
1 INTRODUCTION.....	1
1.1 Controlled Drug Delivery	1
1.1.1 Localized delivery	3
1.2 Polymers for Drug Delivery	5
1.2.1 Bulk versus surface erosion.....	5
1.2.2 Polyanhydrides	7
1.2.3 Polymeric Drugs	7
1.2.4 Salicylic acid-based poly(anhydride-esters)	8
1.3 Inflammation in Wound Healing and Tissue Regeneration	10
1.4 Research Projects	11
1.4.1 Guided bone regeneration device using salicylic acid-based poly(anhydride-esters) and osteoconductive scaffolds	11
1.4.2 Polymeric bone wraps to prevent heterotopic ossification.....	12

1.4.3	Flowable salicylic acid-based poly(anhydride-esters) for injectable barrier applications	13
1.4.4	Tunable drug release profiles from salicylate-based poly(anhydride-ester) matrices using small molecule admixtures	15
1.5	Summary	16
1.6	References	16
2.	GUIDED BONE REGENERATION DEVICE USING SALICYLIC ACID-BASED POLY(ANHYDRIDE-ESTERS) AND OSTEOCONDUCTIVE SCAFFOLDS	21
2.1	Introduction.....	21
2.2	Materials and Methods	24
2.2.1	Scaffold fabrication	24
2.2.2	Polymer synthesis and characterization	24
2.2.3	Polymer capping of scaffolds	25
2.2.4	<i>In vitro</i> drug release	26
2.2.5	Animal model	26
2.2.6	Micro-computerized tomography (microCT)	27
2.2.7	Histology	28
2.2.8	Statistical analyses	30
2.3	Results	30
2.3.1	Polymer degradation.....	31
2.3.2	Animal disposition.....	32
2.3.3	Bone formation within scaffolds	33

2.3.4	Cell densities within scaffolds	37
2.3.5	Regional bone and cell densities within scaffolds.....	39
2.3.6	Host inflammatory response	45
2.4	Conclusions	49
2.5	References	50
3.	POLYMERIC BONE WRAPS TO PREVENT HETEROTOPIC OSSIFICATION	55
3.1	Introduction.....	55
3.2	Materials and Methods	57
3.2.1	Materials	57
3.2.2	Polymer synthesis and characterization	57
3.2.3	Thermal analysis.....	58
3.2.4	Electrospinning	59
3.2.5	Fiber characterization	60
3.2.6	Porosity	60
3.2.7	Mechanical testing	61
3.2.8	<i>In vitro</i> drug release	61
3.2.9	Animal model	62
3.2.10	Radiography	65
3.3	Results and Discussion	65
3.3.1	Characterization of the electrospun mats	65
3.3.2	<i>In vitro</i> drug release	68
3.3.3	<i>In vivo</i> testing	71

3.4	Conclusions	75
3.5	References	76
4.	FLOWABLE SALICYLIC ACID-BASED POLY(ANHYDRIDE-ESTERS) FOR INJECTABLE BARRIER APPLICATIONS	81
4.1	Introduction	81
4.2	Materials and Methods	84
4.2.1	Materials	84
4.2.2	¹ H NMR and FTIR spectroscopies	84
4.2.3	Molecular weight	84
4.2.4	Thermal properties	85
4.2.5	Polymer synthesis	85
4.2.6	Solvent-casting SAA/PEG blended films	87
4.2.7	Rheology	88
4.2.8	Storage stability	88
4.2.9	<i>In vitro</i> drug release	88
4.2.10	<i>In vitro</i> cytotoxicity and proliferation assay	89
4.2.11	TNF- α secretion assay	90
4.3	Results and Discussion	92
4.3.1	SAPAE:PEG blended films	92
4.3.2	SAPAE:PEG copolymers	94
4.3.3	Copolymer characterization	95
4.3.4	Rheology	97
4.3.5	Storage stability	98

4.3.6	<i>In vitro</i> drug release	101
4.3.7	Cytocompatibility	102
4.3.8	Anti-inflammatory activity	105
4.4	Conclusion.....	106
4.5	References	107
5.	TUNEABLE DRUG RELEASE PROFILES FROM SALICYLATE-BASED POLY(ANHYDRIDE-ESTER) MATRICES USING SMALL MOLECULE ADMIXTURES	112
5.1	Introduction.....	112
5.2	Materials and Methods	116
5.2.1	Materials	116
5.2.2	Polymer synthesis and characterization	116
5.2.3	Disc preparation.....	117
5.2.4	Hydrolytic degradation	117
5.2.5	Influence of admixtures on glass transition temperature	118
5.3	Results and Discussion	118
5.3.1	<i>In vitro</i> SA release	119
5.3.2	Admixture effect on glass transition temperature	121
5.4	Conclusions	122
5.5	References	123
6.	APPENDIX: IN VITRO DEGRADATION OF AN AROMATIC POLYANHYDRIDE WITH ENHANCED THERMAL PROPERTIES	128
6.1	Introduction.....	128

6.2	Materials and Methods	130
6.2.1	Materials	130
6.2.2	Polymer synthesis and characterization	130
6.2.3	Polymer <i>in vitro</i> degradation	131
6.2.4	Degradation product analysis via HPLC	132
6.2.5	Diacid concentration determination via UV absorbance	132
6.2.6	Molecular weight analysis	133
6.2.7	Scanning electron microscopy	134
6.2.8	Radiation exposure	134
6.2.9	<i>In vitro</i> cytotoxicity evaluation	134
6.3	Results and Discussion	136
6.3.1	<i>In vitro</i> degradation	136
6.3.2	Morphological changes	139
6.3.3	Molecular weight change due to <i>in vitro</i> degradation	139
6.3.4	Ionizing radiation.....	142
6.3.5	Cytotoxicity	143
6.4	Conclusions	144
6.5	References	145
7	CONCLUSIONS AND FUTURE WORK	147
7.1	Guided bone regeneration device using salicylic acid-based poly(anhydride-esters) and osteoconductive scaffolds	147
7.2	Polymeric bone wraps to prevent heterotopic ossification	148

7.3	Flowable salicylic acid-based poly(anhydride-esters) for injectable barrier applications	150
7.4	Tunable drug release profiles from salicylate-based poly(anhydride-ester) matrices using small molecule admixtures	150
7.5	Summary	151

LIST OF TABLES

Table 2.1. Inflammation Scoring Rubric.	30
Table 2.2. Summary of Group Size.	33
Table 3.1. Electrospinning Polymer Solutions and Flow Rates.....	59
Table 3.2. Average Fiber Diameter and Porosity of Electrospun Mats	66
Table 4.1. Typical M_n , PDI, and T_g for SAA:PEG Polymers.	96
Table 4.2. Shear Viscosities of SAA:PEG Copolymers.....	97
Table 5.1. Representation of 1, 5, and 10 % (w/w) admixtures used for various sample disc compositions.	115
Table 5.2. Theoretical Drug Loading of Samples	119

LIST OF FIGURES

Figure 1.1. Bolus dosing results in the need for frequent administration and difficulty in keeping drug concentrations within therapeutic levels.	2
Figure 1.2. Controlled release formulations can maintain therapeutic drug concentrations.	3
Figure 1.3. Drug distribution (red) with high systemic (A), low systemic (B), and localized (C) delivery.	4
Figure 1.4. Polymer matrix degradation can occur in a manner that is primarily either bulk or surface-eroding. The eroding mechanism has a strong influence on the release profile of encapsulated drugs.	6
Figure 1.5. Polymeric drugs with drugs incorporated as pendant groups (left) or within the polymer backbone (right) through the use of non-bioactive “linker” molecules.	8
Figure 1.6. Synthesis and degradation products of salicylic acid-based poly(anhydride-esters) ¹⁶	9
Figure 1.7. SAPAEs were melt-cast on osteoconductive scaffolds as both a physical barrier against soft tissue growth into the scaffold and to modulate inflammation.	12
Figure 1.8. SAPAE:PEG copolymers have T_g s below 0 °C, resulting in polymers that behave like viscous fluids.	14
Figure 1.9. Visualization of the effect of small molecule admixtures on the SA release profile from SAPAEs.	15
Figure 2.1. Chemical structures of fast-PA and slow-PA.	25

Figure 2.2. Cumulative SA release from SA-PAE capped scaffolds (SA amount was normalized to 1 g of polymer).	32
Figure 2.3. Scaffolds 8 weeks post-surgery with open (A), closed (B), PLGA (C), slow-PA (D), and fast-PA (E) capped scaffolds. Calvaria and new bone growth within the scaffold are grey while the scaffold contrasts white.	34
Figure 2.4. (A) Each histological specimen was divided into 6 zones to determine regional differences in cell density and bone area such that zones labeled T, B, P, and M indicate top, bottom, peripheral, and middle regions, respectively. Stained 3-week post-surgery specimens (mineralized tissue is red and soft tissues is blue) from (B) an open scaffold, (C) closed capped, (D) PLGA capped, (E) slow-PA capped, and (F) fast-PA capped scaffolds are shown. The red arrow indicates the cap area for each scaffold.	35
Figure 2.5. Bone formation and cellular infiltration (mean + standard error) were measured in each scaffold as (A) bone volume by microCT analysis, (B) percentage of bone in available area by histomorphometry, and (C) cell density using histological specimens. Cell density values within a scaffold configuration that were significantly different from the 1 or 3 week values are denoted with a 1 or 3, respectively. Cell density values within a time point that were significantly different from another scaffold configuration are denoted with an o, c, p, s, or f to indicate a significant difference from the open, closed, PLGA, slow-PA, and fast-PA capped scaffolds, respectively.	36
Figure 2.6. Histomorphometry was used to measure the percentage of bone (mean + standard error) in the top region of the different scaffold	

configurations. Values within a time point that are significantly different between scaffold configurations are denoted with an o, c, p, s, or f for open, closed, PLGA, slow-PA, and fast-PA capped scaffolds, respectively. Changes in percent bone area between 3 and 8 weeks was dependent upon scaffold configuration and was significantly greater for the closed, PLGA, and fast-PA capped scaffolds ($p \leq 0.004$), but not for the open scaffold (*, $p = 0.75$) or the slow-PA capped scaffold (**, $p = 0.06$).41

Figure 2.7. Cell density (mean + standard error) was measured in the (A) top and (B) bottom regions of the different scaffold configurations. Cell density values within a scaffold configuration that were significantly different from the 1 or 3 week values are denoted with a 1 or 3, respectively. Cell density values within a time point that were significantly different from another scaffold configuration are denoted with an o, c, p, s, or f to indicate a significant difference from the open, closed, PLGA, slow-PA, and fast-PA capped scaffolds, respectively.43

Figure 2.8. Shown are regions-of-interest located between the scaffold and overlying muscle (M). The ceramic scaffold material is denoted with a white arrowhead and the polymer caps or the voids left after histological processing dissolved the polymer are denoted with a diamond. The fibrous cell layer above the scaffold is denoted with an “F”. An exuberant inflammatory response is apparent at 1, 3, and 8 weeks in the PLGA and at 1 and 3 weeks in the slow-PA capped scaffolds, though the inflammatory response did not appear to involve the muscle in the slow-PA capped

scaffolds. Little or no inflammatory response was apparent in the open scaffold (not shown), closed, or fast-PA capped scaffolds.....	46
Figure 2.9. Histology specimens were scored for apparent inflammation (mean + standard error) using a 9-point scale (Table 2.1), with 9 indicating severe inflammation. Independent of time after surgery, the PLGA-capped scaffolds had a significantly higher inflammation score than all other scaffolds (*, $p \leq 0.006$).	48
Figure 3.1. Bone wrap polymer structures.	58
Figure 3.2. Bone wrap dimensions (A) and placement <i>in vivo</i> (B).	63
Figure 3.3. SEM images (2,500 x) of electrospun blends: 100 % PCL (a), 20 % SAA (b), 40 % SAA (c), 60 % SAA (d), 80 % SAA (e), 20 % SADEM (f), 40 % SADEM (g), 60 % SADEM (h), 80 % SADEM (i). Scale bars are equivalent to 10 μm	66
Figure 3.4. Elastic moduli of dry and wet electrospun mats.	67
Figure 3.5. All polymer wraps maintained their structure throughout 4 weeks of <i>in vitro</i> degradation (80 % SAA at 4 weeks shown).	68
Figure 3.6. Cumulative SA release from SAA-containing electrospun mats.....	69
Figure 3.7. Cumulative SA release from SADEM-containing electrospun mats.	71
Figure 3.8. Radiographs of rats treated with 0 μg , 3.5 μg , 12 μg , or 24 μg BMP-2, unwrapped (U) or wrapped (W).	73
Figure 4.1. Synthetic scheme for the SAA diacid, SAA polymer, and SAA:PEG copolymers.	87

Figure 4.2. Variegated surface of the blended films indicates macroscopic phase separation.....	93
Figure 4.3. DSC spectra for SAA (red), PEG (green), and SAA/PEG blend (blue). The blend spectra indicates phase separation as the spectra values are additive.....	94
Figure 4.4. Resulting copolymers behaved like viscous liquids.....	95
Figure 4.5. ^1H NMR spectra of 2:1 SAA:PEG (g* indicates hydrogen atoms adjacent to a carboxylic acid end group, as opposed to g which indicates hydrogen atoms adjacent to an anhydride group).....	96
Figure 4.6. SAA:PEG copolymer M_n and T_g changes over 3 weeks of storage at different temperatures, with (1:2 d) and without (1:2) desiccant.	100
Figure 4.7. <i>In vitro</i> SA release from SAA:PEG copolymers.....	102
Figure 4.8. <i>In vitro</i> cell viability over 72 hours for cells exposed to SAA:PEG copolymers with ratios of 1:2 (a), 1:1 (b), and 2:1 (c) (* indicates significant decrease from DMSO control, $p < 0.05$). Cell viability was normalized to the DMSO control at 24 hours.....	104
Figure 4.9. TFN- α expression by macrophages exposed to LPS and SAA:PEG copolymers (* indicates significant difference from 10 ng/mL LPS control, $p < 0.05$). TNF- α secretion was normalized to the LPS positive control (set to 1) and the LPS free control (set to 0).	106
Figure 5.1. Hydrolytic degradation scheme of the SAPAE that releases SA and diethylmalonic acid.....	114

Figure 5.2. SA release profiles during the typical lag period of 0-11 days for the polymer alone and against 1, 5, and 10 % (w/w) admixtures (b).	119
Figure 5.3. Cumulative release profiles of polymer and 1 %, 5 %, and 10 % (w/w) admixtures of SA (a), SA:diacid combination (b), and diacid (c) over 30 days. A comparison of the three different admixtures at the same weight percentage (10% w/w) is also shown (d).....	120
Figure 5.4. Glass transition temperatures measured for all samples. The highest point on the y-axis corresponds with the T_g of polymer alone.	122
Figure 6.1. Poly(oCPX) synthesis. ⁸	131
Figure 6.2. HPLC spectra of a diacid standard (A) and the degradation media (B) both exhibit retention times of 1.8 min.	136
Figure 6.3. Cumulative diacid release (mg) into degradation media from 150 mg poly(oCPX) discs in PBS.	137
Figure 6.4. SEM images of disc cross sections at day 0 (A) and day 30 (B). Note the porous structure on the disc surface (area a) which indicative of water penetration with the more uniform section (area b) below.....	139
Figure 6.5. Representative poly(oCPX)GPC spectra (A) before and (B) after 90 day degradation with peak molecular weights labeled.	141
Figure 6.6. Cumulative diacid release into degradation media from 150 mg irradiated poly(oCPX) discs in PBS.	143
Figure 6.7. oCPX diacid did not significantly affect cell viability at 0.5 mg/mL and lower (* indicates a significant difference ($p < 0.05$) in cell viability from the DMSO control). Data are normalized to control viability at 24 hours.....	144

Figure 7.1. Bone wrap with biphasic SAPAE loading	149
--	-----

ABBREVIATIONS, SYMBOLS, AND UNITS

^1H NMR	proton nuclear magnetic resonance	kGy	kiloGray
ANOVA	analysis of variance	kV	kilovolt
Au/Pd	gold/palladium	kVp	kilovolt peak
BMD	bone mineral density	kW	kilowatt
BMP	bone morphogenetic protein	LPS	lipopolysaccharide
BV	bone volume	M	molar
C	Celcius	mg	milligram
cm	centimeter	microCT	micro-computerized tomography
COX	cyclooxygenase	min	minute
Da	Dalton	mL	milliliter
DCM	dichloromethane	mm	millimeter
dL	decaliter	mM	millimolar
DMF	dimethylformamide	M_n	number average molecular weight
DMSO	dimethyl sulfoxide	mPa	milliPascal
ELISA	enzyme-linked immunosorbant assay	MTS	(3-(4,5-dimethylthiazol-2-yl)-5-(3-carboxymethoxyphenyl)-2-(4-sulfophenyl)-2H-tetrazolium)
eq	equivalence	M_w	weight-averaged molecular weight
FBS	fetal bovine serum	ng	nanogram
FDA	US Food and Drug Administration	NIH	National Institutes of Health
FTIR	Fourier transform infrared spectroscopy	nm	nanometer
g	gram	NSAID	nonsteroidal anti-inflammatory drug
GBR	guided bone regeneration	oCPX	poly[α,α' -bis(<i>ortho</i> -carboxyphenoxy)- <i>para</i> -xylene]
GPC	gel permeation chromatography	PBS	phosphate buffered saline
HA	hydroxyapatite	PCL	polycaprolactone
HO	heterotopic ossification	pCPP	poly[1,3-bis-(<i>para</i> -carboxyphenoxy)propane]
hr	hour	PDI	polydispersity index
kg	kilogram	PEG	poly(ethylene glycol)

PLGA	poly(lactic-co-glycolic acid)
psi	pounds per square inch
PTFE	polytetrafluoroethylene
rad	radian
ROI	region of interest
rpm	rotations per minute
RPMI	Roswell-Park-Memorial-Institute cell culture medium
s	second
SA	salicylic acid
SAA	salicylic acid-based polyanhydride ester with an adipic acid linker
SADEM	salicylic acid-based poly(anhydride ester) with a diethylmalonic linker
SAPAE	salicylic acid-based polyanhydride ester
SEM	scanning electron microscopy
TCP	tricalcium phosphate
T _g	glass transition temperature
THF	tetrahydrofuran
T _m	melting temperature
TNF- α	tumor necrosis factor- α
UV	ultraviolet
v/v	volume per volume
w/v	weight per volume
w/w	weight per weight
λ	wavelength
μ A	microAmpere
μ g	microgram
μ L	microliter
μ m	micrometer
°	degree
%	percent
~	approximately

1 INTRODUCTION

Medical innovations in the past century have revolutionized healthcare and greatly improved life expectancy. The development of new drugs and the elucidation of their mechanisms of action have led to a better understanding of how to deliver drugs so as to increase their effectiveness, decrease side effects, and improve patient compliance. One area of pharmaceuticals that is receiving significant attention is the use of biodegradable polymers as drug delivery vehicles.^{1, 2}

1.1 Controlled Drug Delivery

Polymers can provide many benefits in the drug delivery process. Many drug formulations are now employing polymers to stabilize drugs, improve retention times, reduce toxicity, and target specific tissues.³ One of the most important uses for polymers in drug delivery is to control release rates.²

Traditional bolus drug dosing (Figure 1.1), such as is achieved with conventional pills and injections, can present many problems for the patient. In bolus dosing, all of the drug is administered at once, typically via oral or intravenous means; the drug concentration spikes and then falls as the drug molecules are metabolized or eliminated from the body, requiring the administration of another dose.² This frequent dosing can lead to poor patient compliance as the dosing schedule may be interrupted by their daily schedules.²

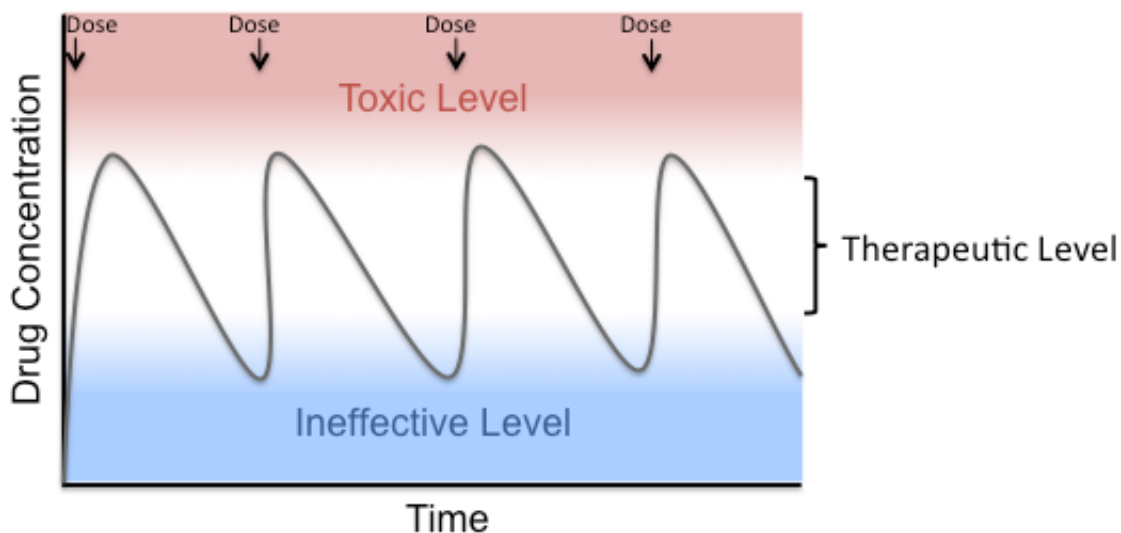


Figure 1.1. Bolus dosing results in the need for frequent administration and difficulty in keeping drug concentrations within therapeutic levels.

Controlling the release of drugs improves dosage efficacy, reduces potential toxicity, and improves patient compliance.² Figure 1.2 illustrates the advantages of controlled drug release over bolus dosing. By developing a system in which drug is released at the same rate as drug metabolism and elimination, concentrations can be maintained at therapeutic levels over sustained periods of time, decreasing the risk of toxicity.³ Sustained release means less frequent dosing, leading to increased compliance.²

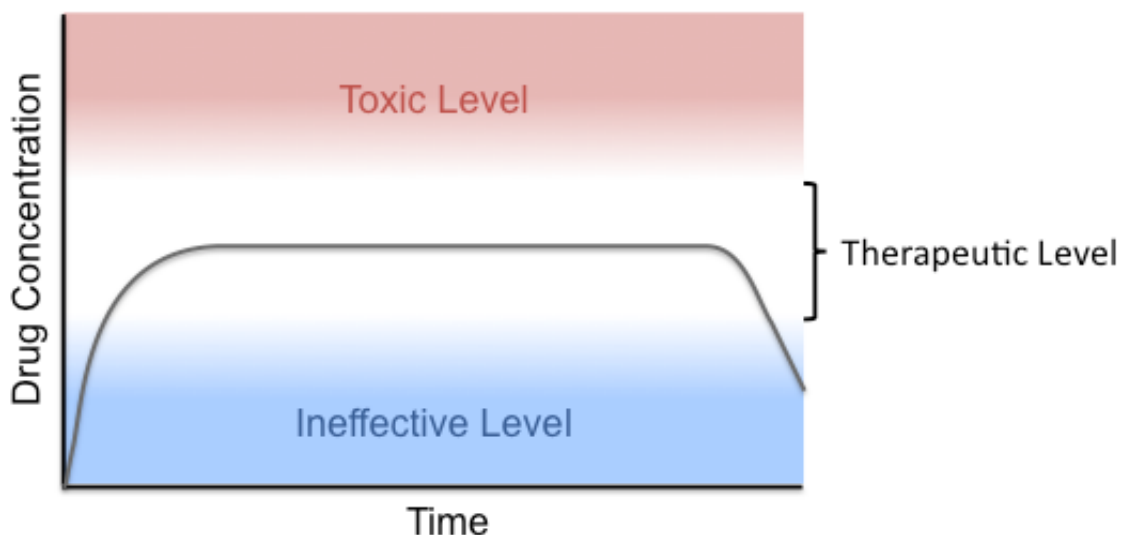


Figure 1.2. Controlled release formulations can maintain therapeutic drug concentrations.

1.1.1 Localized delivery

A significant problem with traditional dosing is that oral and intravenous administration of drugs results in systemic distribution of the drug (Figure 1.3A).¹ By delivering the drug equally throughout the body, higher dosing is needed to reach therapeutic levels in the desired locations.¹ This method also increases side effects, as the drug can interact with cells and organs that are not the intended target, potentially causing toxicity.^{1, 4} As an example, systemic administration of common analgesics such as aspirin or acetaminophen for a headache can cause gastrointestinal bleeding and liver toxicity.⁵ Administering lower amounts of drug can reduce these toxic effects, but also lowers the therapeutic efficacy where the drug is needed (Figure 1.3B).

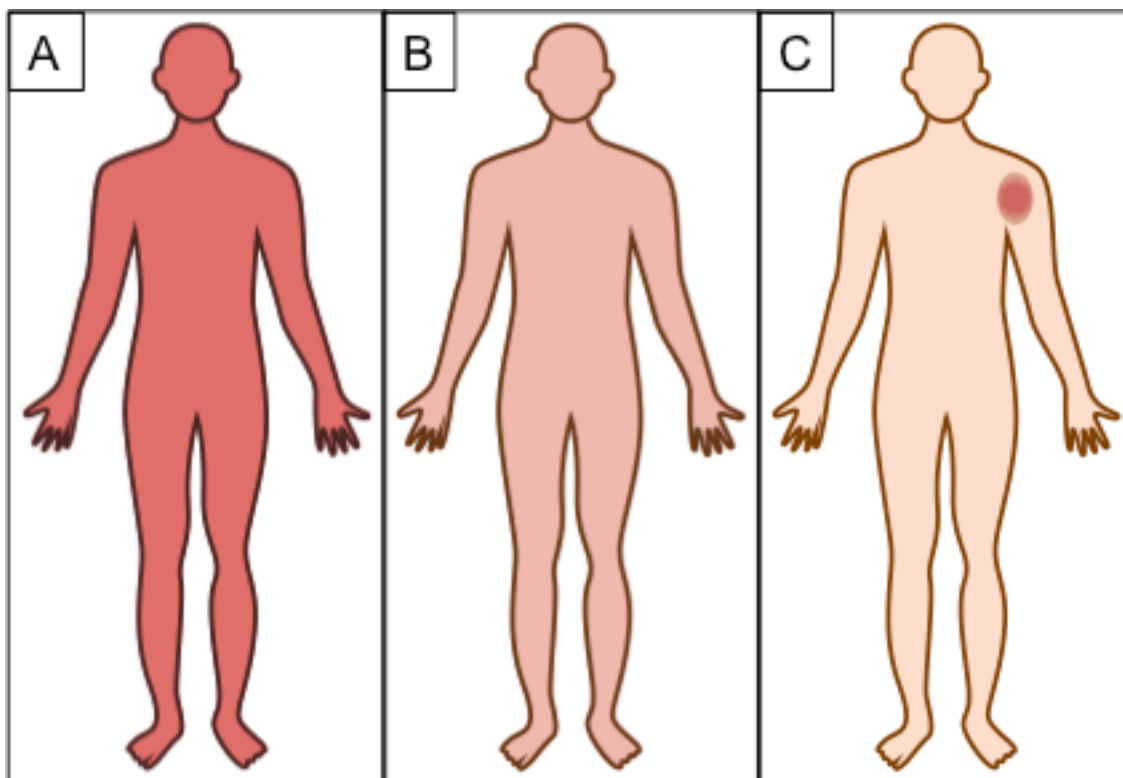


Figure 1.3. Drug distribution (red) with high systemic (A), low systemic (B), and localized (C) delivery.

Polymeric delivery devices offer a way to achieve localized, controlled release.² Implantable polymeric devices have been designed to provide therapeutic levels of drugs to specific areas of the body, while limiting the amount of drug that enters the bloodstream (Figure 1.3C).^{1, 4} This localized release increases drug efficacy by ensuring that the majority of the drug administered to the patient is present at the desired site of therapy, thereby, requiring less total drug to reach therapeutic levels.⁴ The concentration of drug at a specific site decreases potential side effects and toxicity by maintaining the drug only at sites where it will be beneficial.⁴

One example of localized delivery is the GLIADEL[®] Wafer, a delivery system for the chemotherapeutic drug, carmustine. The wafers are directly placed in voids left by resected brain tumors to provide controlled release of carmustine. The locally high drug concentrations allow the device to help prevent recurrence while protecting the body from the harmful effects of the anti-proliferative, such as bone marrow suppression and pulmonary fibrosis.⁶

1.2 Polymers for Drug Delivery

1.2.1 Bulk versus surface erosion

Drugs encapsulated within polymer matrices are released in a manner that depends on the diffusion of the molecules out of the matrix.³ Drug diffusion is increased as the matrix degrades.³ Polymers degrade in different manners that can have a significant effect on the drug release profiles. Polymers typically undergo either bulk or surface erosion (Figure 1.4).⁷ Bulk-eroding polymers swell with water and experience degradation throughout the entire polymer matrix. In this case, the polymer matrices typically maintain their original size throughout most of the degradation process (Figure 1.4, left).⁷ In contrast, surface-eroding polymers minimize water uptake and, therefore, only experience degradation and erosion on the surface areas exposed to aqueous environments. In this case, the polymer matrices decrease in size overall throughout degradation (Figure 1.4, right).⁷

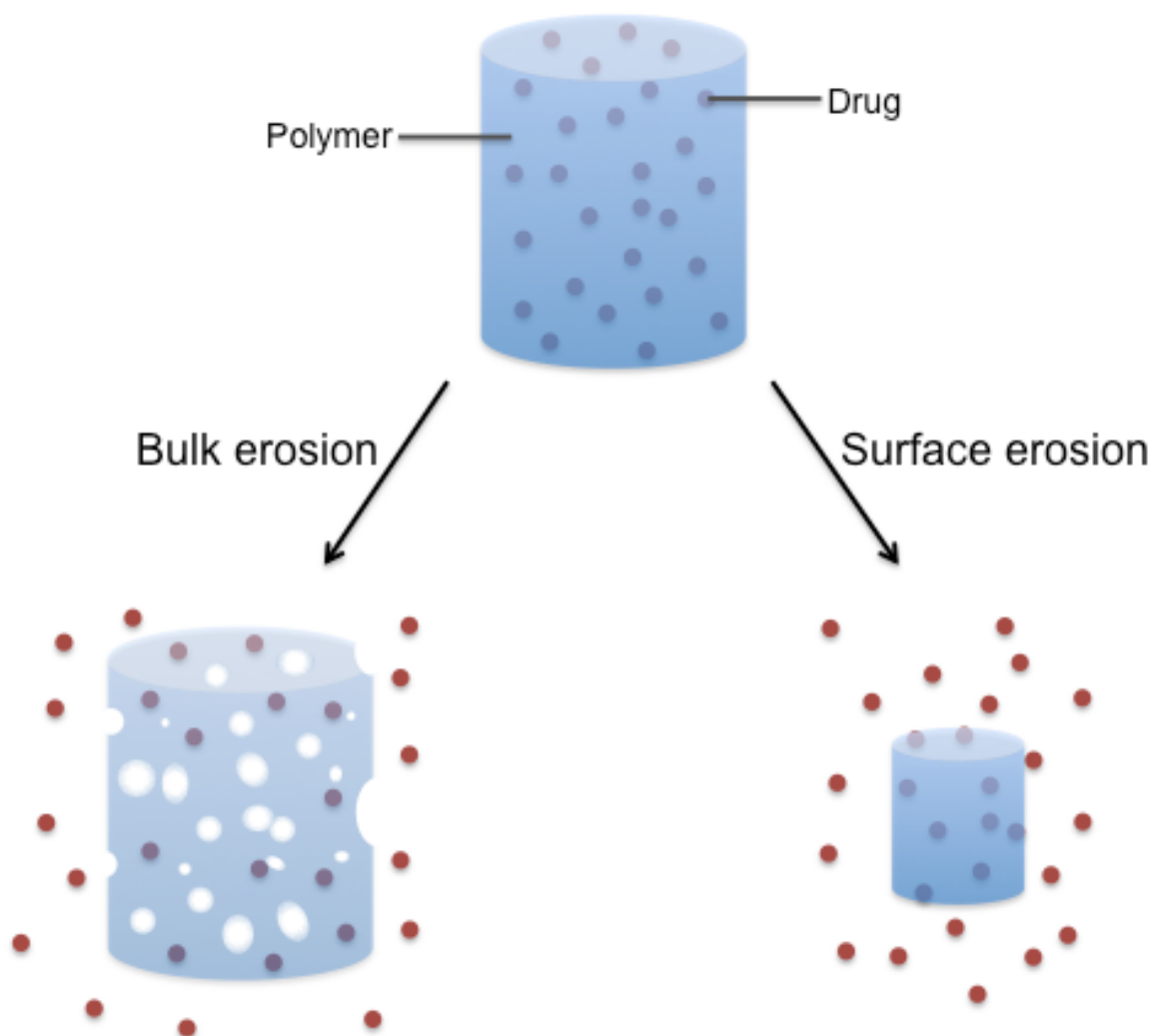


Figure 1.4. Polymer matrix degradation can occur in a manner that is primarily either bulk or surface-eroding. The eroding mechanism has a strong influence on the release profile of encapsulated drugs.

Bulk erosion devices tend to result in a burst release of encapsulated drug while surface erosion devices typically results in near zero-order drug release profiles.⁴ This zero-order release profile allows the attainment of therapies as shown in Figure 1.2. However, no polymer is strictly bulk or surface-eroding; rather, these mechanisms represent two ends of the spectrum. Factors such as

polymer hydrophobicity, crystallinity, degradation product solubility, and bond lability all control water permeation into the polymer matrix, thereby, controlling degradation and erosion. The extent to which a polymeric device is classified as one or the other depends greatly on the device dimensions, specifically the surface area to volume ratio, as this will affect the amount of water uptake.^{7, 8}

1.2.2 Polyanhydrides

Polyanhydrides are a class of hydrolytically degradable polymers that have been widely used in several biomedical applications.⁹ Polyanhydrides are primarily surface eroding, a characteristic that makes them desirable for drug delivery applications as this leads to a near zero-order release of molecules encapsulated within the polymer matrix.^{9, 10} They degrade to release biocompatible acidic byproducts that are easily eliminated from the body.⁴

1.2.3 Polymeric Drugs

To better control release from polymer matrices, drug molecules have been chemically incorporated into the structure of the polymers. This chemical incorporation can be achieved either by attaching a drug to the polymer chains as a pendant group (one chemical bond connecting the drug to the polymer) or by incorporating the drug directly into the polymer backbone (two chemical bonds connecting the drug to the polymer) via “linker” components (Figure 1.5).¹¹⁻¹³ This chemical incorporation of the drug prevents burst release as drug release is controlled by the rate of bond cleavage rather than simple diffusion. Backbone

cleavage can be controlled through the type of linker molecule used by changing the type of bond formed (e.g., anhydride, ester, amide, etc.) and the hydrophobicity of the molecule. With physical encapsulation, maximum drug loading before it affects polymer mechanical and degradation properties depends on drug solubility within the polymer matrix.¹⁴ By chemically incorporating the drug within the polymer, the drug solubility in the polymer is no longer a factor.

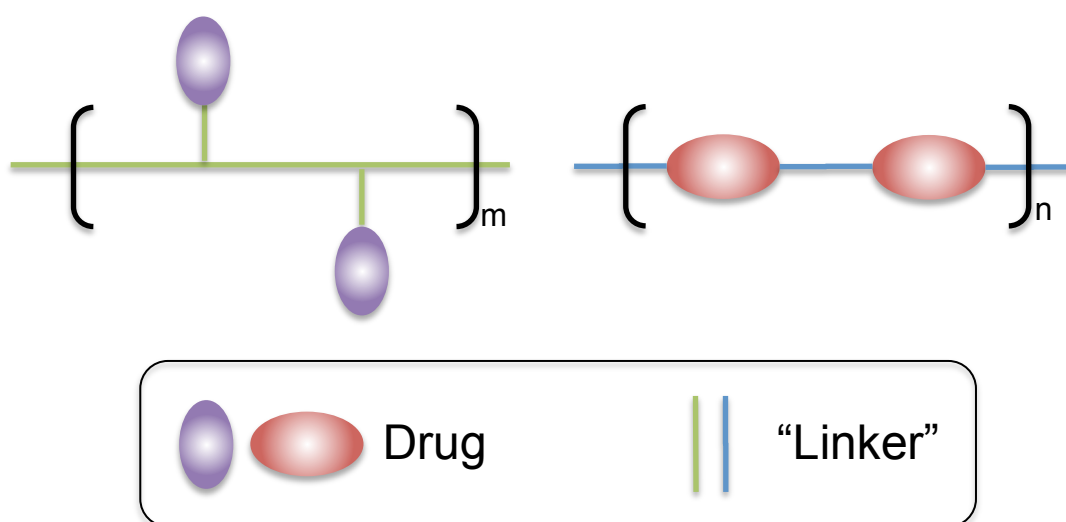


Figure 1.5. Polymeric drugs with drugs incorporated as pendant groups (left) or within the polymer backbone (right) through the use of non-bioactive “linker” molecules.

1.2.4 Salicylic acid-based poly(anhydride-esters)

The Uhrich laboratory has developed a series of salicylic acid-based poly(anhydride-esters) (SAPAEs) that are composed of salicylic acid (SA) and various biocompatible diacid linker molecules.¹⁵⁻¹⁸ Salicylic acid is a nonsteroidal

anti-inflammatory drug (NSAID) that has been used for centuries for its anti-inflammatory, analgesic, antipyretic, antiseptic, and keratolytic properties.¹⁹

SAPAEs exhibit surface erosion in aqueous environments to release free salicylic acid and biocompatible linker molecules (Figure 1.6).²⁰ The linker can be used to alter the degradation rate of the polymer; SAPAEs with more hydrophobic linker molecules exhibit decreased degradation rates.^{16, 21}

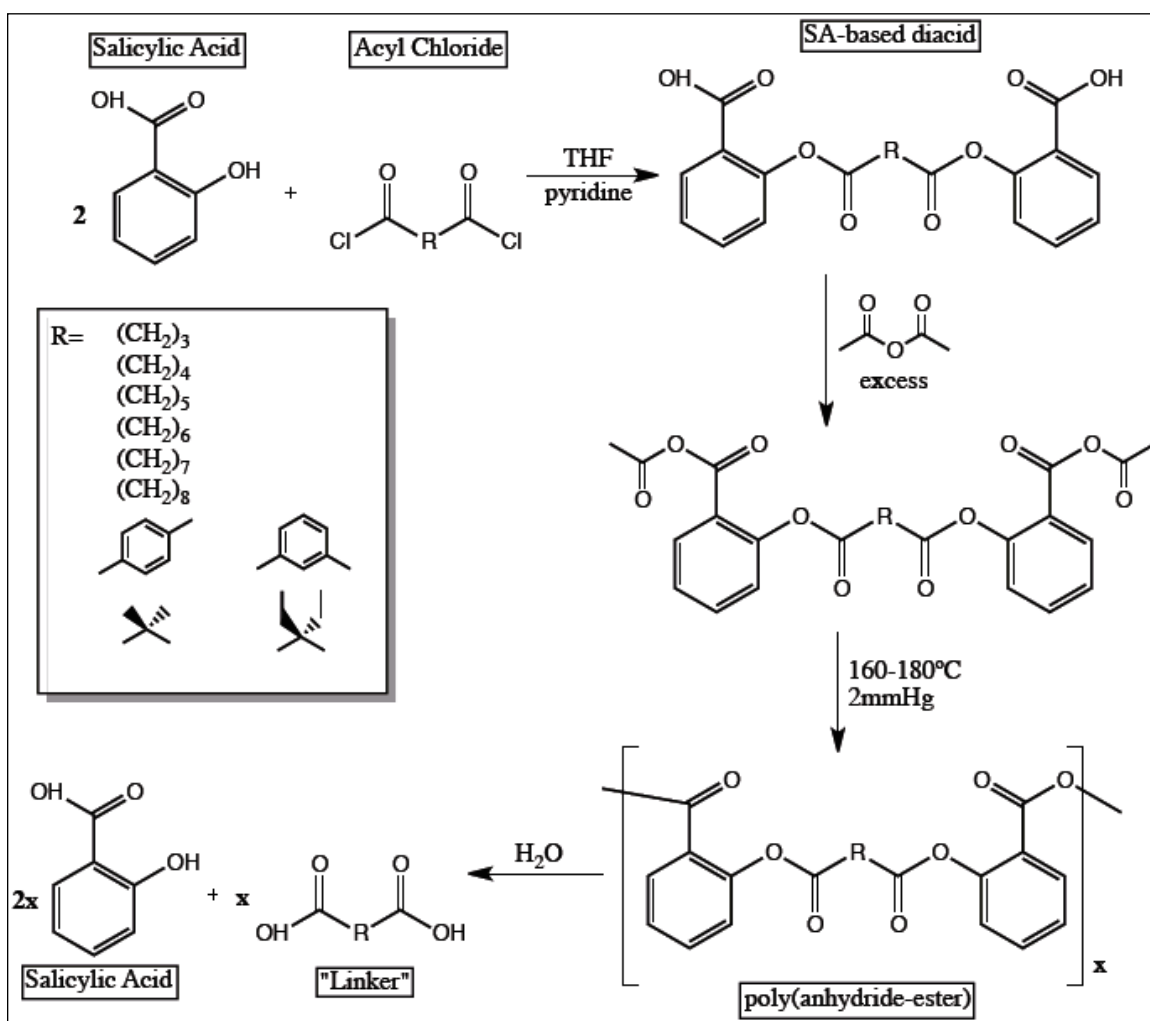


Figure 1.6. Synthesis and degradation products of salicylic acid-based poly(anhydride-esters)¹⁶

The inherent drug loading of SAPAEs can be up to 75 % with linkers such as adipic acid, with the ability to have higher drug loading via admixed free drugs. Polymer systems with physically incorporated SA exhibit altered polymer degradation rates below 40 % SA loading.^{15, 22} The release profile of SA from SAPAEs is observed to have a lag period of little to no drug release followed by zero-order release. The length of the lag period is determined by the composition of the polymer.^{16, 20, 23} The thermal and mechanical properties of SAPAEs allow them to be manipulated into various shapes such as disks, films, microspheres, and fibers.

1.3 Inflammation in Wound Healing and Tissue Regeneration

Wound healing and subsequent tissue regeneration is highly regulated by inflammation.²⁴ The degree and duration of the inflammatory response after injury can determine the rate of healing as well as the quality of new tissue. Having too much or too little inflammation at the injury site can inhibit healing or result in tissue that is structurally and functionally inferior to the original tissue.^{24,}
²⁵ The ability to modulate inflammation at the site of an injury through controlled release of drugs like SA could be used to direct the wound healing response to achieve proper tissue regeneration.

While SA has been shown to affect many cell signaling pathways, its anti-inflammatory properties are most commonly attributed to its involvement in the cyclooxygenase-2 (COX-2) and nuclear factor- κ B (NF- κ B) pathways. COX-2

produces prostaglandins, which induce inflammatory cell recruitment.³⁰ SA is less effective at directly inhibiting COX enzymes than many other NSAIDs,²⁶ but it inhibits activation of C/EBP β , a transcription factor, resulting in decreased COX-2 expression.²⁶⁻²⁹ NF- κ B is a transcription factor that is an important mediator of inflammatory responses that controls the production of inflammatory cytokines such as TNF- α , IFN- γ , IL-1, and many others.³¹ SA inhibits IKK, an enzyme responsible for NF- κ B activation,^{32, 33} thereby, reducing inflammatory responses.

SAPAEs are well suited for controlling wound healing as the release of SA can be easily adjusted to properly modulate inflammation throughout the healing process, allowing enough inflammation as needed for regeneration, while preventing excessive inflammation that could lead to inferior tissue.

1.4 Research Projects

1.4.1 Guided bone regeneration device using salicylic acid-based poly(anhydride-esters) and osteoconductive scaffolds

Successful repair of large bone defects restores anatomy and function. Therapies to promote healing may include inflammation modulation, control of soft tissue infiltration, and bone regeneration.^{34, 35} SAPAEs were combined with osteoconductive ceramic scaffolds and evaluated as a combined guided bone regeneration (GBR) system (Figure 1.7) for concurrent control of inflammation, soft tissue ingrowth, and bone repair in a rabbit cranial defect model. It was hypothesized that the GBR barrier on the scaffolds would prevent soft tissue from

growing into the scaffold and impeding bone regeneration while the SA release would prevent bone resorption and help to decrease inflammation and swelling in the surrounding tissue. Five groups were compared: (1) scaffolds with a solid ceramic cap (as a GBR structure); (2) scaffolds with no cap; (3) scaffolds with a poly(lactide-glycolide) cap, a common biodegradable polymer without any bioactivity; (4) scaffolds with a slow release SAPAE cap; and (5) scaffolds with a fast release SAPAE cap. Animals were sacrificed at 1, 3, and 8 weeks to assess differences in cellular infiltration, bone formation, and inflammation over time. The SAPAE caps suppressed inflammation and displayed no deleterious effect on bone formation.

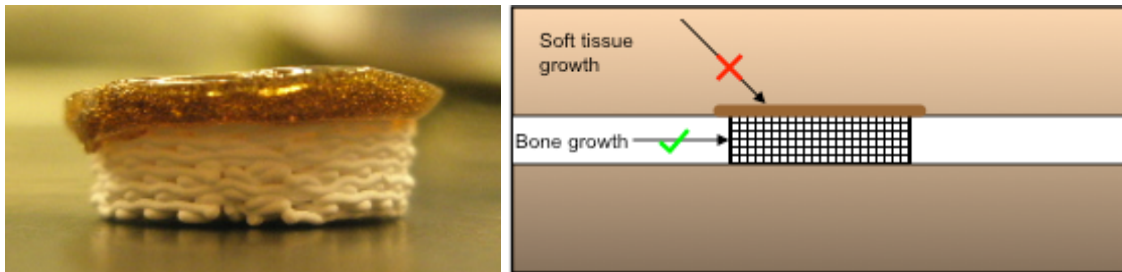


Figure 1.7. SAPAEs were melt-cast on osteoconductive scaffolds as both a physical barrier against soft tissue growth into the scaffold and to modulate inflammation.

1.4.2 Polymeric bone wraps to prevent heterotopic ossification

A drawback of the GBR devices described in Section 1.4.1 is that the SAPAE caps were relatively stiff and did not conform well to the curvature of the skull, thereby, decreasing their efficacy as a physical barrier. To address this

issue, blends of SAPAEs and polycaprolactone (PCL) were electrospun to create more flexible membranes that could be used to wrap bone defects to prevent heterotopic ossification (HO, the formation of mineralized tissue in areas outside of skeletal tissue). PCL was chosen for these blends as it is a widely studied biodegradable polymer that has been used to obtain flexible electrospun fibers.³⁶ Electrospinning parameters were defined and the resulting fibrous mats were characterized by scanning electron microscopy, mechanical testing, and *in vitro* drug release. Additionally, the mats were assessed *in vivo* for their ability to prevent HO. HO is a common occurrence after bone surgery, especially if BMP-2, an osteogenic growth factor, is used to increase the rate of healing.³⁷ A rat femoral defect model was used to observe bone regeneration and HO occurrence for defects filled with BMP-2 loaded collagen sponges with and without the SAPAE:PCL wraps isolating the defect site. Initial animal studies indicate that the SAPAE:PCL blends used prevent HO, but they also inhibit bone regeneration in the defect site. This effect is likely due to the large amount of SA release within the first week after implantation. Current studies are investigating SAPAE:PCL blends that release SA at a slower rate.

1.4.3 Flowable salicylic acid-based poly(anhydride-esters) for injectable barrier applications

Fibrous adhesions are bands of fibrous tissue that join two adjacent surfaces in the body that are not normally connected.³⁸ They can lead to serious medical problems and are a common occurrence after surgery.³⁸⁻⁴⁰ Extending

the concept of using SAPAEs as both drug release systems as well as physical barriers, a device to prevent fibrous adhesion formation was pursued. This effort led to the development and synthesis of SAPAE:poly(ethylene glycol) (PEG) copolymers. These copolymers were designed to have glass transition temperatures (T_g s) below 0 °C, resulting in polymers that behave like viscous fluids at room temperature (Figure 1.8). SAPAE:PEG copolymers of different ratios were synthesized. They were characterized by typical chemical methods. Their shear viscosities were determined both at room and physiological temperatures. The *in vitro* drug release profiles, cytotoxicity, and anti-inflammatory capacity of these polymers were assessed. The shear viscosities, drug release, biocompatibility, and bioactivity of these polymers compare favorably with current fibrous adhesion barriers on the market.

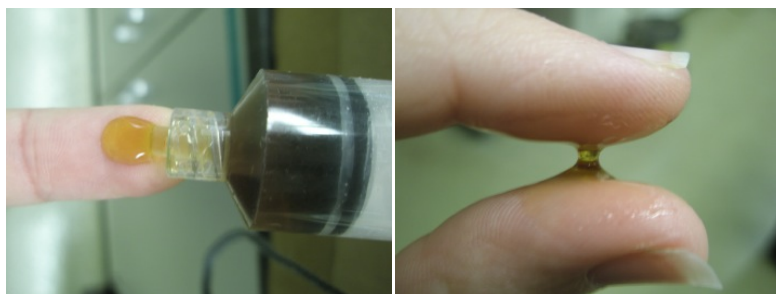


Figure 1.8. SAPAE:PEG copolymers have T_g s below 0 °C, resulting in polymers that behave like viscous fluids.

1.4.4 Tunable drug release profiles from salicylate-based poly(anhydride-ester) matrices using small molecule admixtures

SAPAEs exhibit an initial lag period in drug release, which is characteristic of polyanhydrides.⁴¹ This lag period could be unfavorable in applications where immediate SA release is desired, therefore, an SAPAE that exhibits an 11-day lag period was admixed with various small molecules as a means to shorten or eliminate the lag period. SA, larger SA prodrugs, and 1:1 combinations of the two were physically admixed, each at 1, 5, and 10 % (w/w) to determine the effects of admixture type and amount on the SA release profile. All admixtures resulted in immediate SA release and a decrease in T_g s compared to polymer alone. By varying the amounts of SA and SA prodrugs incorporated into the polymer matrix, immediate and constant SA release profiles over varied time periods were achieved (Figure 1.9).

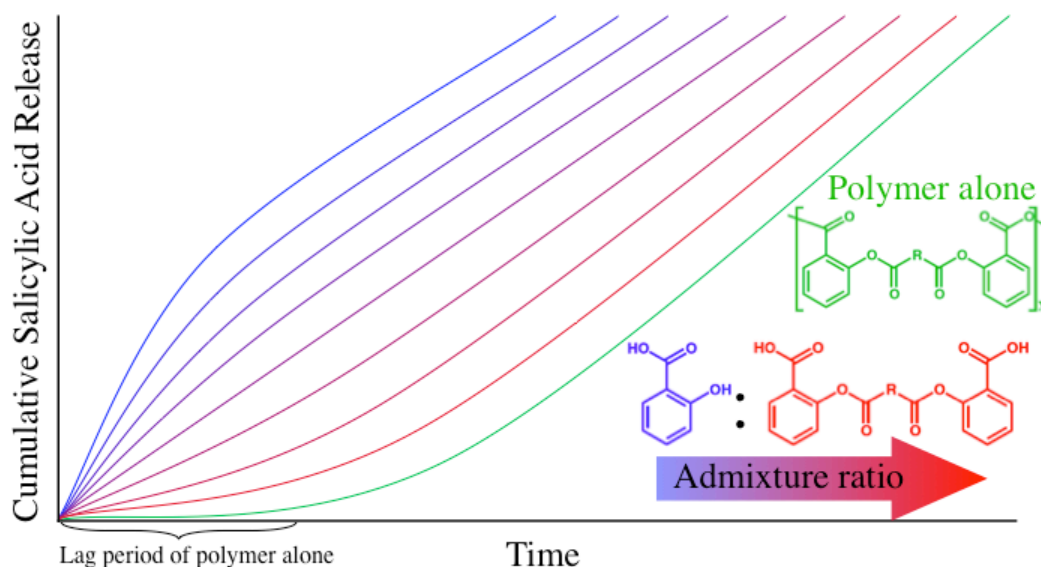


Figure 1.9. Visualization of the effect of small molecule admixtures on the SA release profile from SAPAEs.

1.5 Summary

The localized, controlled delivery of drugs from biodegradable polymer systems is an effective way to improve the therapeutic efficacy of the drugs.² Polymeric drugs are advantageous as they provide both controlled release of drugs, and their physical properties can be modified to meet the needs of various potential applications.⁴² SAPAEs can be used to control the wound healing process by modulating the inflammation responsible for tissue regeneration. The research described herein involves the physical and chemical methods used to adjust drug release profiles and mechanical properties of SAPAEs for various biomedical applications.

1.6 References

1. Domb AJ. Polymeric carriers for regional drug therapy. *Molecular medicine today*. 1995;1(3):134-9.
2. Uhrich KE, Cannizzaro SM, Langer RS, Shakesheff KM. Polymeric systems for controlled drug release. *Chemical reviews*. 1999;99(11):3181-98.
3. Ratner BD. *Biomaterials science : an introduction to materials in medicine*. 2nd ed. Amsterdam ; Boston: Elsevier Academic Press; 2004. xii, 851 p. p.
4. Jain JP, Modi S, Domb AJ, Kumar N. Role of polyanhydrides as localized drug carriers. *Journal of Controlled Release*. 2005;103(3):541-63.
5. Hinson JA, Roberts DW, James LP. Mechanisms of Acetaminophen-Induced Liver Necrosis. 2010;196:369-405.
6. Wang PP, Frazier J, Brem H. Local drug delivery to the brain. *Advanced drug delivery reviews*. 2002;54(7):987-1013.

7. Burkersroda Fv, Schedl L, Göpferich A. Why degradable polymers undergo surface erosion or bulk erosion. *Biomaterials*. 2002;23(21):4221-31.
8. Akbari H, D'Emanuele A, Attwood D. Effect of geometry on the erosion characteristics of polyanhydride matrices. *International Journal of Pharmaceutics*. 1998;160:83-9.
9. Ratner BD, Hoffman AS, Schoen FJ, Lemons JE, editors. *Biomaterials Science: An Introduction to Materials in Medicine*. 2nd ed. San Diego: Elsevier Academic Press; 2004.
10. Whitaker-Brothers K, Uhrich K. Investigation into the erosion mechanism of salicylate-based poly(anhydride esters). *Journal of Biomedical Materials Research Part A*. 2006;76(3):470-9.
11. Erdmann L, Uhrich KE. Synthesis and degradation characteristics of salicylic acid-derived poly(anhydride-esters). *Biomaterials*. 2000;21(19):1941-6.
12. Rosario-Meléndez R, Harris CL, Delgado-Rivera R, Yu L, Uhrich KE. PolyMorphine: An innovative biodegradable polymer drug for extended pain relief. *Journal of Controlled Release*. 2012;162(3):538-44.
13. Ouimet MA, Griffin J, Carbone-Howell AL, Wu W-H, Stebbins ND, Di R, et al. Biodegradable Ferulic Acid-Containing Poly(anhydride-ester): Degradation Products with Controlled Release and Sustained Antioxidant Activity. *Biomacromolecules*. 2013; 14(3) 854-61.
14. Taktguchi T, Kobayashi M, Nagashima C, Yamaguchi A, Nishihara T, Hasegawa K. Effect of prostaglandin E2 on recombinant human bone morphogenetic protein-2-stimulated osteoblastic differentiation in human periodontal ligament cells. *Journal of periodontal research*. 1999;34(7):431-6.
15. Schmeltzer RC, Anastasiou TJ, Uhrich KE. Optimized Synthesis of Salicylate-based Poly(anhydride-esters). *Polymer Bulletin*. 2003;49:441-8.
16. Prudencio A, Schmeltzer RC, Uhrich KE. Effect of Linker Structure on Salicylic Acid-Derived Poly(anhydride-esters). *Macromolecules*. 2005;38:6895-901.

17. Schmeltzer RC, Johnson M, Griffin J, Uhrich K. Comparison of salicylate-based poly(anhydride-esters) formed *via* melt-condensation *versus* solution polymerization. *Journal of Biomaterials Science: Polymer Edition*. 2008;19(10):1295-306.
18. Carbone AL, Uhrich KE. Design and Synthesis of Fast-Degrading Poly(anhydride-esters). *Macromolecular Rapid Communications*. 2009;30(12):1021.
19. Wu KK. Aspirin and salicylate: An old remedy with a new twist. *Circulation*. 2000;102(17):2022-3.
20. Erdmann L, Uhrich KE. Synthesis and degradation characteristics of salicylic acid-derived poly(anhydride esters). *Biomaterials*. 2000;21:1941-6.
21. Carbone AL, Uhrich KE. Design and Synthesis of Fast-Degrading Poly(anhydride-esters). *Macromolecular rapid communications*. 2009;30(12):1021.
22. Tang Y, Singh J. Controlled delivery of aspirin: Effect of aspirin on polymer degradation and *in vitro* release from PLGA based phase sensitive systems. *International Journal of Pharmaceutics*. 2008;357:119-25.
23. Yeagy BA, Prudencio A, Schmeltzer RC, Uhrich KE, Cook TJ. Characterization and *in vitro* degradation of salicylate-derived poly(anhydride-ester microspheres). *Journal of Microencapsulation*. 2006;23(6):643-53.
24. Eming SA, Krieg T, Davidson JM. Inflammation in Wound Repair: Molecular and Cellular Mechanisms. *Journal of Investigative Dermatology*. 2007;127(3):514-25.
25. Diegelmann RF, Evans MC. Wound healing: an overview of acute, fibrotic and delayed healing. *Frontiers in bioscience : a journal and virtual library*. 2004;9:283-9.
26. Amann R, Peskar BA. Anti-inflammatory effects of aspirin and sodium salicylate. *European Journal of Pharmacology*. 2002;447(1):1-9.

27. Wu KK, Liou JY, Cieslik K. Transcriptional Control of COX-2 via C/EBPbeta. *Arteriosclerosis, thrombosis, and vascular biology*. 2005;25(4):679-85.
28. Furst R. Nuclear Factor- B-Independent Anti-Inflammatory Action of Salicylate in Human Endothelial Cells: Induction of Heme Oxygenase-1 by the c-Jun N-Terminal Kinase/Activator Protein-1 Pathway. *Journal of Pharmacology and Experimental Therapeutics*. 2006;318(1):389-94.
29. Tegeder I, Pfeilschifter J, Geisslinger G. Cyclooxygenase-independent actions of cyclooxygenase inhibitors. *FASEB journal : official publication of the Federation of American Societies for Experimental Biology*. 2001;15(12):2057-72.
30. Kindt TJ, Goldsby RA, Osborne BA, Kuby J. *Kuby immunology*. 6th ed. New York: W.H. Freeman; 2007. xxii, 574, A-31, G-12, AN-27, I-27 p. p.
31. Pahl HL. Activators and target genes of Rel/NF-kappaB transcription factors. *Oncogene*. 1999;18(49):6853-66.
32. Pierce JW, Read MA, Ding H, Luscinskas FW, Collins T. Salicylates inhibit I kappa B-alpha phosphorylation, endothelial-leukocyte adhesion molecule expression, and neutrophil transmigration. *J Immunol*. 1996;156(10):3961-9.
33. Yin MJ, Yamamoto Y, Gaynor RB. The anti-inflammatory agents aspirin and salicylate inhibit the activity of I(kappa)B kinase-beta. *Nature*. 1998;396(6706):77-80.
34. Retzepi M, Donos N. Guided Bone Regeneration: biological principle and therapeutic applications. *Clinical oral implants research*. 2010;21(6):567-76.
35. Karakawa A, Sano T, Amano H, Yamada S. Inhibitory Mechanism of Non-steroidal Anti-inflammatory Drugs on Osteoclast Differentiation and Activation. *Journal of Oral Biosciences*. 2010;52(2):119-24.
36. Lee KH, Kim HY, Khil MS, Ra YM, Lee DR. Characterization of nano-structured poly(ε-caprolactone) nonwoven mats via electrospinning. *Polymer*. 2003;44(4):1287-94.

37. Lo KWH, Ulery BD, Ashe KM, Laurencin CT. Studies of bone morphogenetic protein-based surgical repair. *Advanced drug delivery reviews*. 2012;64(12):1277-91.
38. Ward BC, Panitch A. Abdominal adhesions: current and novel therapies. *The Journal of surgical research*. 2011;165(1):91-111.
39. Tingstedt B, Isaksson K, Andersson E, Andersson R. Prevention of Abdominal Adhesions: Present State and What's beyond the Horizon? *European Surgical Research*. 2007;39(5):259-68.
40. Alpay Z, Saed GM, Diamond MP. Postoperative adhesions: from formation to prevention. *Seminars in reproductive medicine*. 2008;26(4):313-21.
41. Whitaker-Brothers K, Uhrich K. Investigation into the erosion mechanism of salicylate-based poly(anhydride-esters). *Journal of biomedical materials research Part A*. 2006;76(3):470-9.
42. Schmeltzer RC, Schmalenberg KE, Uhrich KE. Synthesis and cytotoxicity of salicylate-based poly(anhydride esters). *Biomacromolecules*. 2005;6(1):359-67.

2. GUIDED BONE REGENERATION DEVICE USING SALICYLIC ACID-BASED POLY(ANHYDRIDE-ESTERS) AND OSTEOCONDUCTIVE SCAFFOLDS

2.1 Introduction

A frequent complication with large bone defects is the growth of soft tissue into the defect space, which can preclude osteogenesis.^{1, 2} Guided bone regeneration (GBR) is a technique that employs a barrier to physically exclude cells from migrating into the defect site from anywhere other than the bone at the edges of the defect, thereby, preventing soft tissue ingrowth.¹⁻³ Barrier materials should be biocompatible, biodegradable, and capable of maintaining the defect space without either collapsing or swelling into the void.¹ While materials such as expanded-polytetrafluoroethylene (PTFE) maintain the secluded environment well, they are non-biodegradable and must either be left in place or removed with a second surgery after the defect has healed.¹ Collagen is a common biodegradable GBR material, but native collagen collapses into defect spaces and degrades too quickly *in vivo* to act as a GBR membrane barrier for healing of large defects. Although collagen can be cross-linked to slow the degradation and prevent swelling, the chemicals used to induce the cross-linking can increase cytotoxicity.⁴ GBR membrane barriers composed of synthetic, biodegradable materials such as lactic acid-based polymers can induce foreign body reactions at the implant sites.³ Thus, alternative GBR materials are needed to increase

efficacy and simplify surgical procedures while providing for biocompatibility and biodegradability.

This study evaluates the efficacy of salicylic acid-based poly(anhydride-esters) (SAPAEs) as GBR barrier materials. When placed in an aqueous environment, the anhydride and ester bonds of SAPAEs hydrolyze to release salicylic acid (SA) and biocompatible linker molecules.^{5, 6} Use of different linker molecules between SA moieties dramatically affects the initiation and rate of SAPAE hydrolysis.^{5, 7, 8} Thus, the initiation of hydrolysis, rate of hydrolysis, and amount of SA delivered can be controlled by using different SAPAE polymers.

SA is a nonsteroidal anti-inflammatory drug (NSAID). NSAIDs typically inhibit cyclooxygenase (COX) activity, and COX inhibitors have been found to delay or inhibit new bone formation and fracture union in many animal studies.⁹⁻¹² Clinically, COX inhibitors are used to inhibit heterotopic ossification and studies suggest that COX inhibition can also impair fracture healing in humans.¹³⁻¹⁷ However, COX inhibition also can decrease bone resorption.^{18, 19} This aspect may be important for bone defects in which chronic inflammation is present, as is the case in many periodontal defects, where inflammation can lead to increased osteoclast activity and subsequent bone resorption.²⁰⁻²² There is evidence that the timing of when the COX inhibitor is present has a significant effect on the ability of the drug to affect healing.^{12, 23, 25}

Previous studies of SAPAEs in proximity to bone have had conflicting results. Reynolds et al. found SAPAE disks to decrease inflammation without adverse effects on early bone formation or wound healing in a rat calvarial defect

model when compared to poly(lactic-co-glycolic acid) (PLGA).²⁶ Erdmann et al. compared an SAPAE to a polyanhydride with non-active degradation products as films implanted adjacent to the palatal bone in mice. The SAPAEs produced more new bone growth than the control polymer. The SAPAE films were also found to inhibit bone resorption, unlike the control.²⁷ Harten et al. found that SAPAE microspheres inhibited both new bone formation as well as resorption when compared to a collagen control in a rat femoral defect.²⁸ The differences in results between these studies is likely due to the rate of release and total amount of SA in each of these studies. Harten et al. had significantly higher drug loading than Erdmann et al., which could explain the inhibition of osteogenesis in the femoral defect model.^{27, 28}

The testing of SAPAE polymers with different SA release kinetics for efficacy as GBR barriers using a rabbit parietal bone trephine defect model is described. The SAPAE polymers were capped onto hydroxyapatite- β -tri-calcium phosphate (HA-TCP) lattice scaffolds to act as barriers between the scaffold regeneration site and the overlying periosteum, muscle, and skin. Controls included: scaffolds with PLGA caps, solid HA-TCP caps, and open lattice HA-TCP caps. Bone formation into the scaffolds was quantified by micro-computerized tomography and histology to determine if SAPAE polymers impaired bone regeneration. In addition, cell density within the scaffolds was measured by histology to determine if the SAPAE polymers were altering the regeneration response by affecting cell migration. Finally, inflammation at the trephine defect site was qualitatively assessed by histological observations. The

SAPAE polymers reduced cell density within the scaffolds without negatively affecting the amount of bone formed indicating that the SAPAE polymers may be useful GBR barriers in bone regeneration applications.

2.2 Materials and Methods

2.2.1 Scaffold fabrication

[Scaffold fabrication was performed by Dr. Lukasz Witek, former graduate student at New York University.]

Scaffolds were made using a 3-axis, computer-aided robot which ejected a ceramic ink under mineral oil in a direct-write, layer-by-layer assembly to create 1-cm diameter scaffolds with $250 \times 250 \mu\text{m}^2$ pores as described previously.^{29, 30} Scaffold design and fabrication used custom software (RoboCad 4.0, 3D Inks, Stillwater, OK). The ink was composed of 85% β -tricalcium phosphate (TCP) and 15% hydroxyapatite (HA). Once assembly was complete, the oil was drained and each scaffold was air-dried then fired in a kiln at 1100°C for 4 hours.

2.2.2 Polymer synthesis and characterization

Fast-PA, the faster degrading SAPAE, poly[1,6-bis(o-carboxyphenoxy)hexanoate], was synthesized by melt polymerization as previously described.^{7, 24} Slow-PA, the slower degrading SAPAE, was polymerized from 2,2'-bis(o-carboxyphenoxy)pentanoate and α,α' -bis(o-carboxyphenoxy)-p-xylene in a 1:2 weight ratio in the same manner.^{7, 31} Polymer structures were characterized by ^1H NMR spectroscopy, gel permeation

chromatography, and differential scanning calorimetry before use. Polymer structures are shown in Figure 2.1.

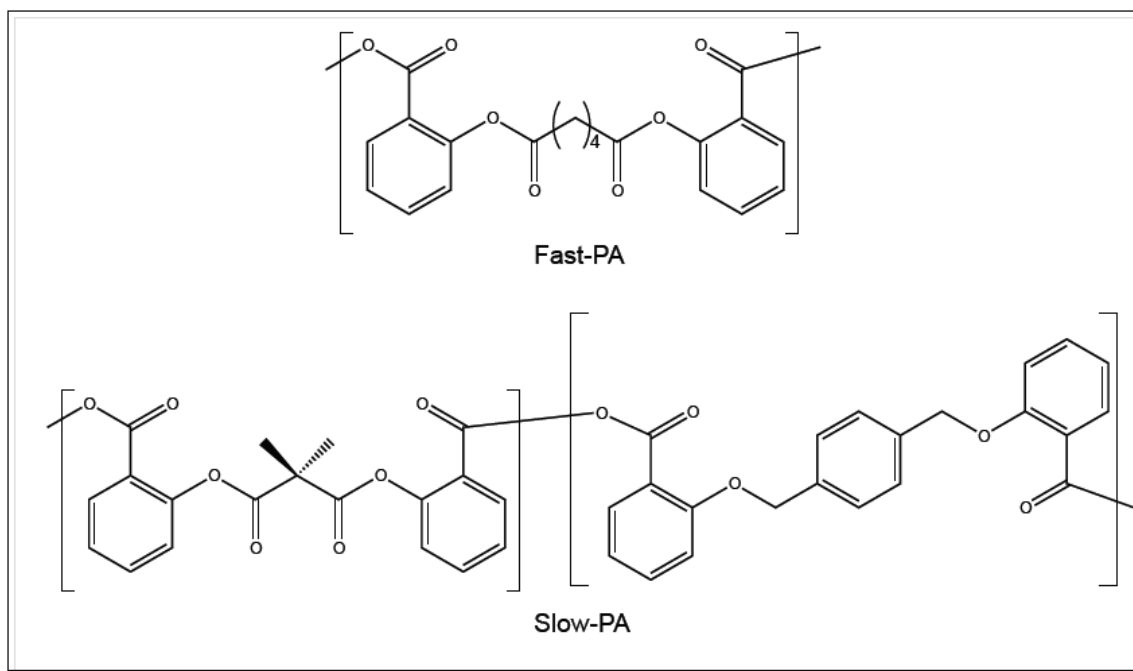


Figure 2.1. Chemical structures of fast-PA and slow-PA.

PLGA [50:50 poly(DL-lactide-co-glycolide), intrinsic viscosity = 0.2 dL/g in hexafluoro-2-propanol] was purchased from DURECT Corp. (Cupertino, CA) and used without additional modification.

2.2.3 Polymer capping of scaffolds

Polymer powders (120 mg) were melted above their glass transition temperature (53 °C for fast-PA, 70 °C for slow-PA, and 45 °C for PLGA) on a piece of aluminum foil over a heating plate set to 180 °C. A flat side of the HA-

TCP scaffold was placed onto the heated polymer, and the construct was removed from heat and cooled to room temperature.

2.2.4 *In vitro* drug release

Polymer-capped scaffolds were placed in glass scintillation vials with 10 mL phosphate buffered saline (PBS), pH 7.4, in an incubator at 37 °C. PBS was collected every 24 hours and replaced with fresh PBS. Polymer degradation products were measured by absorbance ($\lambda = 303$ nm) using high-pressure liquid chromatography (mobile phase: 25 % acetonitrile, 75 % PBS, 1 mL/min, Waters RP18 4.5 x 150 mm column). Data were compared to a calibration curve derived from known SA standards to determine SA concentration in the PBS samples.

2.2.5 Animal model

Skeletally mature, male New Zealand White rabbits weighing between 3.5 and 4.0 kg were purchased from Myrtle's Rabbitry (Thompsons Station, TN) or Covance, Inc. (Princeton, NJ) for this study. Before surgery, rabbits were treated with acepromazine (1 mg/kg), glycopyrolate (0.01 mg/kg), buprenorphine (0.05 mg/kg), and enrofloxacin (10 mg/kg). The rabbits were anesthetized with an intramuscular injection of ketamine (35 mg/kg) and xylazine (5 mg/kg) and an adhesive fentanyl patch (12.5 μ g/hr) was placed in the ear for post-surgical pain relief. The head was shaved, cleaned with isopropanol and chlorohexidine, scrubbed with betadine, and draped.

[Surgeries were performed by Ashley Mitchell, University of Medicine and Dentistry of New Jersey.]

A 4 cm incision was made through the skin and periosteum parallel to the sagittal suture along the midline of the calvaria. The skin and periosteal tissue layers were retracted to expose the parietal bone. A 1 cm defect was created in the right parietal bone posterior to the coronal suture and lateral of the sagittal suture of each rabbit using a hand-powered trephine drill. Care was taken while drilling to avoid disturbing the dura beneath. The site was flushed with saline and a scaffold was inserted into the defect. Defects were filled with a scaffold having one of the following 5 cap structures: porous HA-TCP cap contiguous with the scaffold (open), solid HA-TCP cap fabricated on the scaffold (closed), poly(lactic-co-glycolic) acid (PLGA), slow-PA, and fast-PA (refer to Table 2.2 for group size). The periosteum was sutured over the scaffold and the skin was closed separately thereafter. Animals received antibiotic treatment for 5 days after surgery and pain relief was managed for three days with the applied fentanyl patch. Animals were sacrificed at 1, 3, or 8 weeks after surgery. All animal procedures were approved by the UMDNJ-New Jersey Medical School Institutional Animal Care and Use Committee and followed NIH guidelines for the care and use of laboratory animals.

2.2.6 Micro-computerized tomography (microCT)

Three-dimensional microCT images were made to analyze the bone volume (BV; mm³) and bone mineral density (BMD) of the defect site using a

high-resolution microCT system (Skyscan 1172, Skyscan, Kontich, Belgium). The section of the parietal bone containing the scaffold was excised and fixed in 10 % formalin for 7-10 days. Samples were transferred into 70 % ethanol overnight to prevent drying. All samples were scanned at 90 kVp, an intensity of 112 μ A, and a voxel size of 12 microns isotropic using a 0.5 mm aluminum filter to reduce beam-hardening. X-ray images were reconstructed with NRecon software and analyzed in CTAn, provided by Skyscan. All parameters for scanning and reconstruction remained consistent for all samples.

[MicroCT analysis was performed by Ashley Mitchell, University of Medicine and Dentistry of New Jersey.]

Analysis was based upon an 8.5 mm cylindrical region of interest (ROI) over a fixed distance of 2.11 mm (175 slices per sample). Standard 3-D analysis was performed to retrieve BV and BMD. BV was not normalized to total volume since the same total volume was measured for each sample. BMD is the amount of mineral per unit volume of bone tissue (g/cm^3) and was calibrated against a Micro-Mouse phantom (Cone Instruments, model 090, Solon, OH).

2.2.7 Histology

[Histology was performed by Ashley Mitchell and Brian Kim, University of Medicine and Dentistry of New Jersey.]

Following microCT scanning, samples were dehydrated through grades of ethanol and embedded in poly(methylmethacrylate).³² Sections were cut along the diameter of the scaffold to obtain a lateral view. They were polished and

stained with van Gieson's picrofuchsin (mineralized tissue red) and Stevenel's blue (polychromatic blue stain for soft tissues).³³

All histological specimens were digitally scanned by Micro Optical Solutions, LLC (Amherst, Massachusetts) at 10x magnification. Digital images were received pre-calibrated for use on Image Pro Plus 7.0 image analysis software (Bethesda, Maryland) and the analysis was conducted with that software. Cell nuclei were counted and bone areas were measured within a rectangular region of interest (ROI: 10,000 μm x 2,500 μm) centered to encompass the scaffold area directly underneath the cap visible on the image. Each ROI was divided further into six distinct zones of equal area (3,333 μm x 1,250 μm) to compare different regions of the scaffold. Available area was calculated as the total area for the ROI less the area occupied by the HA-TCP scaffold. Cell counts were normalized against total available area to obtain cells/mm² and bone areas were normalized to obtain the percentage of bone formed relative to the total available area. A qualitative scoring rubric was (Table 2.1) was developed to asses inflammation in the soft tissues above each scaffold.

Table 2.1. Inflammation Scoring Rubric.

Apparent Inflammation Characteristics		Score
Depth of cell layer adjacent to scaffold surface	>50 cells	3
	26-50 cells	2
	10-25 cells	1
	<10 cells	0
Lymphocytic infiltration in soft tissue	Severe	3
	Moderate	2
	Some	1
	None	0
Soft tissue edema	Severe	3
	Moderate	2
	Some	1
	None	0

2.2.8 Statistical analyses

[Statistical analysis was performed by Dr. J. Patrick O'Connor, University of Medicine and Dentistry of New Jersey.]

The microCT data were compared between cap structure groups within each time point (1, 3, and 8 weeks) using analysis of variance (ANOVA). The histomorphometry data were compared between groups using a two-way ANOVA with scaffold configuration and time after surgery as the independent variables and percent bone area or cell density as the dependent variable. Subsequently, Fisher's LSD tests were used to identify significant differences between treatments.

2.3 Results

2.3.1 Polymer degradation

The fast-PA evaluated in this study was chosen as it is the most widely characterized SAPAE and, therefore, is a good polymer for comparison to other applications. Many SAPAEs were developed and assessed for their extended GBR ability. Specifically, a polymer was sought that would remain as a solid physical barrier for up to 8 weeks, the time shown in previous studies to be sufficient for bone regeneration in this type of scaffold.^{30, 34} The final polymer chosen as the slow-PA is a copolymer of monomers that degrade to release SA and monomers that do not degrade to SA. Therefore, it has much lower drug loading than the fast-PA (21 % versus 75 %).

The *in vitro* drug release profiles of the SAPAE-capped scaffolds were studied over 8 weeks (Figure 2.2). The fast-PA exhibited immediate salicylic acid release at approximately 1.9 mg/day in the initial linear period. The slow-PA exhibited an initial lag period of 30 days with minimal SA release after which it began releasing drug at approximately 0.8 mg /day.

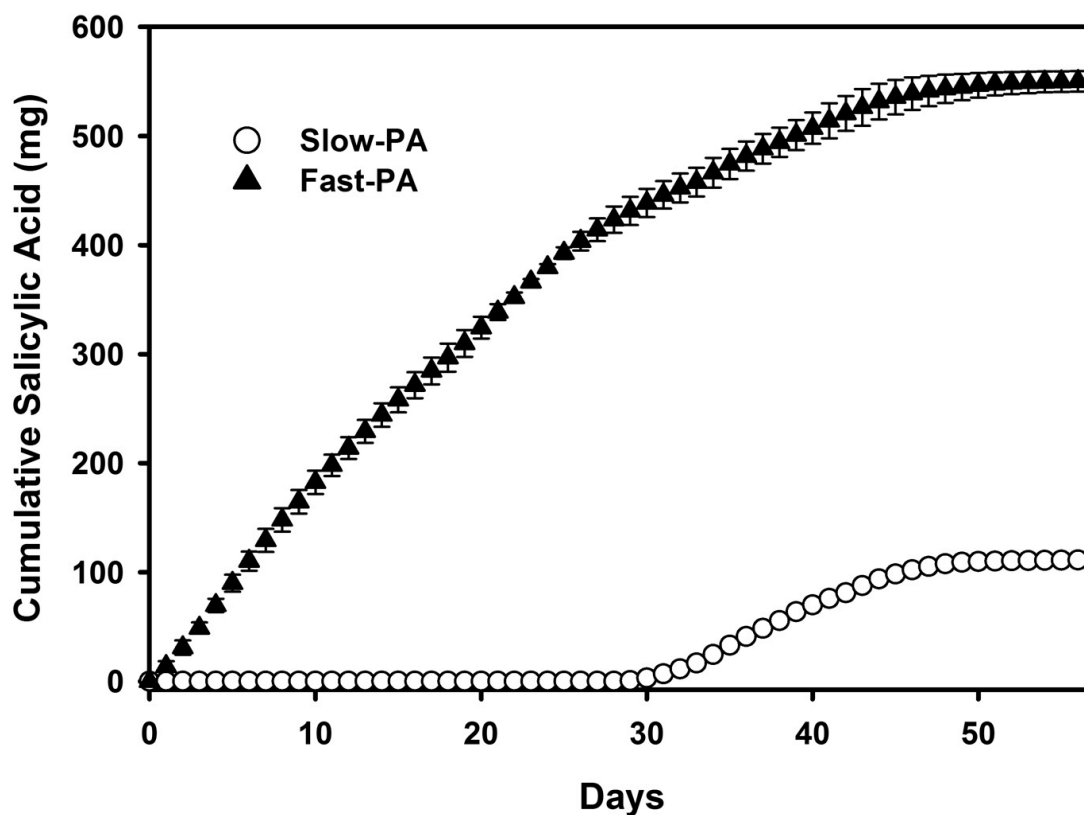


Figure 2.2. Cumulative SA release from SA-PAE capped scaffolds (SA amount was normalized to 1 g of polymer).

2.3.2 Animal disposition

Group size for this study is summarized in Table 2.2. Samples scanned for microCT were also used for histology. No infections or neurological impairment was detected in any rabbit. Three of the 92 rabbits died immediately after surgery, two with implanted PLGA-capped scaffolds and one with a fast-PA-capped scaffold. One of the 1-week fast-PA-capped scaffold specimens was damaged during histological preparation and removed from the study.

Table 2.2. Summary of Group Size.

Scaffold Cap	Initial Group Size	Morbidity & Mortality	Final Group Size		
			1 week	3 weeks	8 weeks
Open	18	0	6	6	6
Closed	18	0	6	6	6
PLGA	19	2	6	6	5
Slow-PA	18	0	6	6	6
Fast-PA	19	2	5	6	6

2.3.3 Bone formation within scaffolds

Bone formation in the scaffolds was analyzed by microCT and histomorphometry. Representative microCT images at 8 weeks of healing for each scaffold design are shown in Figure 2.3. The images show bone within the scaffolds that is contiguous with the surrounding parietal bone. The polymer caps of the scaffolds are not visible in this analysis.

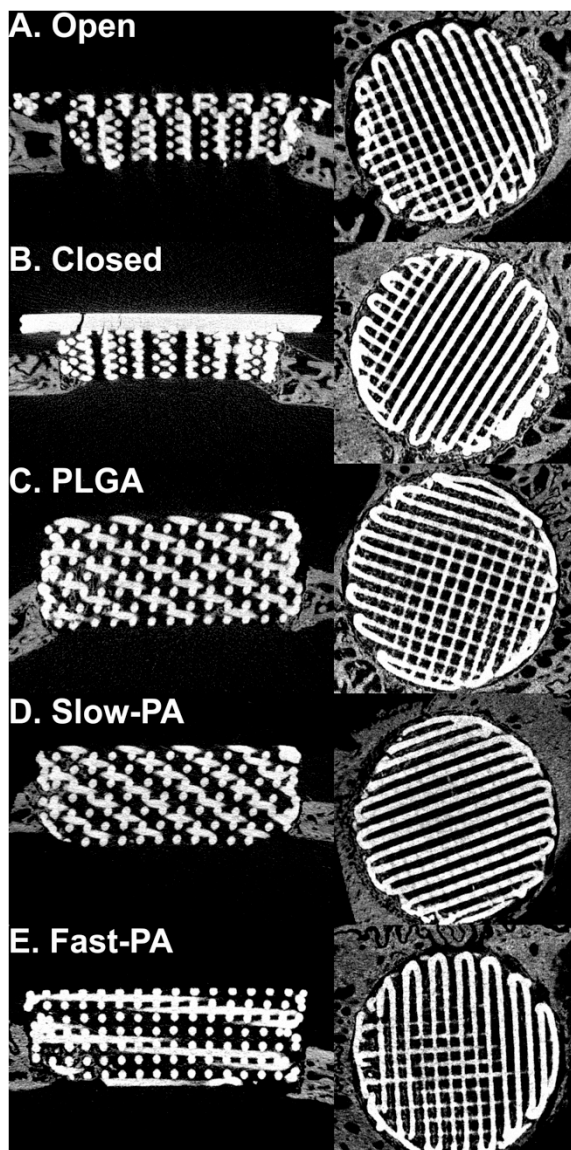


Figure 2.3. MicroCT scans of scaffolds 8 weeks post-surgery with open (A), closed (B), PLGA (C), slow-PA (D), and fast-PA (E) capped scaffolds. Calvaria and new bone growth within the scaffold are grey while the scaffold contrasts white.

Representative histological cross-sections of the scaffolds are shown in Figure 2.4. Bone was evident in all scaffold configurations and appeared to

increase in amount over time. Further, the bone appeared contiguous with the parietal bone indicating that bone formation was occurring by osteo-conduction, as would be expected for the HA-TCP scaffold.

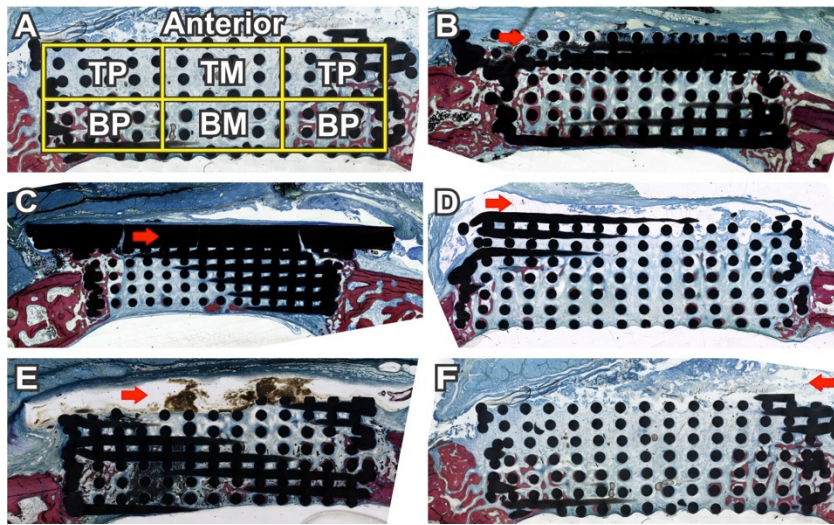


Figure 2.4. (A) Each histological specimen was divided into 6 zones to determine regional differences in cell density and bone area such that zones labeled T, B, P, and M indicate top, bottom, peripheral, and middle regions, respectively. Stained 3-week post-surgery specimens (mineralized tissue is red and soft tissues is blue) from (B) an open scaffold, (C) closed capped, (D) PLGA capped, (E) slow-PA capped, and (F) fast-PA capped scaffolds are shown. The red arrow indicates the cap area for each scaffold.

The amount of mineralized tissue within each implanted scaffold was measured using microCT and histomorphometry (Figures 2.5A and B). The amount of mineralized tissue within the scaffold increased with healing time ($p < 0.001$). However, the cap composition had no apparent effect on the *total*

amount of mineralized tissue within the scaffolds. Similarly, no differences in mineralized tissue density were detected between the different scaffold configurations.

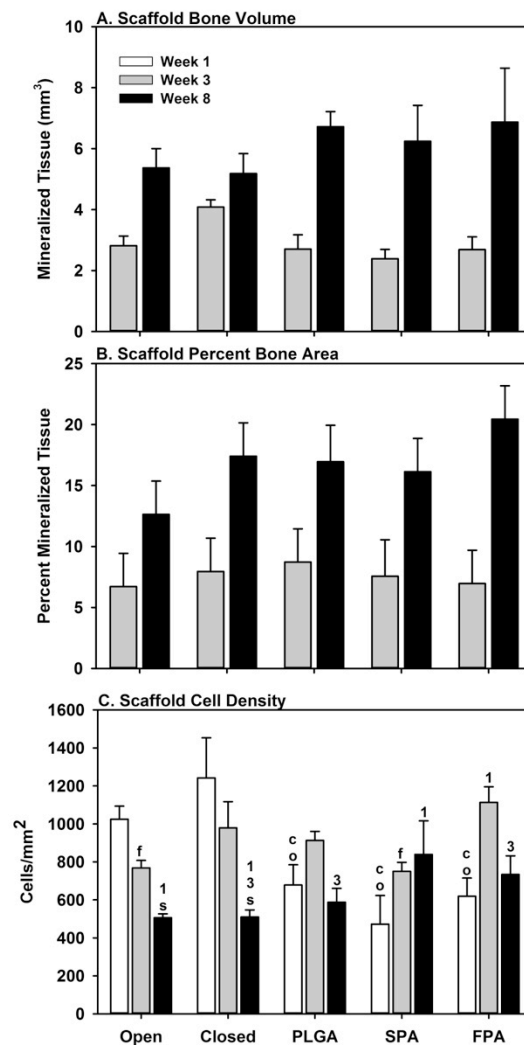


Figure 2.5. Bone formation and cellular infiltration (mean + standard error) were measured in each scaffold as (A) bone volume by microCT analysis, (B) percentage of bone in available area by histomorphometry, and (C) cell density

using histological specimens. Cell density values within a scaffold configuration that were significantly different from the 1 or 3 week values are denoted with a 1 or 3, respectively. Cell density values within a time point that were significantly different from another scaffold configuration are denoted with an o, c, p, s, or f to indicate a significant difference from the open, closed, PLGA, slow-PA, and fast-PA capped scaffolds, respectively.

2.3.4 Cell densities within scaffolds

The caps were designed to prevent inflammation-related cells and granulation tissue that may inhibit or limit bone regeneration from migrating into the scaffold. As an initial assessment of cap effectiveness at isolating the regeneration site, cell numbers were counted within the scaffolds and normalized to area (cell density). Patterns in cell densities were observed between time points within each scaffold configuration (Figure 2.5C). Within the open scaffolds and closed-capped scaffolds, cell density declined with time after surgery. However, cell densities in the polymer-capped scaffolds peaked at 3 weeks for the PLGA-capped and fast-PA-capped scaffolds and at 8 weeks for the slow-PA-capped scaffold.

A 2-way ANOVA using scaffold configuration and time after surgery as independent variables and cell density as the dependent variable was performed. Independent of scaffold configuration, cell density at 8 weeks was lower than at 1 or 3 weeks ($p = 0.016$ and $p < 0.001$, respectively) but no difference between the 1 and 3 week time points was found. Independent of time after surgery,

differences in cell density were only found between the closed-capped scaffolds (mean 910 cells/mm²) and the slow-PA-capped and PLGA-capped scaffolds (means: 687 and 726 cells/mm²; p value: 0.015 and p = 0.043, respectively).

Differences in cell densities between scaffold configuration and time after surgery also were observed (p < 0.001). After 1 week of healing, cell density in the scaffolds with polymer caps (PLGA, slow-PA, and fast-PA) had significantly lower cell density than the closed-capped scaffold group (p ≤ 0.007). The slow-PA-capped scaffolds also had a lower cell density for the entire scaffold than the open scaffolds (p = 0.009). After 3 weeks of healing, only the fast-PA-capped scaffolds had a significantly higher cell density than the slow-PA-capped and open scaffolds (p ≤ 0.006). After 8 weeks of healing, no differences in cell density for the entire scaffold were detected between scaffold configurations.

Cell densities appeared to decrease over time in the open scaffolds and closed-capped scaffolds and increased over time for the polymer-capped scaffolds (Figure 2.5C). These data may reflect how the scaffolds fit into the trephine defect as the curvature of the skull did not match the flat surface of the scaffolds. Thus, the rim of the scaffold cap was never in complete contact with the skull. The polymer caps may have swelled in the aqueous environment to help to provide a better seal between the cap and skull, which was reflected in the overall lower cell densities for the PLGA-capped and slow-PA-capped scaffolds. The reduced number of cells at 1 week in the polymer-capped scaffolds had no negative effect on total bone formation.

The closed-capped scaffolds had the highest cell density across all time points examined which may reflect the osteoconductive properties of the HA-TCP scaffold material and cell migration along that cap surface. In contrast, the PLGA-capped and slow-PA-capped scaffolds had lower cell densities across all time points, suggesting that the polymers were better physical or physical-chemical barriers than solid HA-TCP, potentially due to swelling as discussed earlier. The rapid degradation of the fast-PA-scaffold may have enabled greater cell migration into the scaffold region at later time points. Despite the variations in cell density, the amount of bone within the scaffold was similar between the different scaffold configuration at the 3 or 8 week time points and similar to previous results using HA-TCP scaffolds.^{30, 34} This result suggests that cell density is not a predictor of subsequent bone formation. The cap material may alter the relative number of osteoprogenitor cells within the scaffold relative to other cell types.

2.3.5 Regional bone and cell densities within scaffolds

To measure local effects of the SAPAEs on bone formation and cell density, digital images of the scaffold histological sections were divided into 6 zones: top and bottom of the middle and periphery (Figure 2.4 A). Cell number and mineralized tissue (bone) area were quantified within the six zones of each specimen (see Figure 2.4). These data were combined to measure cell densities and percent bone area within different regions of the scaffold, specifically, the scaffold periphery (top right, top left, bottom right, and bottom left zones), scaffold

middle (top middle and bottom middle zones), scaffold top (top right, middle, and left zones), and scaffold bottom (bottom right, middle, and left zones). Cell densities were determined for each scaffold configuration at 1, 3, and 8 weeks after implantation but bone areas were determined only at 3 and 8 weeks, since no new bone was evident after 1 week.

Independent of scaffold configuration, more mineralized tissue (bone) was present in scaffold periphery, middle, and bottom regions at 8 weeks than at 3 weeks ($p \leq 0.007$, data not shown). However, in the top region, there was significantly less mineralized tissue at 8 weeks in the open scaffolds as compared to all other scaffold configurations ($p < 0.05$; Figure 2.6) and the amount present was similar to that at 3 weeks for the open scaffold ($p = 0.75$). The amount of new bone in the top region of the slow-PA-capped scaffolds was not significantly different between the 3 and 8 week time points, though the difference did approach significance ($p = 0.06$). The fast-PA-capped scaffolds exhibited the greatest increase in bone between the 3 and 8 week time points.

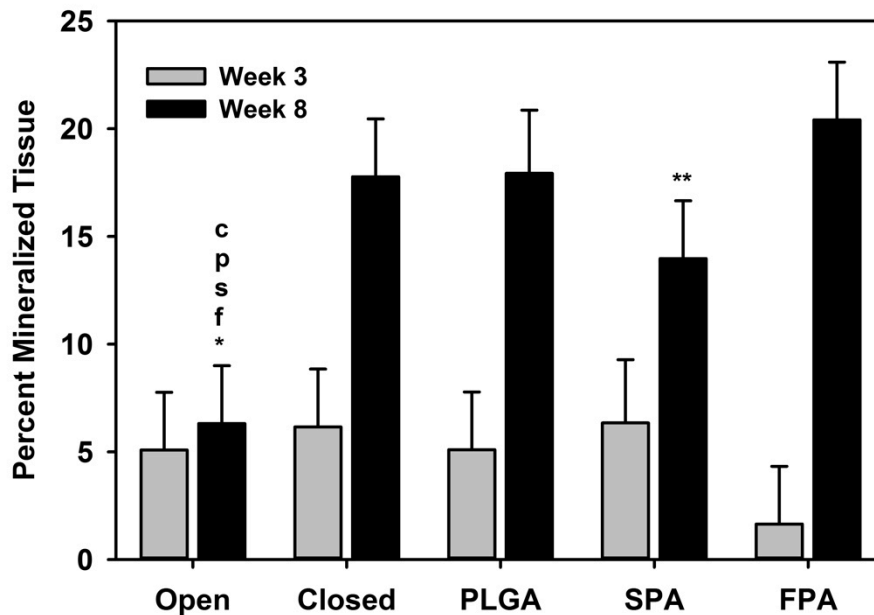


Figure 2.6. Histomorphometry was used to measure the percentage of bone (mean + standard error) in the top region of the different scaffold configurations. Values within a time point that are significantly different between scaffold configurations are denoted with an o, c, p, s, or f for open, closed, PLGA, slow-PA, and fast-PA capped scaffolds, respectively. Changes in percent bone area between 3 and 8 weeks was dependent upon scaffold configuration and was significantly greater for the closed, PLGA, and fast-PA capped scaffolds ($p \leq 0.004$), but not for the open scaffold (*, $p = 0.75$) or the slow-PA capped scaffold (**, $p = 0.06$).

Cell densities within scaffold regions were compared between scaffold configurations and time after surgery to determine if cap composition had any local effects on cell density (Figure 2.7). Significant interactions for cell density

between time after surgery and scaffold configuration were detected for each region ($p < 0.001$). Cell density declined with time in the open and closed-capped scaffolds. In contrast, cell densities increased over time in the slow and fast-PA-capped scaffolds. Cell densities in the peripheral and middle regions were similar to the bottom region values for the open and closed-capped scaffolds and to the top region values for the polymer capped scaffolds (data not shown).

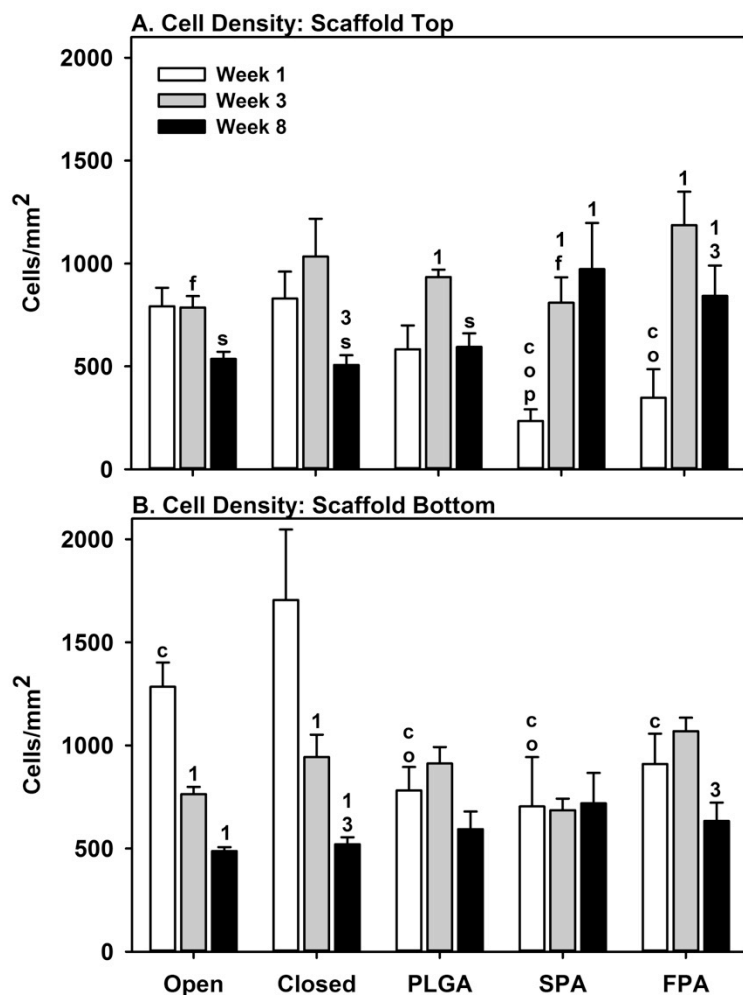


Figure 2.7. Cell density (mean + standard error) was measured in the (A) top and (B) bottom regions of the different scaffold configurations. Cell density values within a scaffold configuration that were significantly different from the 1 or 3 week values are denoted with a 1 or 3, respectively. Cell density values within a time point that were significantly different from another scaffold configuration are denoted with an o, c, p, s, or f to indicate a significant difference from the open, closed, PLGA, slow-PA, and fast-PA capped scaffolds, respectively.

The regional analysis showed that the amount of bone within the top region of the open scaffold was significantly less than all other scaffold configuration after 8 weeks of healing (Figure 2.6). This observation supports the hypothesis that unabated soft tissue ingrowth into the scaffold will limit bone formation. In contrast, cell densities between the open scaffolds and closed-capped scaffolds in the top region were similar, yet the bone formation responses were significantly different (Figures 2.5 and 2.6A). This supports a model in which the osteoconductive properties of the HA-TCP in the closed-capped scaffold facilitated osteoprogenitor cell migration along the surface of the cap to increase the number of osteoprogenitor cells, which lead to more localized bone formation in the top region of the closed-capped scaffolds as compared to the open scaffolds. Importantly, the slow-PA and fast-PA capped scaffolds did promote significantly more bone formation in the top region of the scaffolds than the control open scaffolds, indicating that the SAPAE polymers can be used for guided bone regeneration barriers.

Cell density in the bottom region of the polymer-capped scaffolds did not vary over time (except for 3 vs. 8 weeks in the fast-PA capped scaffolds). In contrast, cell densities in the top region of the SAPAE-capped scaffolds increased with time and appeared to be inversely correlated with polymer degradation (Figures 2.1 and 2.6). These observations indicate that the local cellular milieu within top region of the scaffold did respond to the SAPAE polymers.

2.3.6 Host inflammatory response

In addition to providing a potential physical barrier, the slow-PA and fast-PA caps may also reduce localized inflammation. This effect was qualitatively assessed by examining the inflammatory response in the soft tissues covering each scaffold (Figure 2.8). Void spaces were evident in the cap region of the polymer-capped scaffolds that likely represent the space occupied by the polymer cap, which dissolved during histological processing. The open and closed scaffolds made only with biocompatible HA-TCP showed little histological evidence of inflammation at all time points examined (Figure 2.8A, open scaffold not shown). In contrast, apparent lymphocytic infiltration above the PLGA-capped scaffold that also involved the overlying muscle was evident even after 8 weeks (Figure 2.8B). Voids in the cap region of the PLGA-capped scaffolds were evident at 1 and 3 weeks, suggesting that the PLGA had not completely degraded after 3 weeks. The host response to the slow-PA-capped scaffold appeared different (Figure 2.8C). Slow-PA polymer remnants were evident in the histological sections after 1 week and voids in the cap region of the scaffold indicated that the slow-PA was still present even at 3 weeks, but not by 8 weeks. A robust cellular infiltration above the slow-PA cap was evident at 1 and 3 weeks. However, the cellular infiltration did not significantly invade the overlying muscle suggesting that this potential inflammatory response was quelled. In contrast, little cellular infiltration above the fast-PA-capped scaffolds was evident (Figure 2.8D). Voids in the cap region were evident at 1 week but not by 3 weeks, suggesting that fast-PA cap had almost fully degraded by 3 weeks. For the open

scaffolds (not shown), closed-capped, slow-PA-capped, and fast-PA-capped scaffolds, a prominent, fibrous cell layer adjacent to the HA-TCP scaffold was evident at 8 weeks that was absent or not as well developed in the PLGA-capped scaffolds.

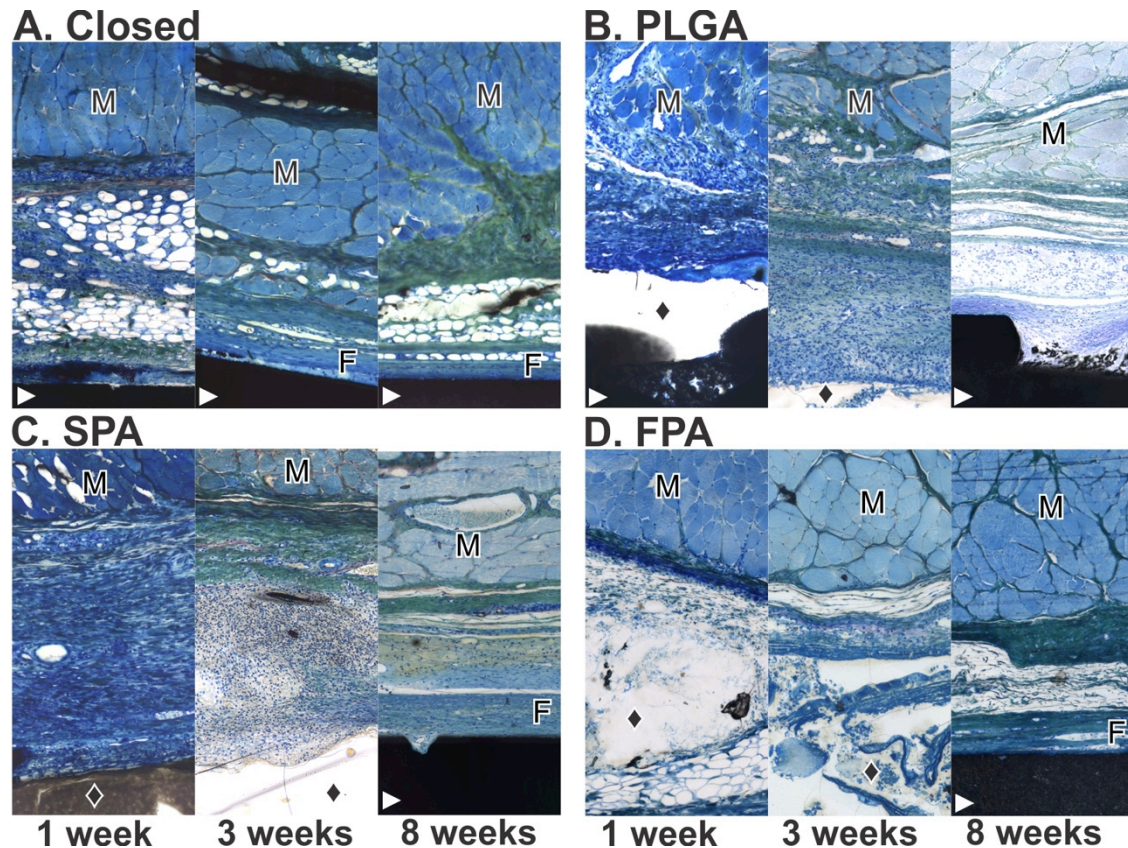


Figure 2.8. Shown are regions-of-interest located between the scaffold and overlying muscle (M). The ceramic scaffold material is denoted with a white arrowhead and the polymer caps or the voids left after histological processing dissolved the polymer are denoted with a diamond. The fibrous cell layer above the scaffold is denoted with an “F”. An exuberant inflammatory response is apparent at 1, 3, and 8 weeks in the PLGA and at 1 and 3 weeks in the slow-PA capped scaffolds, though the inflammatory response did not appear to involve the muscle in the slow-PA capped scaffolds. Little or no inflammatory response

was apparent in the open scaffold (not shown), closed, or fast-PA capped scaffolds.

Differences in the host inflammatory response to the various scaffold configurations were assessed by qualitative scoring of the inflammatory response (Figure 2.9). No significant interaction was found between time after surgery and scaffold configuration. However, independent of scaffold configuration, inflammation scores significantly decreased with time after surgery ($p \leq 0.002$). Also, differences in the host inflammatory response to the scaffold configurations were found independent of time after surgery. The PLGA-capped scaffolds had the highest inflammation scores across all time points (5.1 ± 0.5 , mean \pm standard error) in comparison to all other scaffold configurations ($p \leq 0.006$). The fast-PA-capped scaffolds had the lowest mean inflammation score across all time points (2.0 ± 0.4).

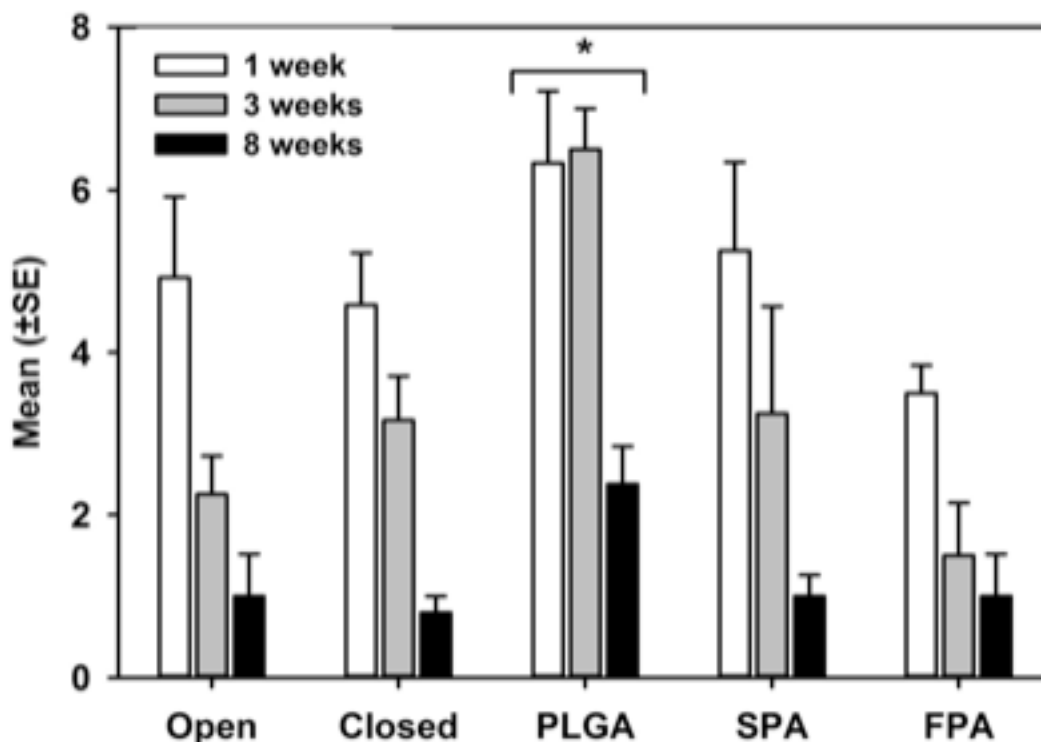


Figure 2.9. Histology specimens were scored for apparent inflammation (mean + standard error) using a 9-point scale (Table 2.1), with 9 indicating severe inflammation. Independent of time after surgery, the PLGA-capped scaffolds had a significantly higher inflammation score than all other scaffolds (*, $p \leq 0.006$).

The anti-inflammatory effect of the SAPAE polymers was evident in the histological analysis (Figures 2.8 and 2.9). An exuberant inflammatory response was associated with the PLGA-capped scaffolds that involved the overlying muscle, was evident even 8 weeks after surgery, and was consistent with *in vivo* responses to PLGA.³⁵⁻³⁷ In contrast, the inflammatory responses to the SAPAE caps were consistent with the *in vitro* degradation profiles of the fast and slow-PA

polymers (Figure 2.2). The inflammatory response present after 3 weeks in the rabbits treated with the slow-PA-capped scaffolds was resolved by 8 weeks, corresponding to the *in vitro* degradation profile of the slow SAPAE beginning after 4 weeks of *in vitro* incubation. The fast-PA begins to degrade immediately *in vitro* and provided for near linear release kinetics of salicylic acid that appeared sufficient to inhibit inflammation *in vivo* even at the earliest time point examined. The SAPAE caps provided a therapeutic amount of anti-inflammatory salicylic acid to reduce inflammation in the overlying soft tissue but which did not significantly inhibit bone formation.

2.4 Conclusions

Our analysis indicates that use of the SAPAE polymers in conjunction with an osteogenic scaffold can be a useful guided bone regeneration device.³⁸ No negative effect of either SAPAE on bone formation was found in this model. The SAPAE polymers degrade *in vivo* and therefore do not require additional procedures to remove, as would a PTFE membrane. The anti-inflammatory SA released by the SAPAE would likely help reduce soft tissue swelling and pain at the surgery site which would provide an additional benefit. However, additional tests are required to optimize the use of these novel devices. Methods for preventing gaps between the edge of the device and the underlying bone must be developed. Such methods could involve better manufacturing procedures to insure a better fit or procedures to glue the device in place. Additional experiments are needed to understand the relationship between polymer

degradation and bone formation rates within the scaffold such that polymer degradation would coincide with maximal bone formation in the scaffold. Current studies are evaluating scaffolds with layered caps incorporating both slow and fast-PA to obtain the early release of SA from the fast-PA with the prolonged barrier properties of the fast-PA.

2.5 References

1. Retzepi M, Donos N. Guided Bone Regeneration: biological principle and therapeutic applications. *Clinical oral implants research*. 2010;21(6):567-76.
2. Stal S, Tjelmeland K, Hicks J, Bhatia N, Eppley B, Hollier L. Compartmentalized bone regeneration of cranial defects with biodegradable barriers: an animal model. *The Journal of craniofacial surgery*. 2001;12(1):41-7.
3. Polimeni G, Koo KT, Pringle GA, Agelan A, Safadi FF, Wikesjo UM. Histopathological observations of a polylactic acid-based device intended for guided bone/tissue regeneration. *Clinical implant dentistry and related research*. 2008;10(2):99-105.
4. Behring J, Junker R, Walboomers XF, Chessnut B, Jansen JA. Toward guided tissue and bone regeneration: morphology, attachment, proliferation, and migration of cells cultured on collagen barrier membranes. A systematic review. *Odontology*. 2008;96(1):1-11.
5. Erdmann L, Uhrich KE. Synthesis and degradation characteristics of salicylic acid-derived poly(anhydride-esters). *Biomaterials*. 2000;21(19):1941-6.
6. Schmeltzer R, Schmalenberg K, Uhrich K. Synthesis and cytotoxicity of salicylate-based poly(anhydride-esters). *Biomacromolecules*. 2005;72A(6):354-62.
7. Prudencio A, Schmeltzer RC, Uhrich KE. Effect of linker structure on salicylic acid-derived poly(anhydride-esters). *Macromolecules*. 2005;38(16):6895-901.

8. Whitaker-Brothers K, Uhrich K. Poly(anhydride-ester) fibers: Role of copolymer composition on hydrolytic degradation and mechanical properties. *J Biomed Mater Res*. 2004;70A:309-18.
9. Cottrell J, O'Connor JP. Effect of non-steroidal anti-inflammatory drugs on bone healing. *Pharmaceuticals*. 2010;3:1668-93.
10. O'Connor JP, Lysz T. Celecoxib, NSAIDs and the skeleton. *Drugs Today (Barc)*. 2008;44(9):693-709.
11. Simon AM, Manigrasso MB, O'Connor JP. Cyclo-oxygenase 2 function is essential for bone fracture healing. *Journal of bone and mineral research : the official journal of the American Society for Bone and Mineral Research*. 2002;17(6):963-76.
12. Goodman SB, Ma T, Mitsunaga L, Miyanishi K, Genovese MC, Smith RL. Temporal effects of a COX-2-selective NSAID on bone ingrowth. *Journal of biomedical materials research Part A*. 2005;72(3):279-87.
13. Pavlou G, Kyrkos M, Tzialogiannis E, Korres N, Tsiridis E. Pharmacological treatment of heterotopic ossification following hip surgery: an update. *Expert opinion on pharmacotherapy*. 2012;13(5):619-22.
14. McLaren AC. Prophylaxis with indomethacin for heterotopic bone after open reduction of fractures of the acetabulum. *Journal of Bone and Joint Surgery*. 1990;72-A(2):245-7.
15. Burd TA, Lowry KJ, Anglen JO. Indomethacin compared with localized irradiation for the prevention of heterotopic ossification following surgical treatment of acetabular fractures. *Journal of Bone and Joint Surgery*. 2001;83-A(12):1783-8.
16. Giannoudis PV, MacDonald DA, Matthews SJ, Smith RM, Furlong AJ, De Boer P. Nonunion of the femoral diaphysis: the influence of reaming and non-steroidal anti-inflammatory drugs. *Journal of Bone and Joint Surgery British Volume*. 2000;82-B:655-8.
17. Burd TA, Hughes MS, Anglen JO. Heterotopic ossification prophylaxis with indomethacin increases the risk of long-bone nonunion. *Journal of Bone and Joint Surgery British Volume*. 2003;85-B(5):700-5.

18. Karakawa A, Sano T, Amano H, Yamada S. Inhibitory Mechanism of Non-steroidal Anti-inflammatory Drugs on Osteoclast Differentiation and Activation. *Journal of Oral Biosciences*. 2010;52(2):119-24.
19. Raisz LG. Prostaglandins and bone: physiology and pathophysiology. *Osteoarthritis Cartilage*. 1999;7(4):419-21.
20. Cochran DL. Inflammation and Bone Loss in Periodontal Disease. *Journal of Periodontology*. 2008;79(8s):1569-76.
21. Thomas MV, Puleo DA. Infection, inflammation, and bone regeneration: a paradoxical relationship. *Journal of dental research*. 2011;90(9):1052-61.
22. Bichara J, Greenwell H, Drisko C, Wittwer JW, Vest TM, Yancey J, et al. The effect of postsurgical naproxen and a bioabsorbable membrane on osseous healing in intrabony defects. *J Periodontol*. 1999;70(8):869-77.
23. Simon AM, O'Connor JP. Dose and time-dependent effects of cyclooxygenase-2 inhibition on fracture-healing. *The Journal of bone and joint surgery American volume*. 2007;89(3):500-11.
24. Schmeltzer RC, Johnson M, Griffin J, Uhrich K. Comparison of salicylate-based poly(anhydride-esters) formed via melt-condensation versus solution polymerization. *Journal of biomaterials science Polymer edition*. 2008;19(10):1295-306.
25. Gerstenfeld LC, Thiede M, Seibert K, Mielke C, Phippard D, Svagr B, et al. Differential inhibition of fracture healing by non-selective and cyclooxygenase-2 selective non-steroidal anti-inflammatory drugs. *Journal of orthopaedic research : official publication of the Orthopaedic Research Society*. 2003;21(4):670-5.
26. Reynolds MA, Prudencio A, Aichelmann-Reidy ME, Woodward K, Uhrich KE. Non-steroidal anti-inflammatory drug (NSAID)-derived poly(anhydride-esters) in bone and periodontal regeneration. *Current drug delivery*. 2007;4(3):233-9.
27. Erdmann L, Macedo B, Uhrich KE. Degradable poly(anhydride ester) implants: effects of localized salicylic acid release on bone. *Biomaterials*. 2000;21(24):2507-12.

28. Harten RD, Svach DJ, Schmeltzer R, Uhrich KE. Salicylic acid-derived poly(anhydride-esters) inhibit bone resorption and formation in vivo. *Journal of biomedical materials research Part A*. 2005;72(4):354-62.
29. Smay J, Cesarano III J, Lewis J. Colloidal Inks for Directed Assembly of 3-D Periodic Structures. *Langmuir*. 2002;18(14):5429-37.
30. Simon JL, Michna S, Lewis JA, Rekow ED, Thompson VP, Smay JE, et al. In vivo bone response to 3D periodic hydroxyapatite scaffolds assembled by direct ink writing. *Journal of biomedical materials research Part A*. 2007;83(3):747-58.
31. Anastasiou TJ, Uhrich KE. Novel Polyanhydrides with Enhanced Thermal and Solubility Properties. *Macromolecules*. 2000;33(17):6217-21.
32. Baron R, Vigney A, Neff L, Silvergate A, Santa Maria A. Processing of undecalcified bone specimens for bone histomorphometry. In: Recker RR, editor. *Bone Histomorphometry: Techniques and Interpretation*. Boca Raton: CRC Press, Inc.; 1983. p. 13-35.
33. Maniatopoulos C, Rodriguez A, Deporter DA, Melcher AH. An improved method for preparing histological sections of metallic implants. *Int J Oral Maxillofac Implants*. 1986;1:31-7.
34. Simon JL, Rekow ED, Thompson VP, Beam H, Ricci JL, Parsons JR. MicroCT analysis of hydroxyapatite bone repair scaffolds created via three-dimensional printing for evaluating the effects of scaffold architecture on bone ingrowth. *Journal of biomedical materials research Part A*. 2008;85(2):371-7.
35. Ibim SE, Uhrich KE, Attawia M, Shastri VR, El-Amin SF, Bronson R, et al. Preliminary in vivo report on the osteocompatibility of poly(anhydride-co-imides) evaluated in a tibial model. *J Biomed Mater Res*. 1998;43(4):374-9.
36. Ibim SM, Uhrich KE, Bronson R, El-Amin SF, Langer RS, Laurencin CT. Poly(anhydride-co-imides): in vivo biocompatibility in a rat model. *Biomaterials*. 1998;19(10):941-51.
37. Tiainen J, Soini Y, Suokas E, Veiranto M, Tormala P, Waris T, et al. Tissue reactions to bioabsorbable ciprofloxacin-releasing polylactide-

polyglycolide 80/20 screws in rabbits' cranial bone. Journal of materials science Materials in medicine. 2006;17(12):1315-22.

38. Mitchell A, Kim B, Cottrell J, Snyder S, Wiltek L, Ricci J, Uhrich KE, O'Connor J. 2013. Development of a guided bone regeneration device using salicylic acid-poly(anhydride-ester) polymers and osteoconductive scaffolds. J Biomed Mater Res Part A 2013:accepted, sections of the chapter are from the pre-peer reviewed version of this article.

3. POLYMERIC BONE WRAPS TO PREVENT HETEROTOPIC OSSIFICATION

3.1 Introduction

Bone grafting can accelerate bone healing in patients with large bone defects or impaired bone healing,. Bone grafting is the second most common procedure performed in the United States with ~ 500,000 procedures performed annually.¹ Autologous bone is the bone graft gold standard, however, it requires a second surgery to harvest the bone, causing donor site morbidity and increased risk of infection.² Allografts nullify these problems but also come with a risk of disease transmission.³ In addition, autograft and allograft availability is limited;³ therefore, other means of promoting bone growth have been explored.⁴

In recent decades, bone morphogenetic proteins (BMPs) have been widely studied and utilized to induce bone formation. The FDA has approved bone regeneration devices containing BMP-2.⁵ Collagen sponges are a common matrix for delivering BMPs, but they exhibit a burst release of the protein.⁶ Various synthetic polymers have been explored as collagen replacements but they still have problems controlling release rate and obtaining physiologically relevant loading.^{5, 7} This lack of control over BMP delivery has causes adverse events in 10-50 % of spinal fusions using BMP-2.⁸

One prevalent problem with BMP-2 therapy is heterotopic ossification (HO), the mineralized bone tissue formation in areas typically occupied by soft tissue.⁸ HO can cause pain and restrict range of movement. Non-steroidal anti-

inflammatory drugs (NSAIDs) are the preferred HO prevention method.⁹⁻¹² However, oral administration of NSAIDs (typically 100 mg/day indomethacin for 1-3 weeks)¹³ causes side effects such as intestinal bleeding, increased bleeding at surgery sites, increased incidence of loose prostheses that limit the feasibility of this treatment.^{11, 14}

The Urich group has previously incorporated salicylic acid (SA), an NSAID, into the backbone of a biodegradable poly(anhydride-ester) (SAPAE).¹⁵⁻¹⁷ SAPAEs can be fabricated into devices for localized, controlled SA release at the implantation site, thereby avoiding systemic side effects.¹⁸ Combining an SAPAE device with BMP-2 delivery may promote bone regeneration while inhibiting HO. In addition, the SAPAE polymeric properties permit their formulation into a physical barrier which can inhibit BMP-2 diffusion from the bone defect site, thus potentially limiting BMP-2 associated side effects.

To evaluate the bone regeneration potential of such a device, polycaprolactone (PCL) and two SAPAEs with different degradation rates were blended at multiple ratios. These blends were electrospun to obtain flexible fibrous mats. PCL was chosen as it has been used previously to increase elasticity in polymer fibers¹⁹ and has been widely studied in electrospun materials. After electrospinning, the fiber diameters, porosity, tensile properties, and *in vitro drug release* characteristics of fibrous mats were determined. These mats were then developed into bone wraps and evaluated *in vivo* for their ability to control bone growth in the presence of BMP-2.

3.2 Materials and Methods

3.2.1 Materials

All chemicals and reagents were purchased from Sigma-Aldrich (Milwaukee, WI) and used as received.

3.2.2 Polymer synthesis and characterization

SAPAEs (Figure 3.1) were synthesized according to previously described methods.^{15, 20, 21} In short, SA was dissolved in tetrahydrofuran (THF) and pyridine. Adipoyl chloride (for the SAA polymer) or diethylmalonyl chloride (for the SADEM polymer) (1 eq) was dissolved in THF and added drop-wise, forming a white suspension. The reaction mixture was stirred overnight, quenched over water and acidified to pH 2 using concentrated hydrochloric acid. The precipitate was filtered, washed with water (3 x 250 mL), and dried *in vacuo* to yield the diacid. Diacid was activated in an excess of acetic anhydride at room temperature, concentrated, and polymerized via melt-condensation polymerization at 180 °C for 4-6 h at 160 rpm. The reaction was cooled to room temperature, dissolved in minimal (~ 10 mL) dichloromethane (DCM) and precipitated over diethyl ether (~ 500 mL). The solvent was decanted and the precipitate was dried *in vacuo* to yield a tan powder. The SAA polymer was characterized as follows: weight average molecular weight (M_w) = 13,400, polydispersity index (PDI) = 1.7, and glass transition temperature (T_g) = 46 °C. The SADEM polymer was characterized as follows M_w = 26,100, PDI = 1.4, and T_g = 70 °C.

Polycaprolactone (M_n 70,000-90,000) was purchased from Sigma-Aldrich (Milwaukee, WI) and used as received.

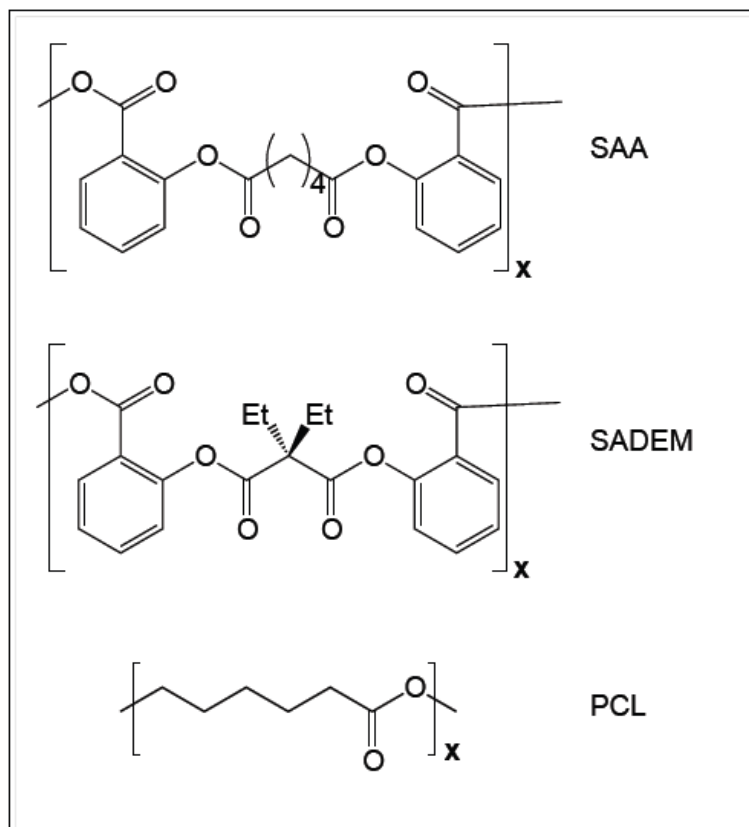


Figure 3.1. Bone wrap polymer structures.

3.2.3 Thermal analysis

DSC measurements were carried out on a TA Instrument Q200 to determine T_g s and melting temperatures (T_m). Samples (4–8 mg) were heated under nitrogen atmosphere to 200 °C at a heating rate of 10 °C/ min and cooled to 0 °C at a rate of 10 °C/min with a two-cycle minimum were performed. TA Instruments Universal Analysis 2000 software, version 4.5A, was used for data analysis. T_g s were calculated as half Cp extrapolated.

3.2.4 Electrospinning

Following synthesis and characterization, SAPAEs and PCL were placed in 20 mL glass scintillation vials and dissolved in DCM and dimethylformamide (DMF, 1:1 volume ratio) at the total weigh percents (w/v) outlined in Table 3.1. Polymers were transferred to a 10 mL syringe with a blunt 18 G stainless steel needle (Popper & Sons, Inc., New Hyde Park, NY). The syringe was placed in a syringe pump set to the flow rates described in Table 3.1. A collecting plate was covered in Reynolds non-stick foil and placed 15 cm from the needle tip. A negative voltage supply was attached to the collecting plate and set at 5 kV. A positive voltage supply was attached to the needle tip and set at 8-15 kV as required to maintain steady fiber extrusion from the needle. To obtain larger, more homogeneous fibrous mats, *in vivo* samples were spun onto a rotating mandrel covered in Reynolds non-stick foil; the charged collecting plate was placed behind the mandrel. Rotating the mandrel at 60 rpm did not lead to fiber alignment (as observed by SEM).

Table 3.1. Electrospinning Polymer Solutions and Flow Rates

% SAPAE	0	20	40	60	80	100
% PCL	100	80	60	40	20	0
Total Polymer Weight % (w/v)	12	15	20	25	35	75
Flow Rate (mL/hr)	5	5	5	5	4	3

3.2.5 Fiber characterization

Fiber morphology was observed on an AMRAY 1830I (AMRAY, INC.) scanning electron microscope. Samples were mounted on aluminum studs and coated with Au/Pd using a SCD 004 Sputter Coater (Bal-Tec, Liechtenstein). ImageJ (NIH) measurement tool determined fiber diameter based on scale bar pixel length. Average fiber diameter was determined from images taken from 4 areas of the sample with 25 fiber measurements per image for a total of 100 measurements per sample.

3.2.6 Porosity

Electrospun mat porosity (ε) was estimated using Equation 1,²² where ρ is density. Mat density was determined on a circular mat sample obtained by using a biopsy punch. Sample thickness was determined using digital calipers (Pro-max S225, Fred V Fowler Co., Newton, MA) and the sample mass was obtained to calculate sample density. PCL density was given by Sigma-Aldrich as 1.145 g/mL. SAPAE densities were determined by pressing polymer disks (13 mm diameter) using a hydraulic press (Carver Model M, Garfield, NJ). Polymer and mold were heated above the polymer T_g before applying force of 10,000 psi for 5 minutes. Polymer disk thickness and mass were determined to calculate density (1.24 g/mL and 1.21 g/mL for the SAA and SADEM polymers, respectively).

$$\varepsilon = \left(1 - \frac{\rho_{mat}}{(\text{PCL weight fraction})\rho_{PCL} + (\text{SAPAE weight fraction})\rho_{SAPAE}} \right) \cdot 100 \quad \text{Equation 1}$$

3.2.7 Mechanical testing

The electrospun mats were cut into dogbone shapes with a ~ 5 mm minimum width and subjected to uniaxial tensile loading at room temperature (EnduraTEC ELF 3200 dynamic mechanical analyzer, Bose Corp., Framingham, MA). Data collection was performed by WinTest software (Version 4.1, Bose Corp.). Sample minimum width and thickness were recorded before testing. Strain was ramped at 0.05 mm/s with an initial displacement of 5 mm between the clamp, and increased until device failure. Electrospun mats were tested both dry and after soaking in PBS for 30 minutes prior to loading to assess any effects initial wetting might have on the properties of the mat. This early time frame is relevant for mat handling during surgery.

With electrospun fibers, the Poisson coefficient is more dependent on the fiber orientation than on the bulk properties of the material.²³ Based on previous electrospun PCL fibers studies, stress was calculated using a Poisson coefficient of 0.45.²² The elastic moduli were determined from the slope of best-fit lines of the initial linear portion of the graphs.

3.2.8 *In vitro* drug release

Electrospun mats (40 x 11 mm) weighing 9-100 mg were rolled into a cylinder such that the cylinder walls were 2 mats thick, mimicking the *in vivo* conformation. A staple maintained the cylindrical shape. Samples were placed into 20 mL glass scintillation vials with 10 mL phosphate buffered saline (PBS, pH 7.4, Sigma-Aldrich). Samples were incubated at 37 °C with agitation at 60

rpm in a controlled environment incubator shaker (New Brunswick Scientific Co., Excella E25, Edison, NJ). All media was collected and replaced with fresh PBS (10 mL) at pre-designated time points for 4 weeks. Spent media was analyzed by UV spectrophotometry using a Perkin Elmer Lambda XLS spectrophotometer (Waltham, MA) to specifically monitor SA release. Measurements were obtained at $\lambda = 303$ nm, the maximum absorbance of SA that does not overlap with other polymer degradation products. Data were calculated against a calibration curve of absorbance values from standard solutions of known SA concentrations in PBS. Polymer remaining after 4 weeks was degraded with basic water (pH > 12) and remaining SA quantified to allow normalization of percent release.

3.2.9 Animal model

Bone wraps were cut from electrospun mats to the dimensions shown in Figure 3.2A. This wrap design was developed to allow fixation of the wrap underneath a custom-fabricated bone plate. The footprint of the plates is 24 x 5 mm with a 10 mm gap between both ends. The wrap's left-most portion (in Figure 3.2A) was fixed beneath the bone plate during surgery while the right-most portion was wound around the bone and threaded through the plate gap (Figure 3.2B). The extra 1 mm in wrap width, compared to the gap, increased friction between the wrap and the plate and prevented migration after implantation.

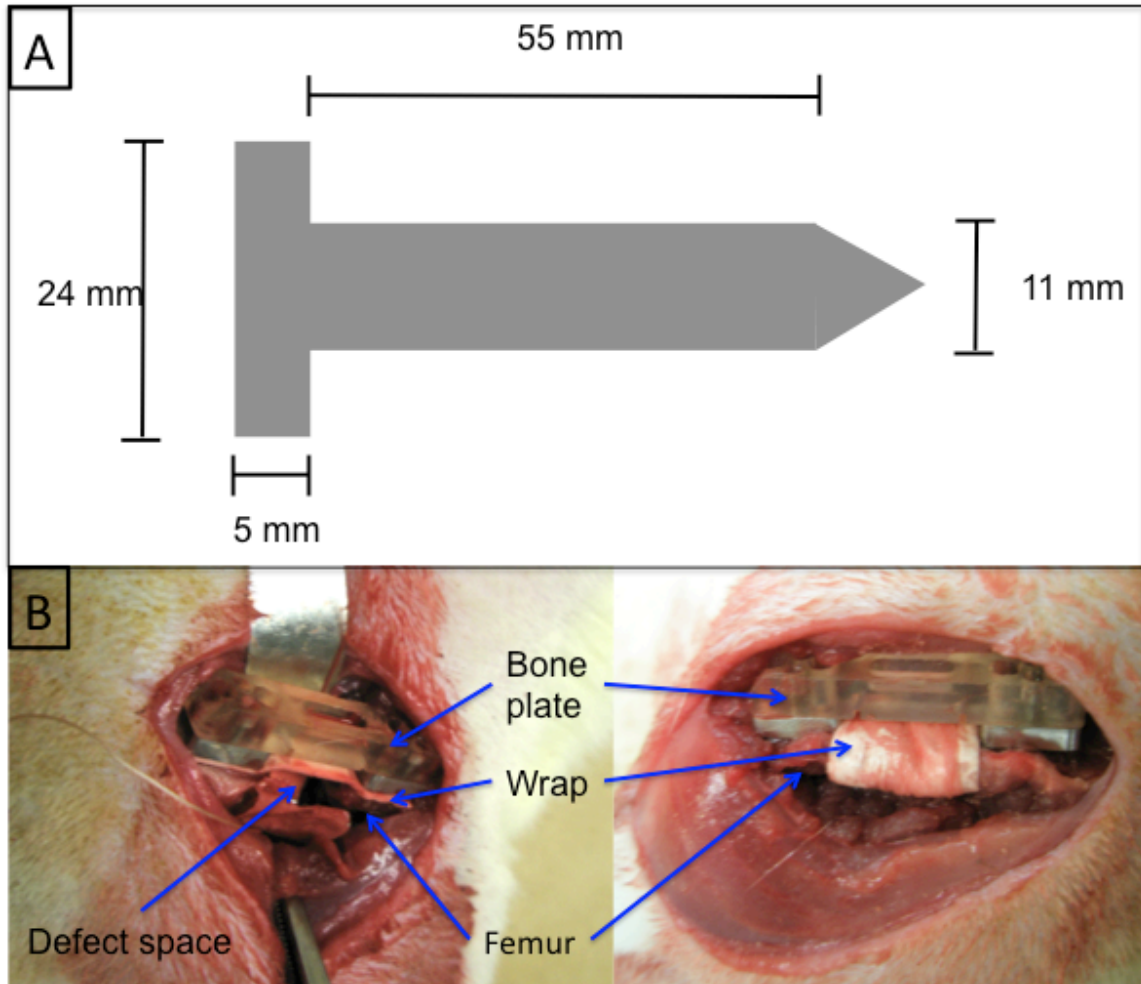


Figure 3.2. Bone wrap dimensions (A) and placement *in vivo* (B).

Male Sprague-Dawley rats weighing 400-450 g were purchased from Taconic Farms (Germantown, NY). Rats were anesthetized with a mixture of ketamine (60 mg/kg) and xylazine (10 mg/kg) by intraperitoneal injection. Additional “quarter” doses of ketamine-xylazine were administered as a booster, if necessary. After a surgical plane of anesthesia was induced, the right hind limb of each rat was shaved and prepared using standard aseptic technique that included a betadine scrub.

[Surgeries were performed by Ashley Mitchell and Sangeeta Subramanian, University of Medicine and Dentistry of New Jersey.]

After preparing the surgical site, the animal was then draped to expose only the right hind limb. A 4 cm incision was created on the lateral surface of the thigh, parallel with the femur. The vastus lateralis and biceps femoris were bluntly dissected to expose the femur. The muscle was retracted to expose the femur and the periosteum was scraped from the femur at the surgical site. A four-hole custom fabricated polyethylene bone plate was positioned on the anterolateral surface of the femur over the left-most portion of the electrospun wraps (Figure 3.2). Using the bone plate as a template, four holes were drilled through the wrap and femur. The wrap and plate were then secured by placing screws into the 4 holes just drilled. Taking care, the wrap was retracted away from femur before sawing. Using a sagittal saw, the femur was cut twice, first at the most distal site, and then at the more proximal site, to create a 5 mm mid-diaphyseal defect. A collagen sponge (15 x 15 x 2.75 mm) was hydrated with buffer (5 mM glutamate, 5 mM NaCl, 2.5 % glycine, 0.5 % sucrose, pH 4.5, 100 μ L) containing 0, 3.5, 12, or 24 μ g recombinant human BMP-2. The collagen sponge was then placed within the defect site and the bone wrap was wound around the sponge filled defect twice to ensure a secure seal. Extra bone wrap length was trimmed just past the bone plate on the second wrap. The wound was closed in layers using interrupted 4-0 resorbable sutures. Triple antibiotic ointment was applied to the wound. The rats were monitored until sternal and alert, and then returned to their cage. At 4 weeks post-surgery, rats were

anesthetized with a mixture of ketamine (60 mg/kg) and xylazine (10 mg/kg) by intraperitoneal injection. All animal procedures were approved by the UMDNJ-New Jersey Medical School Institutional Animal Care and Use Committee and followed NIH guidelines for the care and use of laboratory animals.

3.2.10 Radiography

Radiographs were taken immediately after surgery and weekly thereafter for 4 weeks using a Faxitron X-Ray MX-20 (Faxitron X-ray Corp., Tucson, AZ). Images were created by X-ray exposure to 35 kVp for 120 s.

3.3 Results and Discussion

3.3.1 Characterization of the electrospun mats

SAPAE homopolymer fibers shattered when removed from the collecting foil, and therefore, were not further characterized. The SEM images (Figure 3.3) show that the SAPAE:PCL blends resulted in well-formed, randomly aligned fibers with negligible beading. Image analysis was used to evaluate fiber diameters. Average fiber diameter ranged from 0.6-1 μm (Table 3.2). Neither SAPAE:PCL ratio, nor the use of SADEM rather than SAA, exhibited a noticeable effect on fiber diameter. Similarly, neither parameter affected mat porosity (Table 3.2); the average porosity was 74.5 %. This porosity compares well with previous literature, in which the typical electrospun PCL porosity is >70 %.^{24, 25}

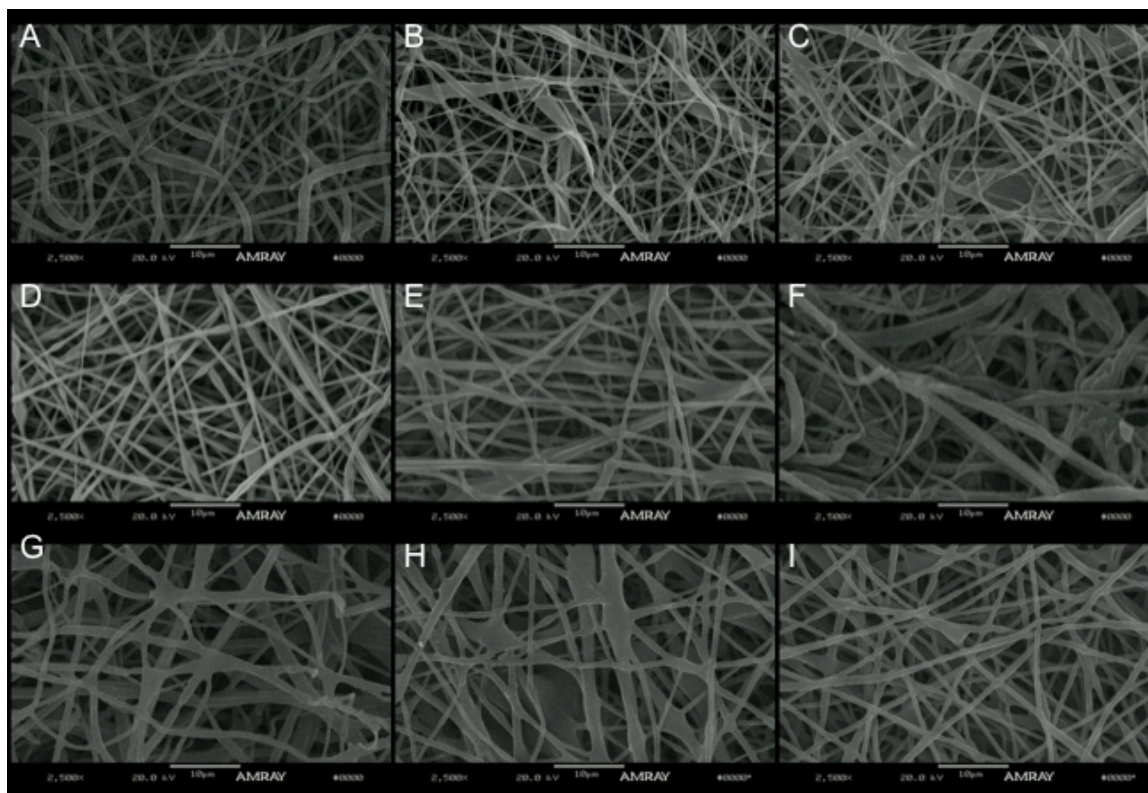


Figure 3.3. SEM images (2,500 x) of electrospun blends: 100 % PCL (a), 20 % SAA (b), 40 % SAA (c), 60 % SAA (d), 80 % SAA (e), 20 % SADEM (f), 40 % SADEM (g), 60 % SADEM (h), 80 % SADEM (i). Scale bars are equivalent to 10 μm .

Table 3.2. Average Fiber Diameter and Porosity of Electrospun Mats

Sample	Fiber Diameter (μm)	Porosity (%)
PCL	0.72 ± 0.20	74
20 % SAA	0.65 ± 0.25	71
20 % SADEM	0.75 ± 0.28	81
40 % SAA	0.60 ± 0.27	69
40 % SADEM	0.96 ± 0.42	75
60 % SAA	0.68 ± 0.17	82
60 % SADEM	0.85 ± 0.30	64
80 % SAA	0.88 ± 0.26	77
80 % SADEM	0.92 ± 0.29	77

To characterize their mechanical properties, polymer mats were subjected to uniaxial strain. Electrospun PCL mats elastic moduli range from 27.5 kPa²⁶ to 31 MPa²⁷ in literature. The elastic modulus for the 100% PCL mats was 40 ± 12 kPa. In this study, the elastic moduli increased as the SAPAE content increased (Figure 3.4). The 60 and 80 % SAA and 80% SADEM samples did not follow the trend of increasing stiffness. This effect is likely due to the tested sample thickness. The samples were very thin (< 0.1 mm) mats. Thin samples have a decreased ability to delocalize stress, meaning that defects in thin films are more likely to cause device failure at low stresses.²⁸ Decreased trendlines R^2 values used to determine the sample moduli support this theory. Soaking the mats in PBS for 30 minutes prior to tensile testing did not have a noticeable effect on the elastic moduli, therefore, mat mechanics are not expected to change during the implantation process.

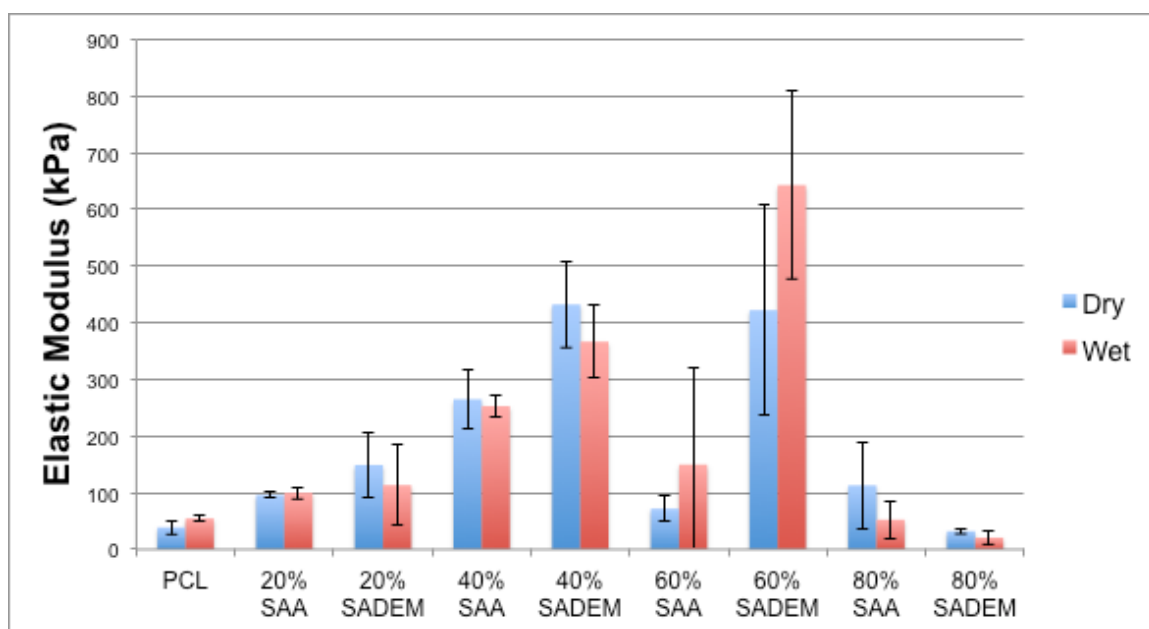


Figure 3.4. Elastic moduli of dry and wet electrospun mats.

3.3.2 *In vitro* drug release

For the *in vitro* drug release studies, polymer mats were cut and rolled to simulate the shape of the wrap *in vivo* (Figure 3.5), then placed in PBS (pH 7.4) at 37 °C to simulate physiological conditions. SA release from the wraps was monitored over 4 weeks by sampling the degradation media. An important finding during the *in vitro* degradation studies was that all of the polymer blends maintained their structural integrity throughout the 4 weeks (Figure 3.5). Polymer remaining after 4 weeks was degraded with basic water and remaining SA was quantified and used to normalize cumulative release.



Figure 3.5. All polymer wraps maintained their structure throughout 4 weeks of *in vitro* degradation (80 % SAA at 4 weeks shown).

All SAA blends released a majority of the loaded SA within the first week, with some samples releasing almost 50 % in the first day, and all released > 75 % within the first 3 days (Figure 3.6). After the first week, SA release significantly decreased (< 3 % SA release/week for all groups). Release profiles for all SAA blends were similar, with no correlation to SAA % in the blend. After 4 weeks, the 20 % SAA group had released 85.6 % SA, the 40 % SAA group had released 96.8 % SA, the 60 % SA group had released 92.5 % SA, and the 80 % SAA group had released 98.3 % SA.

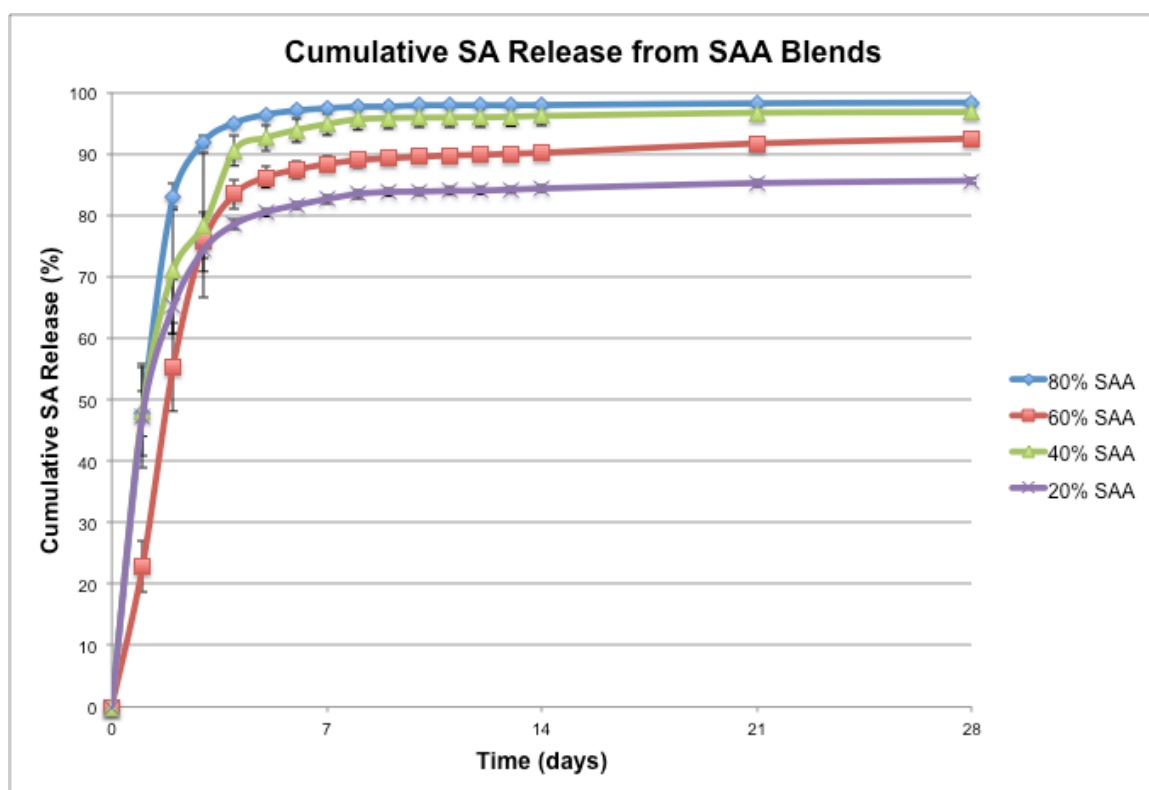


Figure 3.6. Cumulative SA release from SAA-containing electrospun mats.

The SADEM blends exhibited drastically different release profiles (Figure 3.7) than the SAA blends. In the first week, very little SA release was observed. This lag time correlates with previous studies indicating that the SADEM polymer has a much longer lag time before SA release than the SAA polymer blends.^{17, 29} The 20 % SADEM blend released at 0.5 %/day for the first 2 weeks, then at 1.8 %/day for the next 2 weeks for a cumulative 32.5 % release. The 40 % SADEM blend released at 0.2 %/day for 2 weeks then at 1.4 %/day for the next 2 weeks for a cumulative 21.5% release. The 60 % SADEM blend released at < 0.1 %/day for 2 weeks then at 0.7 %/day for the next 2 weeks for a cumulative 9.9% release. The 80 % SADEM blend released at 0.2 %/day for 10.5 days then at 1.7 %/day until day 28 for a cumulative 31% release.

Neither the SAA blends nor the SADEM blends exhibited a trend correlating to SAPAE weight percent. Differences mat thickness may account for the discrepancies between groups.

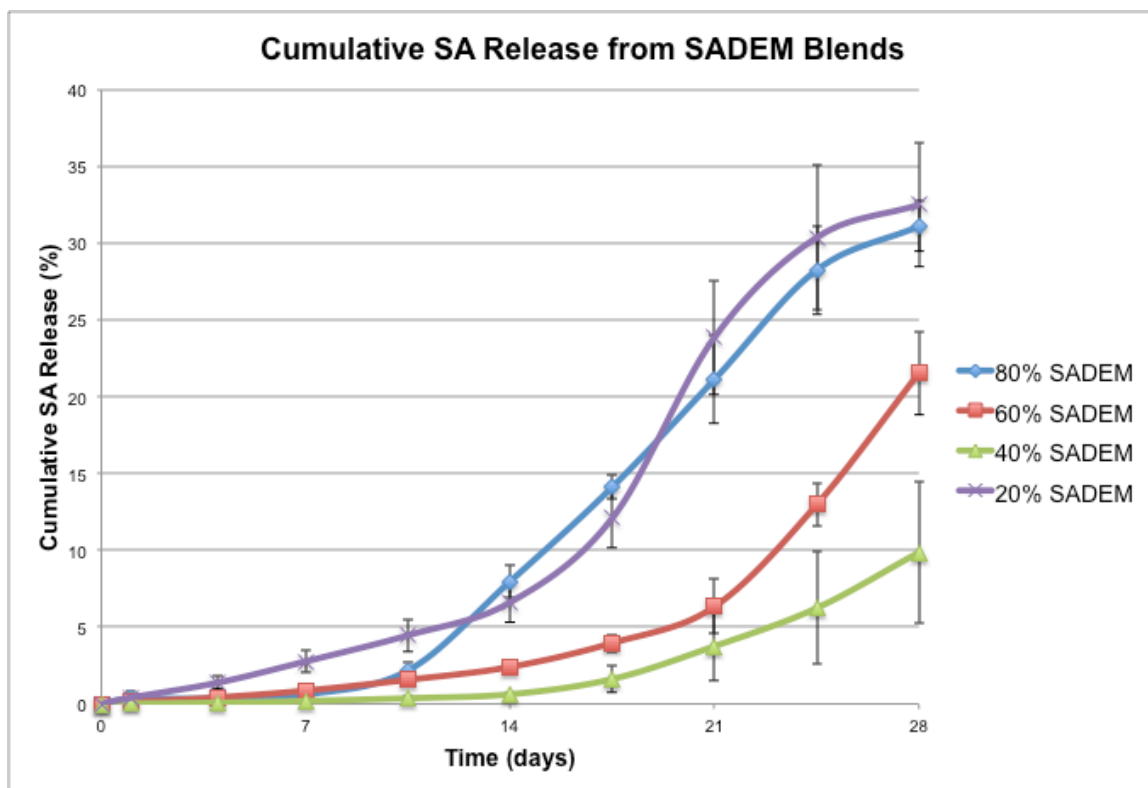


Figure 3.7. Cumulative SA release from SADEM-containing electrospun mats.

3.3.3 *In vivo* testing

Electrospun mats were used as bone wraps in a rat femoral segmental defect (~ 5 mm) model. The purpose of the wraps was two-fold: first, to act as guided bone regeneration membranes, keeping BMP-2 collagen loaded sponges within the defect and preventing soft tissue infiltration into the defect space, and second, to provide locally high SA concentrations to inhibit HO that might be caused by BMP-2 release.

For this study, 40 % SAPAE wraps were chosen, as wraps with higher SAPAE content would tear when attempting to maneuver the wrap during surgery. The SAA blend was chosen as it released more SA in the 4-week time

frame than the SADEM blends; any SA effect on HO would be more likely to be observed with an SAA blend than with an SADEM blend.

Previous studies have shown a dose-dependent biphasic bone regeneration response to BMP-2. Low BMP-2 concentrations do not stimulate much bone growth and high BMP-2 concentrations cause HO and inflammation.³⁰⁻³² One study calculated 12 μ g as the optimal dose for a 5 mm rat femoral segmental defect.³⁰ However, the presence of these wraps may affect optimum BMP-2 because SA acts on similar cell signaling pathways as BMP-2; SA inhibits COX-2 transcription³³ while BMP-2 has been found to promote COX-2 transcription in osteoblasts.³⁴ Additionally, the prostaglandins produced by COX-2 work synergistically with BMP-2 to cause osteoblast differentiation.³⁵ The wrap may also change the optimum BMP-2 dose by altering molecule diffusion into and out of the defect site. This study includes BMP-2 doses of 0, 3.5, 12, and 24 μ g to understand how the BMP-2-loaded collagen sponges interact with the SAA bone wraps and to determine the best BMP-2 dose to be used in subsequent SAPAE wrap studies.

Radiographs were taken over 4 weeks to assess the progression of bone growth. Scans from week 4 are shown in Figure 4.8. Mineralized bone tissue appears in the radiographs as a light gray. The metal screws and plates are also light gray. Two animals in the 0 μ g BMP-2 wrapped group were sacrificed at week 3 due to bone plate loosening. One animal in the 24 μ g BMP-2 wrapped group was not scanned properly at 4 weeks.

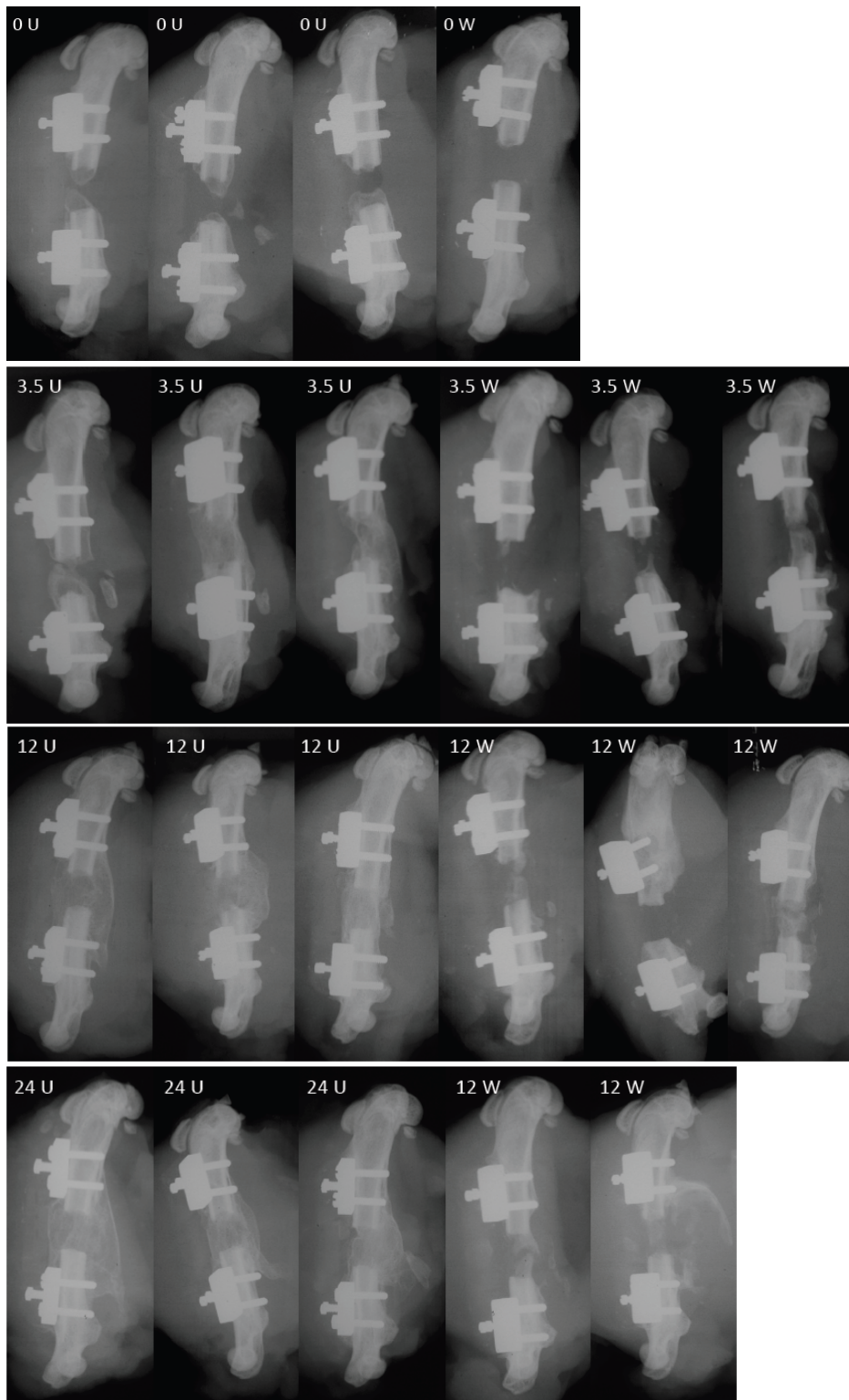


Figure 3.8. Radiographs of rats treated with 0 µg, 3.5 µg, 12 µg, or 24 µg BMP-2, unwrapped (U) or wrapped (W).

In rats with 0 μg BMP-2, the wrapped defects (Figure 3.8: 0W) exhibited significantly less bone formation compared to defects without wraps (Figure 3.8: 0U). Even without BMP-2 treatments, HO occurred in one of the rats in the unwrapped group with orthotopic bone (bone growth contiguous with and outward from the original bone surface) occurring in all 3 rats in this group. The wraps appeared to completely prevent HO, orthotopic bone, and new bone within the defect site.

In the unwrapped groups, BMP-2 treatment enhanced bone formation, both within the defect space as well as in the surrounding muscle tissue (Figure 3.8: 3.5U, 12U, 24U). As BMP-2 concentration increased, so did the bone volume in the surrounding tissues and along the original bone surface.

In the wrapped groups with BMP-2 (Figure 3.8: 3.5W, 12W, 24W), bone formation was delayed and the overall bone formation was decreased. Differences in bone formation were more variable within the wrapped groups than in the corresponding unwrapped groups. With 3.5 μg BMP-2, one animal exhibited good healing within the defect space with only a small amount of HO occurring along the wrap edge. The other animals in this group exhibited minimal bone growth.

Similarly for the 12 μg BMP-2 group (Figure 3.8: 12W), two animals exhibited growth bridging the defect space with small areas of HO along the wrap edging while the other animal exhibited no bone growth. In the 24 μg (Figure 3.8:

24W) group, both animals in the wrapped group exhibited healing within the defect space and had varying degrees of HO.

3.4 Conclusions

SAPAEs were blended with PCL and electrospun to create fibrous mats with mechanical properties and drug release profiles that could be adjusted by controlling SAPAE:PCL ratios and the SAPAE type. Bone wraps with 40 % SAA were assessed *in vivo* for their ability to control bone regeneration when combined with BMP-2 (0, 3.5, 12, or 24 µg). The wraps significantly reduced HO when compared to no wraps. This effect may be attributed to the SA release or the wrap's physical presence preventing BMP-2 diffusion out of and osteoprogenitor cells into the defect space. Previous studies have shown that SAPAE effect on bone formation seems to be dependent on dosing, with higher SA loading resulting in prevention of osteogenesis.^{18, 36, 37} The SAA wraps release > 75 % loaded SA in the first few days after implantation which may stop the inflammatory reaction necessary for bone regeneration.^{38, 39} This effect is not expected to be an issue with the SADEM:PCL blends which exhibit a lag period before SA release.

HO in the wrapped groups typically occurred in small areas, along the wrap surface, as opposed to the large bone masses contiguous with the femur seen in the unwrapped groups. Large bone masses are more likely to lead to adverse symptoms in patients,⁹ so the HO observed with the wraps is preferable to the HO that occurs without the wraps.

Micro-computerized tomography will be performed on the samples obtained in this study to quantify differences in bone formation. Histology will also be performed to assess local inflammation. Additional studies are currently being performed to assess the efficacy of PCL and SADEM:PCL bone wraps with 12 µg BMP-2 for comparison to the SAA:PCL wraps described here. These studies should elucidate the relative effect of SA release and physical barrier presence on HO. They will also assess the temporal effect of SA release on bone regeneration.

3.5 References

1. Mamidwar SS. Preface: Bone Graft Materials. *Journal of Long-Term Effects of Medical Implants*. 2010;20(4):269.
2. Pollock R, Alcelik I, Bhatia C, Chuter G, Lingutla K, Budithi C, et al. Donor site morbidity following iliac crest bone harvesting for cervical fusion: a comparison between minimally invasive and open techniques. *European Spine Journal*. 2008;17(6):845-52.
3. Abbas G, Bali SL, Abbas N, Dalton DJ. Demand and supply of bone allograft and the role of orthopaedic surgeons. *Acta orthopaedica Belgica*. 2007;73(4):507-11.
4. Nandi SK, Roy S, Mukherjee P, Kundu B, De DK, Basu D. Orthopaedic applications of bone graft & graft substitutes: a review. *The Indian journal of medical research*. 2010;132:15-30.
5. Lo KWH, Ulery BD, Ashe KM, Laurencin CT. Studies of bone morphogenetic protein-based surgical repair. *Advanced drug delivery reviews*. 2012;64(12):1277-91.
6. Geiger M, Li RH, Friess W. Collagen sponges for bone regeneration with rhBMP-2. *Advanced drug delivery reviews*. 2003;55(12):1613-29.

7. Boerckel JD, Kolambkar YM, Dupont KM, Uhrig BA, Phelps EA, Stevens HY, et al. Effects of protein dose and delivery system on BMP-mediated bone regeneration. *Biomaterials*. 2011;32(22):5241-51.
8. Carragee EJ, Hurwitz EL, Weiner BK. A critical review of recombinant human bone morphogenetic protein-2 trials in spinal surgery: emerging safety concerns and lessons learned. *The Spine Journal*. 2011;11(6):471-91.
9. Randelli F, Pierannunzii L, Banci L, Ragone V, Aliprandi A, Buly R. Heterotopic ossifications after arthroscopic management of femoroacetabular impingement: the role of NSAID prophylaxis. *Journal of Orthopaedics and Traumatology*. 2010;11(4):245-50.
10. Rapuano BE, Boursiquot R, Tomin E, MacDonald DE, Maddula S, Raghavan D, et al. The effects of COX-1 and COX-2 inhibitors on prostaglandin synthesis and the formation of heterotopic bone in a rat model. *Archives of Orthopaedic and Trauma Surgery*. 2007;128(3):333-44.
11. Vuolteenaho K, Moilanen T, Moilanen E. Non-Steroidal Anti-Inflammatory Drugs, Cyclooxygenase-2 and the Bone Healing Process. *Basic & Clinical Pharmacology & Toxicology*. 2008;102(1):10-4.
12. Cullen N, Perera J. Heterotopic ossification: pharmacologic options. *The Journal of head trauma rehabilitation*. 2009;24(1):69-71.
13. Xue D, Zheng Q, Li H, Qian S, Zhang B, Pan Z. Selective COX-2 inhibitor versus nonselective COX-1 and COX-2 inhibitor in the prevention of heterotopic ossification after total hip arthroplasty: a meta-analysis of randomised trials. *International Orthopaedics*. 2009;35(1):3-8.
14. Chao ST, Joyce MJ, Suh JH. Treatment of heterotopic ossification. *Orthopedics*. 2007;30(6):457-64; quiz 65-6.
15. Erdmann L, Uhrich KE. Synthesis and degradation characteristics of salicylic acid-derived poly(anhydride-esters). *Biomaterials*. 2000;21(19):1941-6.
16. Schmeltzer RC, Anastasiou TJ, Uhrich KE. Optimized synthesis of salicylate-based poly(anhydride-esters). *Polym Bull*. 2003;49(6):441-8.

17. Prudencio A, Schmeltzer RC, Uhrich KE. Effect of linker structure on salicylic acid-derived poly(anhydride-esters). *Macromolecules*. 2005;38(16):6895-901.
18. Harten RD, Svach DJ, Schmeltzer R, Uhrich KE. Salicylic acid-derived poly(anhydride-esters) inhibit bone resorption and formation in vivo. *Journal of biomedical materials research Part A*. 2005;72(4):354-62.
19. Lee KH, Kim HY, Khil MS, Ra YM, Lee DR. Characterization of nano-structured poly(ϵ -caprolactone) nonwoven mats via electrospinning. *Polymer*. 2003;44(4):1287-94.
20. Prudencio A, Schmeltzer RC, Uhrich KE. Effect of Linker Structure on Salicylic Acid-Derived Poly(anhydride-esters). *Macromolecules*. 2005;38(16):6895-901.
21. Schmeltzer RC, Schmalenberg KE, Uhrich KE. Synthesis and cytotoxicity of salicylate-based poly(anhydride esters). *Biomacromolecules*. 2005;6(1):359-67.
22. Del Gaudio C, Bianco A, Grifioni M. Electrospun bioresorbable trileaflet heart valve prosthesis for tissue engineering: in vitro functional assessment of a pulmonary cardiac valve design. *Ann Ist Super Sanità*. 2007;44(2):178-86.
23. Heo S-J, Nerurkar NL, Baker BM, Shin J-W, Elliott DM, Mauck RL. Fiber Stretch and Reorientation Modulates Mesenchymal Stem Cell Morphology and Fibrous Gene Expression on Oriented Nanofibrous Microenvironments. *Annals of Biomedical Engineering*. 2011;39(11):2780-90.
24. Simonet M, Schneider OD, Neuenschwander P, Stark WJ. Ultraporous 3D polymer meshes by low-temperature electrospinning: Use of ice crystals as a removable void template. *Polymer Engineering & Science*. 2007;47(12):2020-6.
25. Lowery JL, Datta N, Rutledge GC. Effect of fiber diameter, pore size and seeding method on growth of human dermal fibroblasts in electrospun poly(ϵ -caprolactone) fibrous mats. *Biomaterials*. 2010;31(3):491-504.
26. Eriskin C, Kalyon DM, Wang H. Functionally graded electrospun polycaprolactone and β -tricalcium phosphate nanocomposites for tissue engineering applications. *Biomaterials*. 2008;29(30):4065-73.

27. Zhang X, Thomas V, Vohra YK. In vitro biodegradation of designed tubular scaffolds of electrospun protein/polyglyconate blend fibers. *Journal of Biomedical Materials Research Part B: Applied Biomaterials*. 2009;89B(1):135-47.
28. Stachewicz U, Peker I, Tu W, Barber AH. Stress Delocalization in Crack Tolerant Electrospun Nanofiber Networks. *ACS Applied Materials & Interfaces*. 2011;3(6):1991-6.
29. Ouimet MA, Snyder SS, Uhrich KE. Tunable drug release profiles from salicylate-based poly(anhydride-ester) matrices using small molecule admixtures. *Journal of Bioactive and Compatible Polymers*. 2012;27(6):540-9.
30. Angle SR, Sena K, Sumner DR, Virkus WW, Viridi AS. Healing of rat femoral segmental defect with bone morphogenetic protein-2: a dose response study. *Journal of musculoskeletal & neuronal interactions*. 2012;12(1):28-37.
31. Brown KV, Li B, Guda T, Perrien DS, Guelcher SA, Wenke JC. Improving Bone Formation in a Rat Femur Segmental Defect by Controlling Bone Morphogenetic Protein-2 Release. *Tissue Engineering Part A*. 2011;17(13-14):1735-46.
32. Zara JN, Siu RK, Zhang X, Shen J, Ngo R, Lee M, et al. High Doses of Bone Morphogenetic Protein 2 Induce Structurally Abnormal Bone and Inflammation In Vivo. *Tissue Engineering Part A*. 2011;17(9-10):1389-99.
33. Wu KK, Liou JY, Cieslik K. Transcriptional Control of COX-2 via C/EBPbeta. *Arteriosclerosis, thrombosis, and vascular biology*. 2005;25(4):679-85.
34. Chikazu D, Li X, Kawaguchi H, Sakuma Y, Voznesensky OS, Adams DJ, et al. Bone Morphogenetic Protein 2 Induces Cyclo-oxygenase 2 in Osteoblasts via a Cbfa1 Binding Site: Role in Effects of Bone Morphogenetic Protein 2 In Vitro and In Vivo. *Journal of Bone and Mineral Research*. 2002;17(8):1430-40.
35. Taktguchi T, Kobayashi M, Nagashima C, Yamaguchi A, Nishihara T, Hasegawa K. Effect of prostaglandin E2 on recombinant human bone morphogenetic protein-2-stimulated osteoblastic differentiation in human periodontal ligament cells. *Journal of periodontal research*. 1999;34(7):431-6.

36. Erdmann L, Macedo B, Uhrich KE. Degradable poly(anhydride ester) implants: effects of localized salicylic acid release on bone. *Biomaterials*. 2000;21(24):2507-12.
37. Reynolds MA, Prudencio A, Aichelmann-Reidy ME, Woodward K, Uhrich KE. Non-steroidal anti-inflammatory drug (NSAID)-derived poly(anhydride-esters) in bone and periodontal regeneration. *Current drug delivery*. 2007;4(3):233-9.
38. Goodman SB, Ma T, Mitsunaga L, Miyanishi K, Genovese MC, Smith RL. Temporal effects of a COX-2-selective NSAID on bone ingrowth. *Journal of biomedical materials research Part A*. 2005;72(3):279-87.
39. Simon AM, O'Connor JP. Dose and time-dependent effects of cyclooxygenase-2 inhibition on fracture-healing. *The Journal of bone and joint surgery American volume*. 2007;89(3):500-11.

4. FLOWABLE SALICYLIC ACID-BASED POLY(ANHYDRIDE-ESTERS) FOR INJECTABLE BARRIER APPLICATIONS

4.1 Introduction

Fibrous adhesions are bands of fibrous tissue that join two surfaces in the body that are not normally connected. They generally form after injury to an area that results in increased inflammation. Surgery, trauma, infections, radiation, and ischemia can all lead to adhesion formation, with surgery being the most common cause.^{1, 2} Adhesions are a serious problem that can lead to many complications, including chronic pain, infertility, and intestinal obstruction.² Fibrous adhesions have an enormous impact on the healthcare system. It has been estimated that 95 % of abdominal and pelvic surgeries, including gynecologic, result in adhesions.³ Adhesion related problems account for 6 % of hospital readmissions and 1 % of all hospitalizations in the United States.^{4, 5} Over 400,000 abdominal adhesiolysis procedures, a surgery to dissect fibrous adhesions, are performed annually.⁶ While adhesiolysis can help alleviate some pain and complications associated with adhesions, the effect is often temporary as the adhesions tend to grow back after the procedure.⁴

Adhesion-related complications often lead to additional surgeries, which is particularly alarming when one takes into account that the presence of adhesions makes such secondary surgeries even more difficult and dangerous, increasing surgery time, hospital stay, complications, blood loss, morbidity, and mortality.^{4, 6-}

¹⁰ While there has been some effort to develop devices to reduce adhesion

formation, no device has been proven to significantly reduce the incidence of adhesion-related complications.⁶

The physiological pathway that leads to abdominal adhesion formation has been well studied. After surgery, fibrinogen from blood in the peritoneal cavity form a fibrin matrix. This matrix forms into transient fibrinous bands degrade by fibrinolysis or become a scaffold for fibroblasts to create permanent fibrous adhesions. The occurrence of fibrinolysis is dependent upon the levels of different cytokines and enzymes, with the first 7-10 days after surgery being the most critical for adhesion formation.^{11, 12}

Both physical and pharmaceutical methods have been investigated to prevent adhesion formation.^{2, 4, 13} Various solids, gels, and fluids have been explored as physical barriers, the main purpose of which is to separate surfaces where adhesions could potentially form. The FDA has approved only 5 barrier devices for human use. However, FDA approved devices are not efficacious enough at reducing adhesion related complications to warrant their ubiquitous use.¹⁴⁻¹⁷

Drugs tested for adhesion prevention include primarily those that affect the clotting cascade, the inflammatory process, cell proliferation, extracellular matrix production, or oxidative stress.⁴ Systemic administration of such drugs at therapeutic levels can cause undesired side effects and delay healing after surgery.² Some attempts have been investigated to inject drugs into the peritoneal cavity; however, most of these studies have shown low efficacy in laboratory testing primarily because the mesothelial membrane lining the

peritoneal cavity quickly absorbs drugs and subsequently distributes them throughout the body.⁴

The Urich laboratory developed salicylic acid-based poly(anhydride-esters) (SAPAEs) that hydrolytically degrade to release salicylic acid (SA) and biocompatible linker molecules.¹⁸ SA, a non-steroidal anti-inflammatory drug (NSAID), has been found to inhibit cyclooxygenase-2 (COX-2) activity which is expressed in adhesion fibroblasts but not in normal peritoneal fibroblasts.¹⁹ Other COX-2 inhibitors have been found to inhibit adhesion formation in animal models.²⁰⁻²² SA is a desirable agent for adhesion prevention as it not only has anti-inflammatory properties, but also acts as an analgesic, potentially reducing post-surgical pain.²³ SAPAEs exhibit high drug loading capacities (up to 75 %) and are able to be manipulated into various geometries depending on the application needs.^{18, 24-27} An SAPAE adhesion prevention material will allow for sustained release of salicylic acid at the site of implantation while also maintaining a temporary physical presence to block adhesion formation.

The research described herein describes the development and characterization of SAPAE:poly(ethylene glycol) (PEG) copolymers with desirable mechanical and drug release properties for an adhesion prevention device. The copolymers exhibited mechanical properties similar to or better than current injectable barrier devices on the market. *In vitro* drug release showed PEG content controls SA release rates and cell studies confirmed cytocompatibility and anti-inflammatory activity.

4.2 Materials and Methods

4.2.1 Materials

All chemicals and reagents, including poly(ethylene glycol) (PEG) 20,000 Da, were purchased from Sigma-Aldrich (Milwaukee, WI) and used as received.

4.2.2 ^1H NMR and FTIR spectroscopies

^1H spectra were recorded on a Varian 500 MHz spectrometer using deuterated dimethyl sulfoxide (DMSO- d_6) as the solvent and internal reference. FTIR spectra were obtained using a Thermo Nicolet/Avatar 360 spectrometer. Samples were dissolved in dichloromethane and solvent-cast on NaCl plates. Each spectrum was an average of 32 scans.

4.2.3 Molecular weight

Gel permeation chromatography (GPC) was used to determine polymer number-averaged molecular weight (M_n) and polydispersity index (PDI) using a Perkin-Elmer liquid chromatography system consisting of a Series 200 refractive index detector, a Series 200 LC pump, and an ISS 200 autosampler. Sample automation and data processing were performed using a Dell OptiPlex GX110 computer running Perkin-Elmer TurboChrom 4 software with a Perkin-Elmer Nelson 900 Series Interface and 600 Series Link. Polymer samples dissolved in dichloromethane (DCM, 10 mg/mL) were filtered through 0.45 μm poly(tetrafluoroethylene) syringe filters. Samples were resolved on a Jordi divinylbenzene mixed-bed GPC column (7.8 \times 300 mm, Alltech Associates,

Deerfield, IL), with a DCM mobile phase and a flow rate of 1.0 mL/min. Molecular weights were calibrated relative to broad polystyrene standards (Polymer Source Inc., Dorval, Canada).

4.2.4 Thermal properties

Differential scanning calorimetry (DSC) measurements were carried out on a TA Instrument Q200 to determine glass transition (T_g) and melting (T_m) temperatures. Measurements on samples (4–8 mg) heated under nitrogen atmosphere to 200 °C at a heating rate of 10 °C/min and cooled to –50 °C at a rate of 10 °C/min with a two-cycle minimum were performed. TA Instruments Universal Analysis 2000 software, version 4.5A, was used to analyze the data. T_g s were calculated as half C_p extrapolated.

4.2.5 Polymer synthesis

SA-based diacid was synthesized according to previously described methods (Figure 4.1).²⁸ Briefly, SA (2 equivalents (eq)) was dissolved in tetrahydrofuran (THF) and pyridine (4 eq). Adipoyl chloride (1 eq) was dissolved in THF and added drop-wise forming a white suspension. The reaction mixture was stirred overnight, quenched over water and acidified to pH 2 using concentrated hydrochloric acid. The precipitate was filtered, washed with water (3 x 250 mL), and dried *in vacuo* to yield diacid.

For the SAPAE homopolymer used in this study (referred to hereafter as SAA, Figure 4.1), diacid was activated in an excess of acetic anhydride at room

temperature, concentrated, and polymerized via melt-condensation polymerization at 180 °C for 5 h at 100 rpm *in vacuo* to yield a tan foam. M_n = 9,000 Da, PDI = 1.2. T_g = 45 °C.

For the SAPAE copolymers (referred to hereafter as SAA:PEG, Figure 4.1), diacid and poly(ethylene glycol) bis(carboxymethyl) ether (M_n 600, Sigma-Aldrich) were combined in weight ratios of 1:2, 1:1, and 2:1 and activated in an excess of acetic anhydride at room temperature, concentrated, and polymerized via melt-condensation polymerization at 180 °C for 3 h at 100 rpm *in vacuo* to yield a brown viscous liquid. Yield: 2.00 g (67%), brown viscous liquid. ^1H NMR (500 MHz, DMSO- d_6 , δ) for SAA:PAE copolymer: 8.21 (br, ArH), 7.93 (br, ArH), 7.77 (br, ArH), 7.39 (br, ArH), 4.41 (s, CH_2), 4.02 (s, CH_2), 3.46 (s, CH_2), 2.51 (br, CH_2), 1.65 (br, CH_2), peak integration varied with SAA:PEG ratio. IR (solvent-cast DCM): 1775 cm^{-1} (C=O, anhydride), 1745 cm^{-1} (C=O, ester).

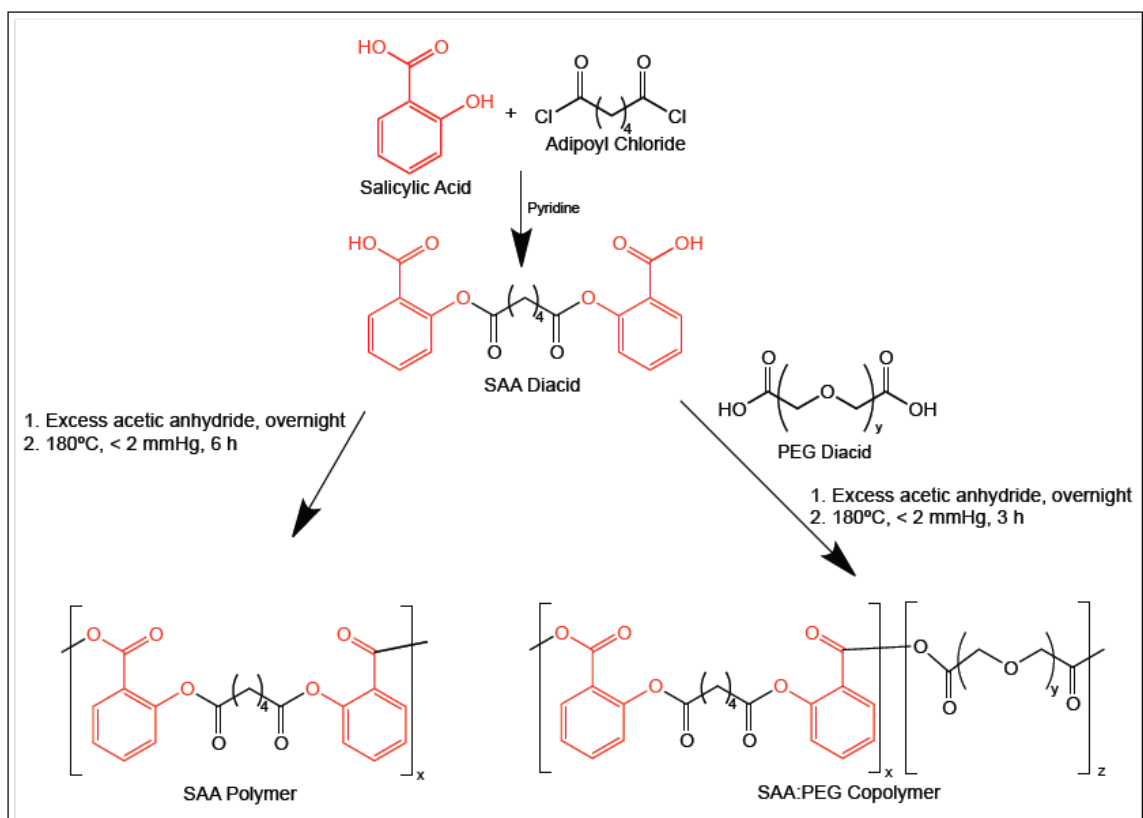


Figure 4.1. Synthetic scheme for the SAA diacid, SAA polymer, and SAA:PEG copolymers.

4.2.6 Solvent-casting SAA/PEG blended films

SAA (250 mg) and PEG 20,000 (250 mg) were dissolved in 1 mL dichloromethane and cast into a Teflon drying dish (3 cm diameter). The dish was left to evaporate overnight in a hood before being placed into a vacuum desiccator for 24 hr at room temperature to remove any remaining solvent.

4.2.7 Rheology

A Rheometrics SR-2000 parallel plate rheometer with the temperature set to 25 or 37 °C (TA Instruments, New Castle, DE) was used for rheological measurements. The top plate was lowered to 0.5 mm. Oscillatory shear studies were performed ramping the frequency from 0.1 to 10 rad/s at 2 % shear strain. The SAA:PEG copolymers shear viscosity was evaluated by ramping shear rates from 0.1 to 1 rad/s for the 2:1 ratio, 0.1 to 100 rad/s for the 1:1 ratio, and 1 to 500 rad/s for the 1:2 ratio. Samples were analyzed in triplicate.

4.2.8 Storage stability

SAA:PEG copolymers (~ 0.5 g) were placed in 50 mL centrifuge tubes at -20 °C, 4°C, or 25 °C. Tubes were flushed with dry nitrogen before storage. Copolymer samples (1:2 ratio) were studied both with and without desiccant (Drierite, W A Hammond Drierite Co. Ltd., Xenia, OH). A Kimwipe (Kimberly-Clark, Irving, TX) taped to the tube cap suspended the desiccant away from the polymer. All other ratios were tested without desiccant only. M_n and T_g were analyzed for all samples each week for 3 weeks. Samples were studied in singlet due to the amount of time required for sample analysis.

4.2.9 *In vitro* drug release

Polymers (50 ± 1 mg) were placed in aluminum pans (6.3 mm diameter) to contain polymer spreading. Polymer-filled pans were placed in 20 mL Wheaton glass scintillation vials containing 10 mL phosphate buffered saline (PBS) at pH

7.4. Samples were incubated at 37 °C with agitation at 60 rpm in a controlled environment incubator shaker (New Brunswick Scientific Co., Excella E25, Edison, NJ). All media was collected and replaced with fresh PBS (10 mL) at pre-designated time points for 14 days. Spent media was analyzed by UV spectrophotometry using a Perkin Elmer Lambda XLS spectrophotometer (Waltham, MA) to specifically monitor SA release. Measurements were obtained at $\lambda = 303$ nm, the maximum absorbance of SA that does not overlap with other polymer degradation products. Data were calculated against a calibration curve of absorbance values from standard solutions of known SA concentrations in PBS. Polymer remaining after 14 days was degraded using basic water (pH > 12) and SA was quantified to allow normalization of percent release. Samples were studied in triplicate.

4.2.10 *In vitro* cytotoxicity and proliferation assay

Polymer cytocompatibility was performed by culturing NCTC clone 929 (strain L) mouse areolar fibroblast cells (ATCC, Manassas, Virginia) in media containing the dissolved polymers. These L929 fibroblast cells are a standard cell type for cytocompatibility testing as recommended by ASTM.²⁹ Cell culture media consisted of Dulbecco's Modified Eagle's Medium (DMEM, Sigma-Aldrich, St. Louis, MO), 10 % v/v fetal bovine serum (Atlanta Biologicals, Lawrenceville, GA), 1 % L-glutamate (Sigma) and 1 % penicillin/streptomycin. The polymers were dissolved in dimethyl sulfoxide (DMSO) at 100, 50, 10, 5, and 1 mg/mL. These solutions were then diluted with cell culture media to achieve

concentrations of 1, 0.5, 0.1, 0.05, and 0.01 mg/mL and 1 % DMSO. A control with 1 % DMSO in media without polymer was prepared. Three 96-well plates were seeded at an initial concentration of 2,000 cells per well with each experimental group plated in triplicate. For the L929 fibroblasts, cell viability was determined by using a CellTiter 96®AQueous One Solution Cell Proliferation Assay (MTS, Promega, Madison, WI) at 24, 48, and 72 hours. After 2 hr incubation with MTS, the absorbance was recorded with a microplate reader at $\lambda = 490$ nm. One-way ANOVAs followed by Bonferroni's all-pairs comparison were used to determine significance (significantly different if $p < 0.05$).

4.2.11 TNF- α secretion assay

[Differentiation of monocytes was performed by Dr. Jeffrey Barminko, former graduate student in the Department of Biomedical Engineering, Rutgers University.]

Human blood-derived monocytes (Blood Center of New Jersey, East Orange, NJ) were used to determine the polymer efficacy on decreasing inflammatory cytokine secretion. The cell isolation and purification protocol used was previously described by Kim et al.³⁰ Briefly, peripheral blood mononuclear cells were collected from blood of healthy donors by density gradient separation using Ficoll-PLUS (GE Healthcare, Piscataway, NJ). Red blood cells were lysed by incubation in ammonium-potassium-chloride lysing buffer for 5 min, washed with PBS and counted. Monocytes were cultured on 175 cm² flasks (BD, Franklin Lakes, NJ) at a concentration of 8×10^6 cells/mL in Roswell Park

Memorial Institute (RPMI) 1640 media (GIBCO BRL, Rockville, MD). RPMI media was supplemented with 10 % fetal bovine serum (FBS) (GIBCO BRL), 100 units/mL penicillin (GIBCO BRL), 100 µg/mL streptomycin (GIBCO BRL) and 400 mM L-glutamine (GIBCO BRL). Monocytes were allowed to adhere for 2 h and then washed 3 times with PBS to remove non-adherent cells. Monocytes were cultured for 7 days at 37 °C and 5 % CO₂ in RPMI supplemented with 5 ng/mL granulocyte-macrophage colony-stimulating factor (GM-CSF) (R&D Systems, Minneapolis, MN) to generate macrophages.

After 7 days of culture, macrophages were washed once with PBS and then detached with trypsin-EDTA (GIBCO) for 30 minutes at room temperature. Cells were re-suspended in culture medium (RPMI), counted, re-plated at 8×10^3 cells/well in a 96 well plate, and allowed to attach overnight. The following day, the media was replaced with the various sample groups: polymer containing media (0.2 mg/mL polymer, 10 ng/mL lipopolysaccharide (LPS), 1% DMSO), a positive control (10 ng/mL LPS, 1% DMSO), and a negative control (no LPS, 1% DMSO). All cell studies were performed in triplicate. LPS (10 ng/mL) induced macrophage TNF- α secretion. After 48 h, media was collected and TNF- α secretion was determined with an enzyme-linked immunosorbent assay kit against human TNF- α (BioLegend, San Diego, CA). A CellTiter 96®AQueous One Solution Cell Proliferation Assay (Promega, Madison, WI) was used to ensure that differences in TNF- α secretion were not due to differences in cell viability. A one-way ANOVA followed by Bonferroni's all-pairs comparison was used to determine significance (significantly different if $p < 0.05$).

4.3 Results and Discussion

4.3.1 SAPAE:PEG blended films

SAPAE homopolymers are hard and glassy at physiological temperatures, making them unfeasible as adhesion barrier devices on their own. The first method attempted to create an adhesion barrier material used SAA, the most well characterized SAPAE, blended with PEG. PEG was chosen as it has favorable mechanical characteristics, has been used in other barrier devices, and can inhibit protein adsorption to surfaces, thereby decreasing the likelihood of cell adhesion to the barrier as it degrades.³¹

The polymers were concurrently dissolved and solvent-cast to create a film. The resulting film crumbled when removed from the Teflon dish it had been cast in. Unlike typical solvent cast films of SAA, the film surface was not smooth (Figure 4.2).

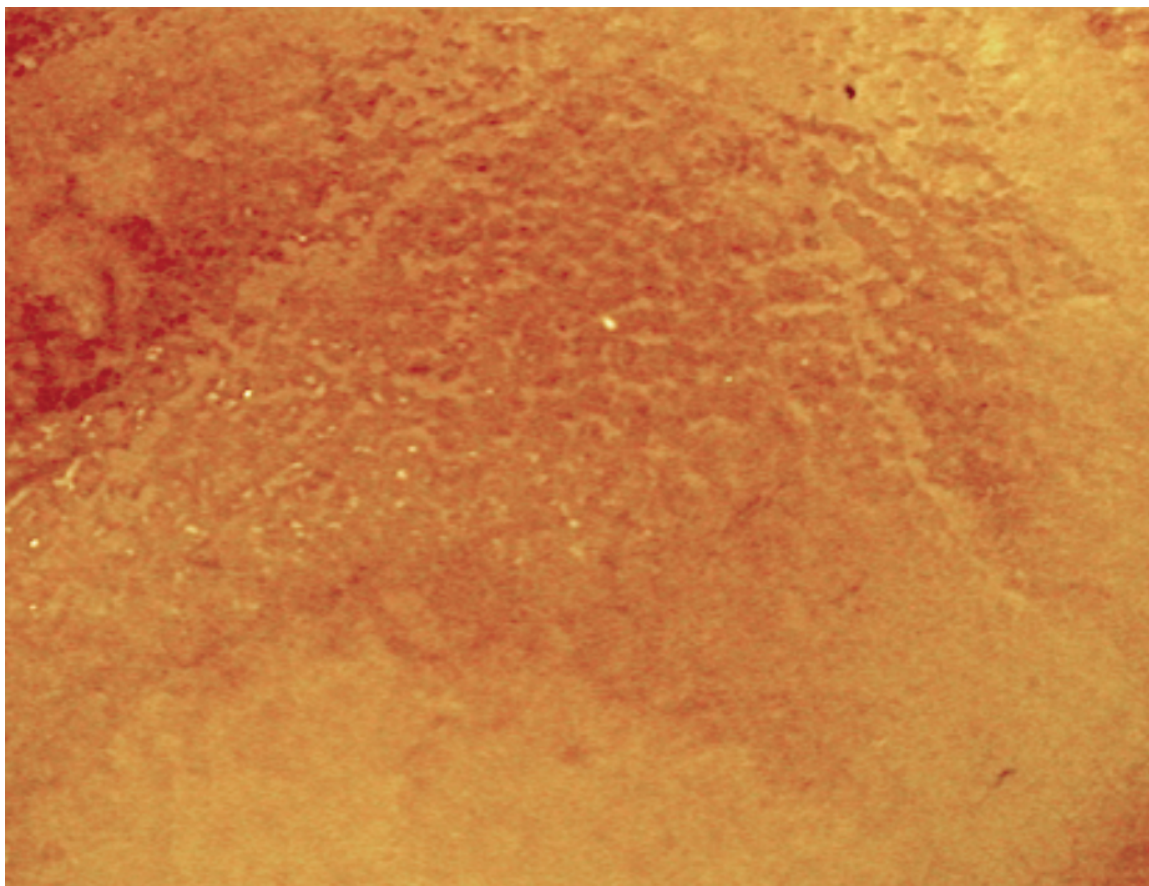


Figure 4.2. Variegated surface of the blended films indicates macroscopic phase separation.

DSC spectra of SAA, PEG, and the SAA/PEG film are shown in Figure 4.3. If the polymer blend were completely miscible, the thermal transitions for the blend would have intermediary values between the homopolymer values transitions.³² The thermal transition for the blend appears to be more additive than intermediary as the SAA T_g drop and PEG T_m are still visible despite their overlap. The DSC curves and film topography indicate immiscibility and phase separation.

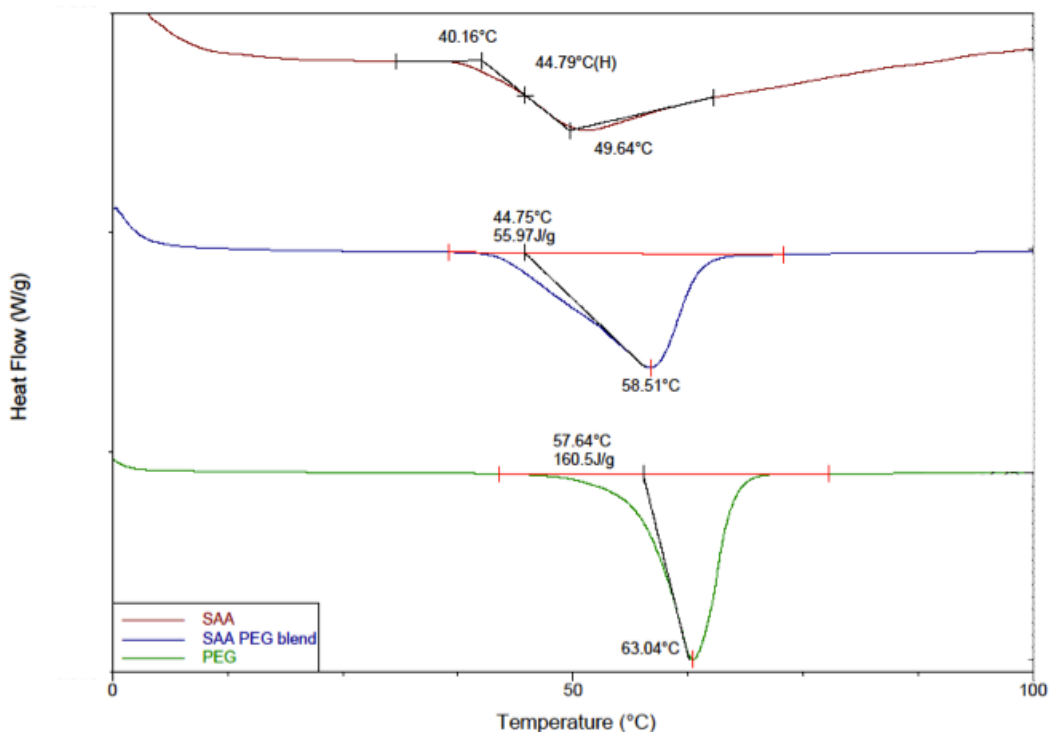


Figure 4.3. DSC spectra for SAA (red), PEG (green), and SAA/PEG blend (blue). The blend spectra indicates phase separation as the spectra values are additive.

4.3.2 SAPAE:PEG copolymers

Due to the poor mechanical properties and phase separation, which could result in uneven degradation and drug release, other methods of incorporating PEG with SAA were pursued. Copolymers containing SAA repeat units and PEG repeat units were considered, as previous research had created similar copolymers of PEG moieties and aromatic polyanhydride units.³³ Carboxylic acid-terminated PEG chains (Sigma-Aldrich) were purchased for copolymerization with SAA monomers to allow the copolymers to be formed using standard melt polymerization techniques (Figure 4.1).

4.3.3 Copolymer characterization

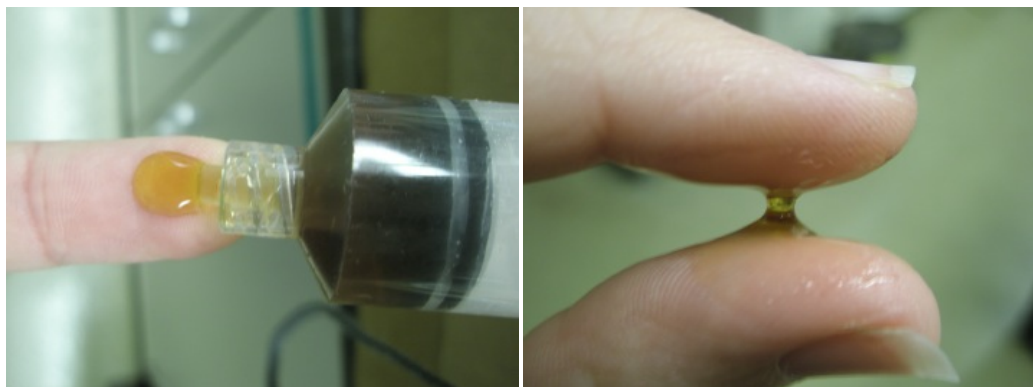
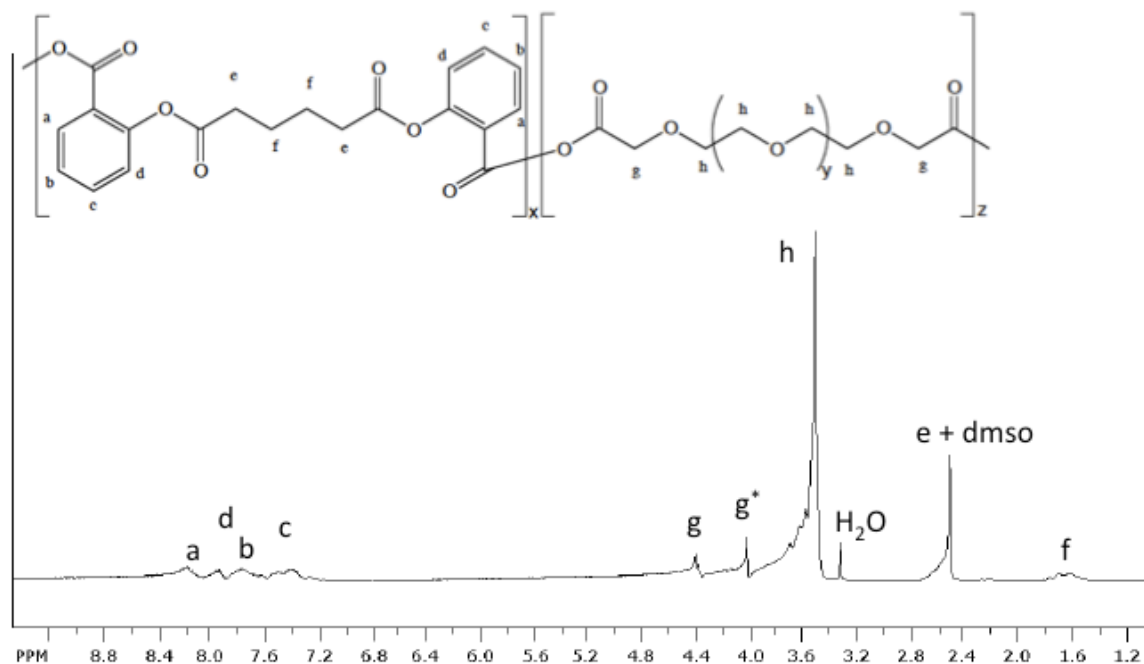


Figure 4.4. Resulting copolymers behaved like viscous liquids.

The resulting copolymers formed brown viscous liquids at room temperature (Figure 4.4). These liquids were very sticky, a good quality for an adhesion barrier as this property will help the material adhere to the administered site and remain in place throughout the healing process⁴. ¹H NMR (Figure 4.5 and FTIR spectroscopies were used to confirm the products. ¹H NMR peak integrations confirmed that theoretical and experimental SAA:PEG ratios were similar. FTIR confirmed the presence of anhydride and ester bonds in the various polymers. Typical M_n , PDI, and T_g values for the copolymer ratios studied are summarized in Table 4.1. The significant decrease in copolymer T_g s as compared to the homopolymer (45 °C) is typical for polyanhydride copolymers containing PEG moieties.^{34, 35}

Table 4.1. Typical M_n , PDI, and T_g for SAA:PEG Polymers.

SAA:PEG Ratio	M_n (Da)	PDI	T_g (°C)
2:1	23,700	44.6	-5
1:1	16,500	22.2	-25
1:2	39,200	31.7	-35
1:0 (SAA homopolymer)	9,000	1.2	45

**Figure 4.5.** ^1H NMR spectra of 2:1 SAA:PEG (g^* indicates hydrogen atoms adjacent to a carboxylic acid end group, as opposed to g which indicates hydrogen atoms adjacent to an anhydride group).

4.3.4 Rheology

With T_g s below 0 °C, the polymers behaved as viscous liquids at room temperature, as opposed to the glassy SADEM homopolymers. To assess the copolymer mechanical properties, rheological studies were performed. Initial oscillatory measurements demonstrated a phase angle of approximately 90°. This data indicates that the polymers primarily undergo viscous deformation with negligible elastic deformation. The results of subsequent linear shear viscosity ramping measurements are given in Table 4.2. Shear viscosities decreased by an order-of-magnitude as PEG content increased. Increasing the sample temperatures from 25 °C to 37 °C resulted in a decrease in shear viscosity by about half an order-of-magnitude. These patterns suggest an ability to tailor copolymer rheological properties by changing PEG content.

Table 4.2. Shear Viscosities of SAA:PEG Copolymers

SAA:PEG Ratio	Shear Viscosity at 25 °C (mPa•s)	Shear Thinning Observed (25 °C, rad/s)	Shear Viscosity at 37 °C (mPa•s)	Shear Thinning Observed (37 °C, rad/s)
2:1	6.5×10^7 $\pm 1.8 \times 10^7$	N/A	8.5×10^6 $\pm 3.7 \times 10^6$	N/A
1:1	7.3×10^6 $\pm 0.8 \times 10^6$	2	1.6×10^6 $\pm 0.4 \times 10^5$	10
1:2	2.2×10^5 $\pm 0.1 \times 10^5$	100	6.9×10^4 $\pm 0.1 \times 10^4$	200

These shear viscosity values compare well with Intercoat® (Ethicon, Somerville, NJ), an injectable adhesion barrier currently on the market.

Intercoat[®] is a carboxymethylcellulose and PEG blend with a viscosity of about $2.1 \times 10^5 \text{ mPa}\cdot\text{s}$,³⁶ similar to the 1:2 SAA:PEG copolymer described here. Additionally, evidence suggests that as the viscosity of a barrier increases, so does the efficacy.³⁶ This result indicates that the SAA:PEG copolymers may have mechanical properties suitable for the prevention of adhesions. However, a balance must be made between the ability of a material to remain in place in vivo and the ease of surgical application. While both the 1:1 and 1:2 copolymers can be extruded from a syringe, the 2:1 copolymer can only be extruded with extreme effort. The ease of application is an important consideration for surgical use⁴ and suggests that the optimal SAA:PEG ratio is below 2:1 for injectable applications.

4.3.5 Storage stability

Copolymer storage stability is an issue as their degradation over time affects both physicochemical properties and drug release rates. Copolymers were stored in the freezer, refrigerator, and at ambient temperatures. The molecular weight and glass transition temperatures were monitored weekly for 3 weeks to assess the rate of degradation of samples under the various conditions (Figure 4.6). As only one data set was taken, variability is observed, resulting in increases in M_n and T_g at some time points. GPC column issues resulting in fluctuating baselines could also have affected M_n measurements. However, there is a general trends observed between groups. Colder environments slowed the rate of polymer degradation. This fact can be seen in the dramatic differences in 0 and 3 week M_n and T_g values for polymers at 25 °C as compared

to the slight differences between 0 and 3 weeks for samples maintained at -20 °C. As PEG is hygroscopic, it is expected to increase polymer degradation rates, thus, the copolymer with the greatest amount of PEG (1:2 copolymer) was stored both with and without desiccant to reduce degradation rates. The desiccant effect is most obvious on the molecular weight, with only slight differences observed in the T_g . Due to these results, all copolymers were subsequently stored in the freezer in a secondary container with desiccant.

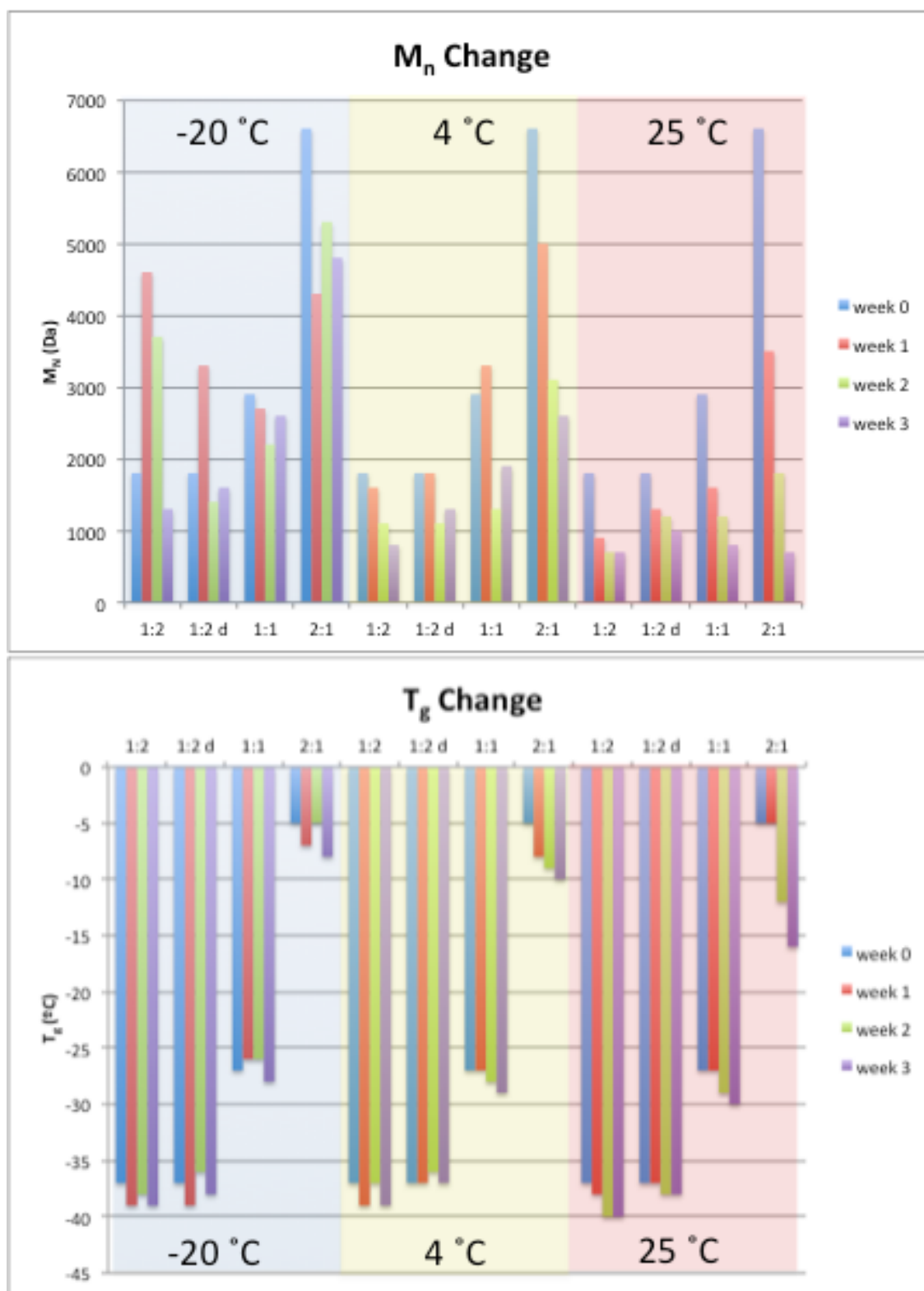


Figure 4.6. SAA:PEG copolymer M_n and T_g changes over 3 weeks of storage at different temperatures, with (1:2 d) and without (1:2) desiccant.

4.3.6 *In vitro* drug release

SAPAEs are hydrolytically degradable and the incorporation of hydrophilic PEG moieties was expected to significantly effect drug release rates. Figure 4.7 shows the SA release profiles from the SAA:PEG copolymers. The 1:2 copolymer completely degraded in less than a week, with 77 % of incorporated SA released within the first 24 hours. The 1:1 and 2:1 copolymers exhibit lesser release within the first day (37 % and 15 %, respectively). The initial release correlated with the PEG content where increasing PEG led to greater SA release. In comparison, the SAA homopolymer exhibits a 2-day lag period.³⁷ For the 1:1 and 2:1 copolymers, after the initial release, the release rate stabilized to give a more linear profile. Average release after day 1 was 3.5 % from the 1:1 samples and 2.8 % from the 2:1 samples. On day 14, basic water was used to completely degrade remaining polymer to determine total SA content. SA content from remaining polymer was used to normalize cumulative release data. After 14 days, the 1:1 and 2:1 copolymers released 85 % and 52 % SA, respectively.

As the critical period for adhesion prevention is the first 7-10 days after injury,^{11, 12} the 1:2 copolymer would not appear to be a good candidate as it does not provide drug release or physical barrier properties over this time period. The rate of degradation *in vitro* and *in vivo* may vary dramatically. However, the amount of polymer used and how it is placed in the body will have an effect on polymer duration *in vivo*. Additionally, the increased shear stress *in vivo* would most likely result in increased degradation rates. Alternatively, if the initial

inflammatory response is correctly modulated (inflammatory cytokine concentrations in the peritoneal cavity peak within the first 24 hours after abdominal surgery),³⁸ drug release and physical presence may not be as important at later times and the polymer may not need to remain in the body for 10 days.

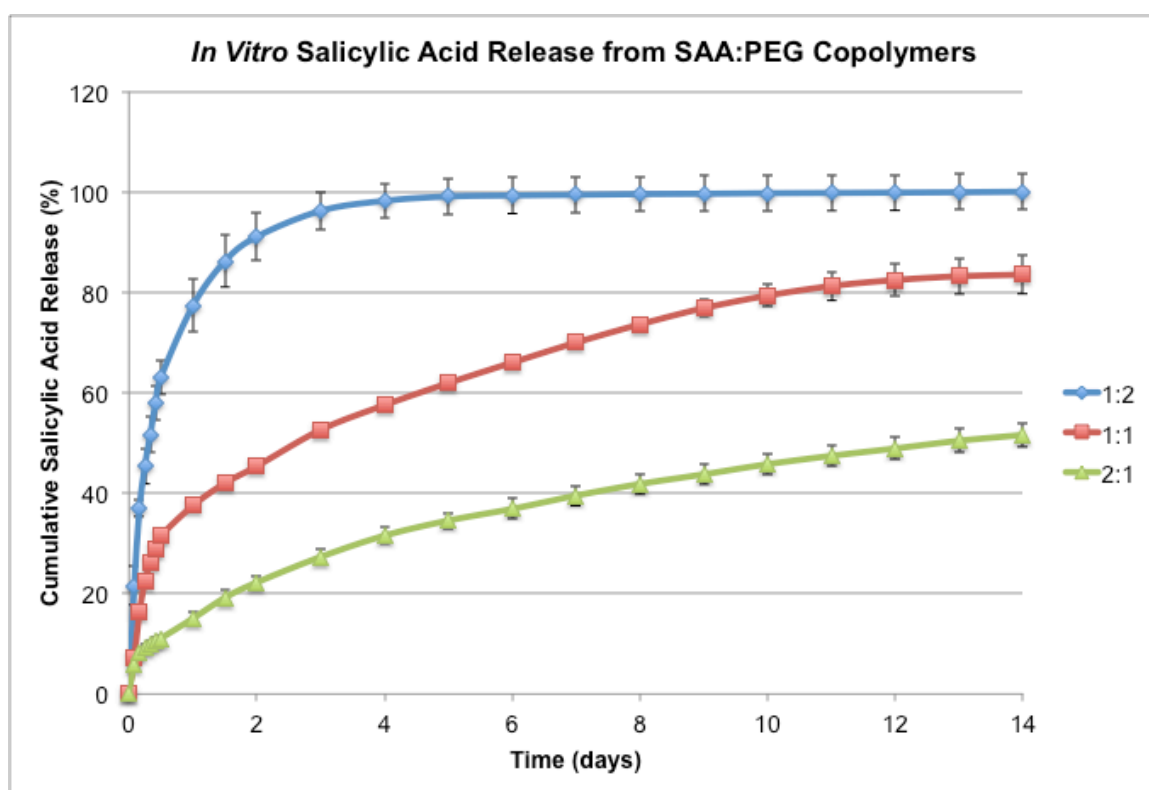


Figure 4.7. *In vitro* SA release from SAA:PEG copolymers.

4.3.7 Cytocompatibility

Copolymer (0.01 to 1 mg/mL) cytocompatibility was evaluated over 3 days (Figure 4.8). All polymers were cytotoxic when dissolved at 1 mg/mL, compared

to the 1 % DMSO control. The polymers with higher drug loading (1:1 and 2:1) were also toxic at 0.5 mg/mL. Below these levels, no significant toxicity over the three days was observed. It should be noted, however, that in these studies, the polymers were dissolved in solution, which increases polymer degradation rate compared to expected *in vivo* degradation.

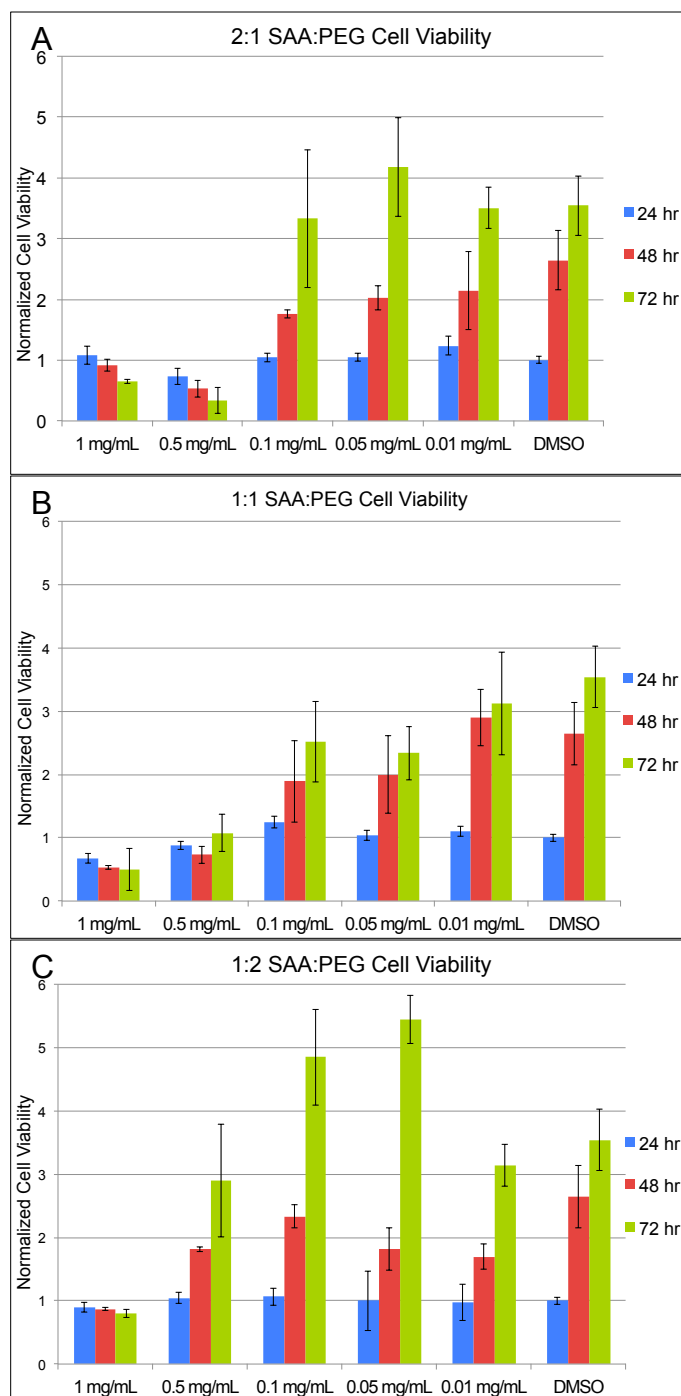


Figure 4.8. *In vitro* cell viability over 72 hours for cells exposed to SAA:PEG copolymers with ratios of 1:2 (a), 1:1 (b), and 2:1 (c) (* indicates significant decrease from DMSO control, $p < 0.05$). Cell viability was normalized to the DMSO control at 24 hours.

These levels of cytotoxicity are an important consideration for *in vivo* use. Rapid polymer degradation could lead to locally toxic effects if too much polymer is used or if the polymer is placed in an area of the body that could not absorb the polymer degradation products quickly. This rapid degradation should not pose a problem in the peritoneal cavity, where most problematic fibrous adhesions occur, as the peritoneal cavity absorbs fluids rapidly.⁴

4.3.8 Anti-inflammatory activity

Many inflammatory cytokines, such as TNF- α , can lead to adhesion cell phenotype differentiation.³⁸ Macrophages were exposed to 10 ng/mL LPS to elicit an immune response resulting in TNF- α secretion. ELISA was used to monitor the copolymer effect on macrophage TNF- α production. The copolymers exhibited TNF- α knockdown in a dose-dependent manner correlating with the amount of SA loading in the polymer (Figure 4.9). At 0.2 mg/mL, 2:1 and 1:1 copolymers significantly decreased TNF- α expression while the 1:2 copolymer reduced expression but not statistically significantly. Cytotoxicity assays were performed to confirm that TNF- α knockdown was not due to cell death (data not shown).

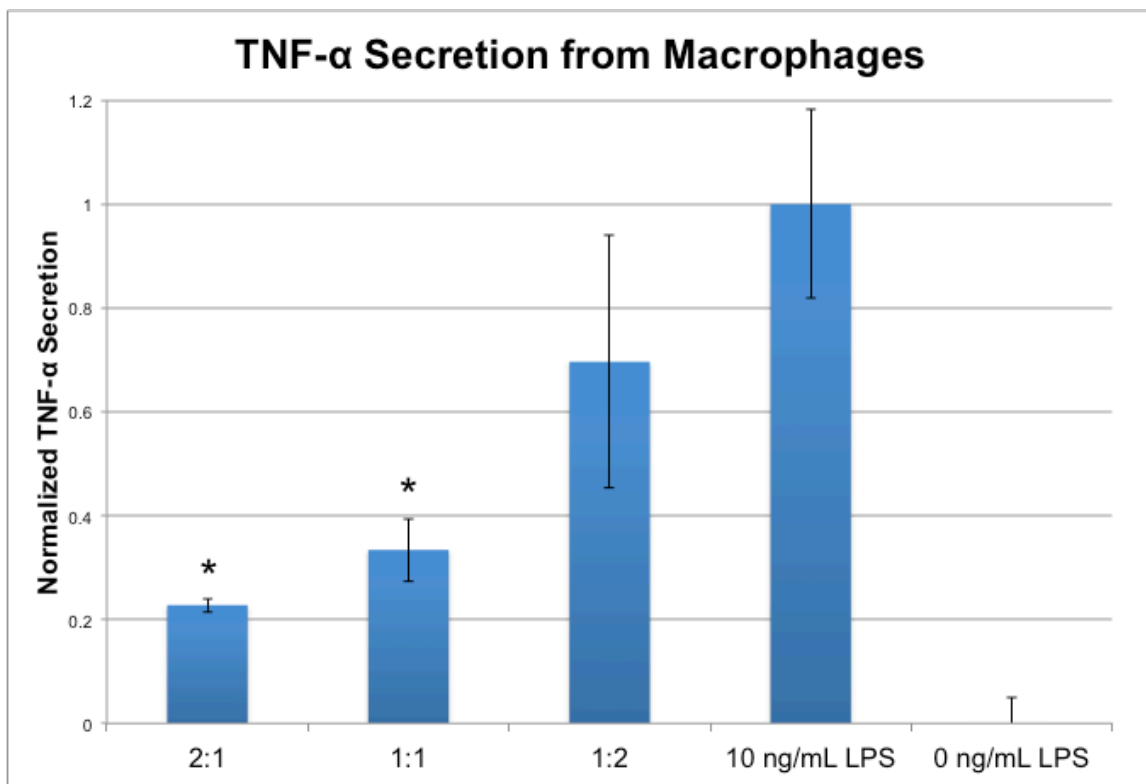


Figure 4.9. TNF- α expression by macrophages exposed to LPS and SAA:PEG copolymers (* indicates significant difference from 10 ng/mL LPS control, $p < 0.05$). TNF- α secretion was normalized to the LPS positive control (set to 1) and the LPS free control (set to 0).

4.4 Conclusion

Fibrous adhesions are a prevalent medical issue. Currently employed physical barrier devices and pharmaceutical regimens are not efficacious at preventing adhesion related complications.^{2, 4, 13} The SAA:PEG copolymers described herein combine these two approaches. The polymers could be used as an injectable barrier substance to physically prevent adhesion formation between tissue surfaces. They could also provide controlled, sustained SA release which

may be able to prevent fibroblast differentiation into the adhesion phenotype. While the mechanical and drug release properties of these biocompatible polymers suggest they would be effective adhesion barrier devices, subsequent studies are required to assess adhesion prevention efficacy *in vivo*.

4.5 References

1. Alpay Z, Saed GM, Diamond MP. Postoperative Adhesions: From Formation to Prevention. *Seminars in Reproductive Medicine*. 2008;26(4):313-21.
2. Tingstedt B, Isaksson K, Andersson E, Andersson R. Prevention of Abdominal Adhesions-Present State and What's beyond the Horizon? *Eur Surg Res*. 2007;39:259-68.
3. Ellis H, Moran BJ, Thompson JN, Parker MC, Wilson MS, Menzies D, et al. Adhesion-related hospital readmissions after abdominal and pelvic surgery: a retrospective cohort study. *The Lancet*. 1999;353:1476-80.
4. Ward BC, Panitch A. Abdominal Adhesions: Current and Novel Therapies. *Journal of Surgical Research*. 2011;165(1):91-111.
5. Stanciu D, Menzies D. The magnitude of adhesion-related problems. *The Association of Coloproctology of Great Britain and Ireland*. 2007;9(Supplement 2):35-8.
6. Al-Jaroudi D, Tulandi T. Adhesion Prevention in Gynecologic Surgery. *Obstetrical and Gynecological Survey*. 2004;59(5):360-7.
7. van der Krabben AA, Dijkstra FR, Nieuwenhuijzen M, Reijnen MMPJ, Schaapveld M, Van Goor H. Morbidity and mortality of inadvertent enterotomy during adhesiotomy. *British Journal of Surgery*. 2000;87:467-71.
8. Van Goor H. Consequences and complications of peritoneal adhesions. *The Association of Coloproctology of Great Britain and Ireland*. 2007;9(Supplement 2):25-34.

9. Pathogenesis, consequences, and control of peritoneal adhesions in gynecologic surgery. *Fertility and sterility*. 2008;90(5):S144-S9.
10. Moran BJ. Adhesion-related small bowel obstruction. *Colorectal disease : the official journal of the Association of Coloproctology of Great Britain and Ireland*. 2007;9 Suppl 2:39-44.
11. van der Wal JB, Jeekel J. Biology of the peritoneum in normal homeostasis and after surgical trauma. *Colorectal disease : the official journal of the Association of Coloproctology of Great Britain and Ireland*. 2007;9 Suppl 2:9-13.
12. Duron JJ. Postoperative intraperitoneal adhesion pathophysiology. *Colorectal disease : the official journal of the Association of Coloproctology of Great Britain and Ireland*. 2007;9 Suppl 2:14-24.
13. Alpay Z, Saed GM, Diamond MP. Postoperative adhesions: from formation to prevention. *Seminars in reproductive medicine*. 2008;26(4):313-21.
14. Wiseman DM, Pharm S MR. Disorders of Adhesions or Adhesion-Related Disorder: Monolithic Entities of Part of Aomething Bigger-CAPPS? *Seminal Reproductive Medicine*. 2008;26:356-68.
15. diZerga GS, Tulandi T. Prevention of intra-abdominal adhesions in gynaecological surgery. *Reproductive biomedicine online*. 2008;17(3):303-6.
16. Wilson MS. Practicalities and costs of adhesions. *Colorectal disease : the official journal of the Association of Coloproctology of Great Britain and Ireland*. 2007;9 Suppl 2:60-5. Epub 2007/10/27.
17. Wilson MS, Menzies D, Knight AD, Crowe AM. Demonstrating the clinical and cost effectiveness of adhesion reduction strategies. *Colorectal disease : the official journal of the Association of Coloproctology of Great Britain and Ireland*. 2002;4(5):355-60.
18. Erdmann L, Uhrich KE. Synthesis and degradation characteristics of salicylic acid-derived poly(anhydride esters). *Biomaterials*. 2000;21:1941-6.

19. Saed GM, Munkarah AR, Diamond MO. Cyclooxygenase-2 is expressed in human fibroblasts isolated from intraperitoneal adhesions but not from normal peritoneal tissues. *Fertility and sterility*. 2003;79(6):1404-8.
20. Golan A, Maymon R, Winograd I, Bukovsky I. Prevention of post-surgical adhesion formation using aspirin in a rodent model: a preliminary report. *Hum Reprod*. 1995;10(7):1797-800.
21. Muzii L, Marana R, Brunetti L, Margutti F, Vacca M, Mancuso S. Postoperative adhesion prevention with low-dose aspirin: effect through the selective inhibition of thromboxane production. *Hum Reprod*. 1998;13(6):1486-9.
22. Sandoval MA, Hernandez-Vaquero D. Preventing peridural fibrosis with nonsteroidal anti-inflammatory drugs. *European spine journal : official publication of the European Spine Society, the European Spinal Deformity Society, and the European Section of the Cervical Spine Research Society*. 2008;17(3):451-5.
23. O'Neil MJ, editor. *The Merck Index*. 14th ed. Whitehouse Station, NJ: Merck & Co., Inc.; 2006.
24. Schmeltzer RC, Anastasiou TJ, Uhrich KE. Optimized Synthesis of Salicylate-based Poly(anhydride-esters). *Polymer Bulletin*. 2003;49:441-8.
25. Prudencio A, Schmeltzer RC, Uhrich KE. Effect of Linker Structure on Salicylic Acid-Derived Poly(anhydride-esters). *Macromolecules*. 2005;38:6895-901.
26. Schmeltzer RC, Johnson M, Griffin J, Uhrich K. Comparison of salicylate-based poly(anhydride-esters) formed *via* melt-condensation *versus* solution polymerization. *Journal of Biomaterials Science: Polymer Edition*. 2008;19(10):1295-306.
27. Carbone AL, Uhrich KE. Design and Synthesis of Fast-Degrading Poly(anhydride-esters). *Macromolecular Rapid Communications*. 2009;30(12):1021.
28. Prudencio A, Schmeltzer RC, Uhrich KE. Effect of linker structure on salicylic acid-derived poly(anhydride-esters). *Macromolecules*. 2005;38(16):6895-901.

29. International A. Standard Practice for Direct Contact Cell Culture Evaluation of Materials for Medical Devices. ASTM F813. West Conshohocken, PA2012.
30. Kim J, Hematti P. Mesenchymal stem cell-educated macrophages: A novel type of alternatively activated macrophages. *Experimental Hematology*. 2009;37(12):1445-53.
31. Tziampazis E, Kohn J, Moghe PV. PEG-variant biomaterials as selectively adhesive protein templates: model surfaces for controlled cell adhesion and migration. *Biomaterials*. 2000;21(5):511-20.
32. Brostow W, Chiu R, Kalogeras IM, Vassilikou-Dova A. Prediction of glass transition temperatures: Binary blends and copolymers. *Materials Letters*. 2008;62(17-18):3152-5.
33. Hou S, McCauley LK, Ma PX. Synthesis and Erosion Properties of PEG-Containing Polyanhydrides. *Macromolecular Bioscience*. 2007;7(5):620-8.
34. Vogel B, Mallapragada S. Synthesis of novel biodegradable polyanhydrides containing aromatic and glycol functionality for tailoring of hydrophilicity in controlled drug delivery devices. *Biomaterials*. 2005;26(7):721-8.
35. Cai Q, Zhu KJ, Zhang J. Salicylic Acid and PEG-Contained Polyanhydrides: Synthesis, Characterization, and In Vitro Salicylic Acid Release. *Drug Delivery*. 2005;12(2):97-102.
36. diZerega GS, Cortese S, Rodgers KE, Block KM, Falcone SJ, Juarez TG, et al. A modern biomaterial for adhesion prevention. *Journal of Biomedical Materials Research Part B: Applied Biomaterials*. 2007;81B(1):239-50.
37. Ouimet MA, Snyder SS, Uhrich KE. Tunable drug release profiles from salicylate-based poly(anhydride-ester) matrices using small molecule admixtures. *Journal of Bioactive and Compatible Polymers*. 2012;27(6):540-9.
38. Sammour T, Kahokehr A, Soop M, Hill AG. Peritoneal Damage: The Inflammatory Response and Clinical Implications of the Neuro-Immuno-Humoral Axis. *World Journal of Surgery*. 2010;34(4):704-20.

5. TUNEABLE DRUG RELEASE PROFILES FROM SALICYLATE-BASED POLY(ANHYDRIDE-ESTER) MATRICES USING SMALL MOLECULE ADMIXTURES

5.1 Introduction

Salicylic acid (SA), the major metabolite of aspirin, has been used for centuries for its analgesic, anti-inflammatory, and antipyretic effects.¹ Recently, SA has been found to be beneficial for many other applications such as wound healing, diabetes, arthritis, and cancer treatment.²⁻⁶ The best results are obtained when SA is maintained at therapeutic levels at the desired area for as long as it is needed.⁷ Oral SA delivery is systemic and potentially causes gastrointestinal problems, while not maintaining steady SA concentrations at the desired location.⁸ Localized delivery from polymers can help overcome undesired side effects and allow for higher localized SA levels than systemic delivery.^{9, 10}

Previous attempts to control localized SA release involve the physical mixture of SA into a biodegradable polymer matrix.¹¹⁻¹⁵ This type of drug incorporation, however, generally results in a burst of SA,¹¹⁻¹⁴ where large amounts of drug are released before the rate stabilizes.¹⁶ Burst profiles of drugs are unpredictable,¹⁶ and can lead to toxic SA concentrations. Additionally, maximum drug loading is limited before the drug affects matrix mechanical and degradation properties.¹¹

Many drug-eluting polymer matrices exhibit a burst release and fail to sustain drug release for the duration polymer degradation.¹¹⁻¹⁴ Wang *et al.* have demonstrated sustained release with minimal control over the degradation profile by altering polymer composition. Although the authors were able to obtain zero-order release, the amount of SA required to achieve this (40% in poly(lactic-co-glycolic acid) (PLGA)) significantly increased polymer degradation rates.¹⁵

To better control SA concentrations, salicylate-based poly(anhydride-esters) (SAPAEs) were developed in which SA is chemically incorporated into the polymer backbone via a biocompatible linker molecule. These polymers have been studied both *in vitro*^{17, 18} and *in vivo*,^{19, 20} have been found to be biocompatible, and result locally reduce inflammation.²¹ They hydrolytically degrade to provide near zero-order SA release after an initial lag period, when minimal-to-no drug is released. SAPAEs are designed to fully degrade over a matter of days to many months.^{22, 23} The chemical SA incorporation enables inherent drug loading capacities up to 85% (w/w), with the ability to physically admix additional drug to obtain even higher loading.²⁴

The lag period length and the subsequent release rate is a direct function of the linker structure as shown for various polyanhydrides.^{23, 25, 26} Polymers with linear aliphatic linkers release SA faster with a shorter lag period than those comprised of branched aliphatic linkers.²³ Diethylmalonic acid, a branched aliphatic linker was chosen for this study (Figure 5.1) as previous studies indicated this SAPAE had a lag period longer than 1 week.²⁷

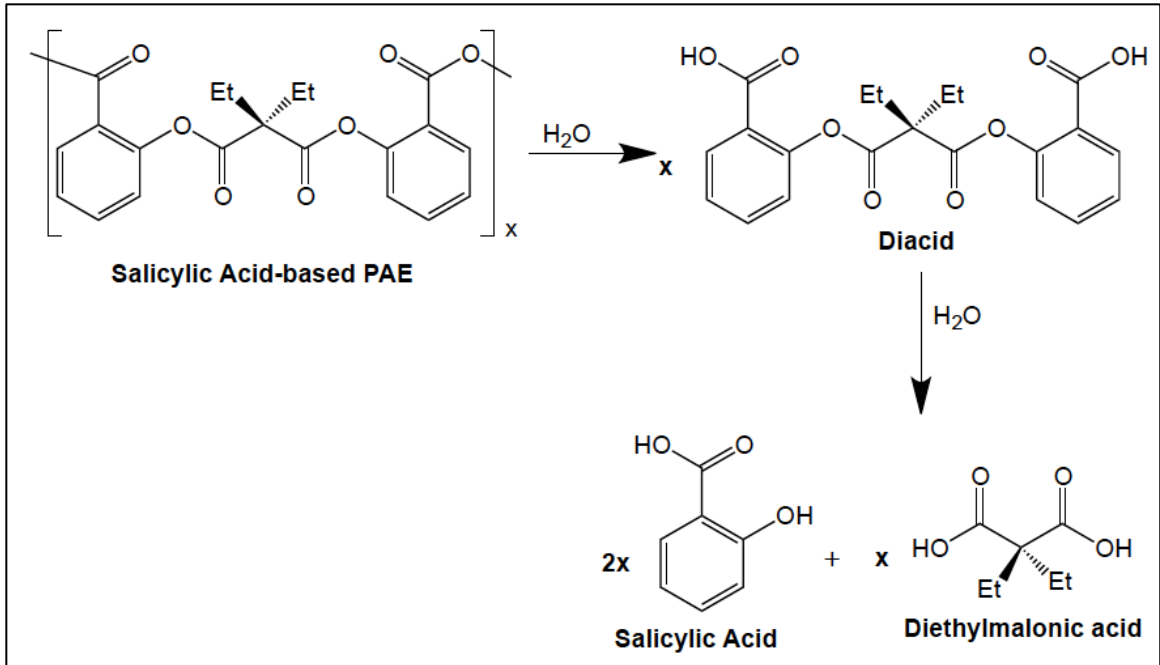


Figure 5.1. Hydrolytic degradation scheme of the SAPAE that releases SA and diethylmalonic acid.

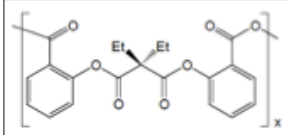
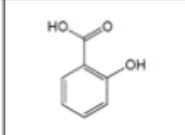
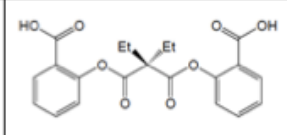
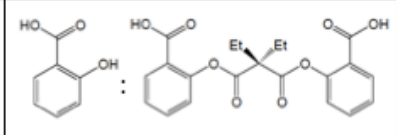
While the SAPAE release rate can be easily changed for different applications via the linker molecule, the lag period is an important consideration. A lag period may be beneficial for applications, such as bone regeneration, where an initial inflammatory response is desired and localized reduced inflammation is beneficial at a later time point.^{28, 29} On the other hand, a lag period could be a disadvantage if SA was desired immediately following implantation, as for instances where inflammation is already present (e.g., arthritis and diabetes).

One method used to adjust lag period length is admixing small molecules into the polymer matrix to act as channeling agents.³⁰ As these channeling agents are solubilized, pores are created in the disc surface, increasing water

penetration and subsequent polymer degradation.³¹ This effect has been observed using salt leaching techniques,³² as well as admixing molecules such as drugs^{15, 33} or inert polymer precursors into the polymer matrix.^{34, 35} For example, PLGA monomers (10% w/w) acting as channeling agents in drug-loaded PLGA discs resulted in the absence of a lag period in drug release.³⁵

To overcome the SAPAE lag period, free SA and a degradable polymer precursor, hereafter referred to as diacid (Figure 5.1), were physically admixed with the SAPAE at different ratios and weight percentages as described in Table 5.1. The SAPAE chosen was comprised of a branched, aliphatic linker (diethylmalonic acid) exhibiting a lag period of approximately 11 days. Polymer and admixed drugs were compressed into discs and drug release was monitored *in vitro* for 30 days. The admixture effects on drug release and thermal properties of the polymer matrices were determined.³⁶

Table 5.1. Representation of 1, 5, and 10 % (w/w) admixtures used for various sample disc compositions.

Polymer Alone	SA 1, 5, and 10 % (w/w)	Diacid 1, 5, and 10 % (w/w)	SA:Diacid (1:1) 1, 5, and 10 % (w/w)
			

5.2 Materials and Methods

5.2.1 Materials

Acetic anhydride was purchased from Fisher (Fair Lawn, NJ). All other chemicals and reagents were purchased from Sigma-Aldrich (Milwaukee, WI) and used as received.

5.2.2 Polymer synthesis and characterization

SAPAE was synthesized according to previously described methods.^{23, 37, 38} In short, SA (2 equivalents (eq)) was dissolved in tetrahydrofuran (THF) and pyridine (4 eq). Diethylmalonyl chloride (1 eq) was dissolved in THF and added drop-wise forming a white suspension. The reaction mixture was stirred overnight, quenched over water and acidified to pH 2 using concentrated hydrochloric acid. The precipitate was filtered, washed with water (3 x 250 mL), and dried *in vacuo* to yield diacid. Diacid was activated in an excess of acetic anhydride at room temperature, concentrated, and polymerized via melt-condensation polymerization at 180 °C for 6 h at 160 rpm. The reaction was cooled to room temperature, dissolved in minimal (~ 10 mL) dichloromethane and precipitated over diethyl ether (~ 500 mL). The solvent was decanted and the precipitate was dried *in vacuo* to yield a tan powder. The resulting polymer had a weight average molecular weight (M_w) of 15,600, PDI of 1.7, and T_g of 88 °C.

5.2.3 Disc preparation

SA, diacid, and SA:diacid (1:1 by weight) mixture were separately mixed with polymer at 1, 5, and 10 % (w/w) (Table 5.1) and ground with mortar and pestle to achieve a homogenous mixture. Polymer discs were prepared by pressing ground polymer mixtures (160 ± 5 mg) into 13 mm diameter x 1 ± 0.5 mm thick discs in an IR pellet die (International Crystal Laboratories, Garfield, NJ) with a bench-top hydraulic press (Carver model M, Wabash, IN) at 10,000 psi for 5 min at room temperature. Discs were prepared in triplicate to give a total of 30 discs.

5.2.4 Hydrolytic degradation

Discs were placed in 20 mL Wheaton glass scintillation vials containing 10 mL 0.1 M phosphate buffered saline (PBS) at pH 7.4. Samples were incubated at 37 °C with agitation at 60 rpm in a controlled environment incubator shaker (New Brunswick Scientific Co., Excella E25, Edison, NJ). All samples were studied in triplicate. Media was collected and replaced with fresh PBS (10 mL) at pre-designated time points for 30 days. Spent media was analyzed by UV spectrophotometry using a Perkin Elmer Lambda XLS spectrophotometer (Waltham, MA) to specifically monitor SA release. Measurements were obtained at $\lambda = 303$ nm, the maximum absorbance of SA that did not overlap with other polymer degradation products. Data were calculated against a calibration curve of absorbance values from standard solutions of known SA concentrations in

PBS. All pH measurements were performed using an Accumet® AR15 pH meter (Fisher Scientific, Fair Lawn, NJ).

5.2.5 Influence of admixtures on glass transition temperature

Differential scanning calorimetry (DSC, Thermal Advantage Q200) was performed on all samples prior to degradation to monitor the T_g of all polymer systems as deformation after implantation may affect drug release *in vivo* due to the changes in surface area for these surface-eroding polymers. Samples (3-8 mg) were analyzed by heating under nitrogen gas. Data were collected at heating and cooling rates of 10 °C/min from -10 °C to 200 °C with a two-cycle minimum. TA Instruments Universal Analysis 2000 software, version 4.5A was used to analyze the data. T_g s were calculated as half C_p extrapolated.

5.3 Results and Discussion

Free SA and diacid were physically admixed into SAPAE matrices to attain immediate drug release commonly observed with physical mixtures¹⁶ with the zero-order characteristics of SAPAEs. Addition of these molecules at all weight percentages increased SA release during the typical lag period of polymer alone while having little effect on the release rate at later times. The amount of SA released was dependent upon both the type of molecules admixed and the weight percentage within the matrix (Table 5.2 and Figure 5.2).

Table 5.2. Theoretical Drug Loading of Samples

Admixture Type	None	SA			Diacid			SA:Diacid (1:1)		
Admixture Amount (%)	—	1	5	10	1	5	10	1	5	10
Drug Loading (%)	72.2	72.5	73.6	75.0	72.2	72.1	71.9	72.4	72.9	73.5

5.3.1 *In vitro* SA release

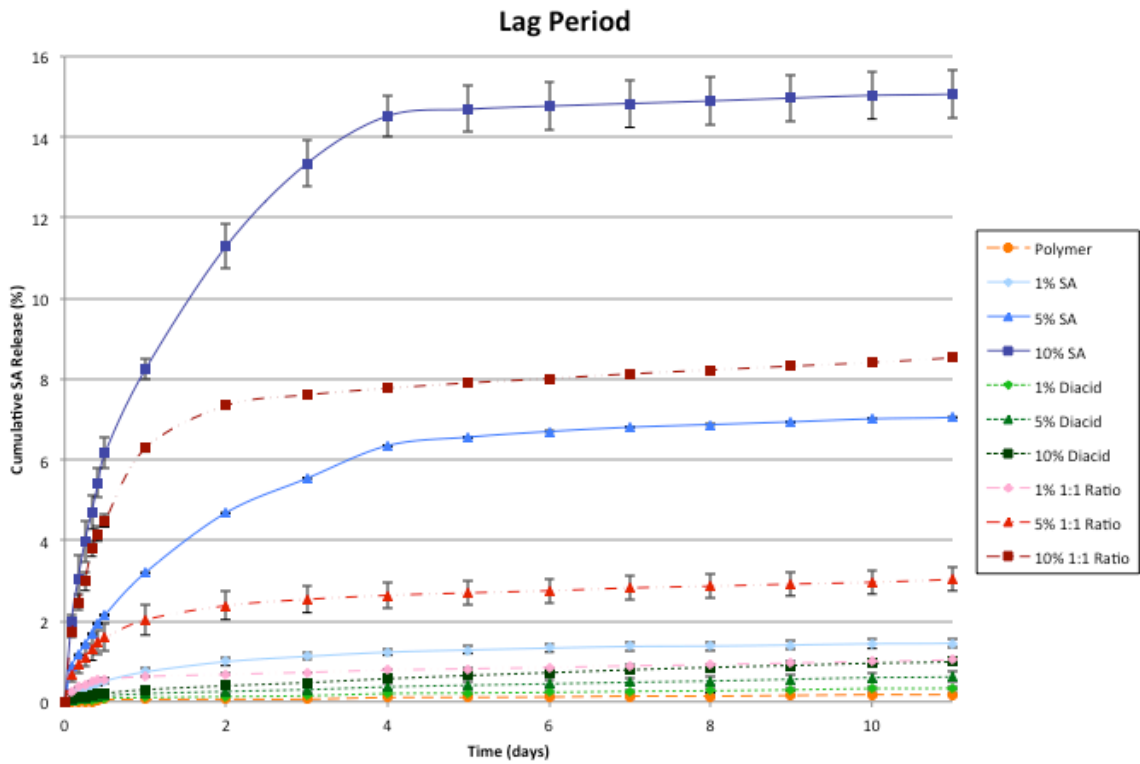


Figure 5.2. SA release profiles during the typical lag period of 0-11 days for the polymer alone and against 1, 5, and 10 % (w/w) admixtures (b).

In vitro drug release was measured by quantifying the SA concentrations in PBS over 30 days using UV spectrophotometry. The inflection points in the profiles for the polymer alone was used to define the lag period and subsequent

period of zero-order drug release. The polymer alone (Figure 5.2) displayed a lag period of 11 days. The pH of spent media was monitored through the lag periods with the greatest pH differential observed as 0.6, which should have negligible effects on polymer degradation rates. As shown in Figure 5.2, the lag period for polymer alone was overcome by all admixtures within the first 24 hours where SA samples exhibited the highest SA concentration for their respective weight percentages, followed by the 1:1 mixture, and then diacid.

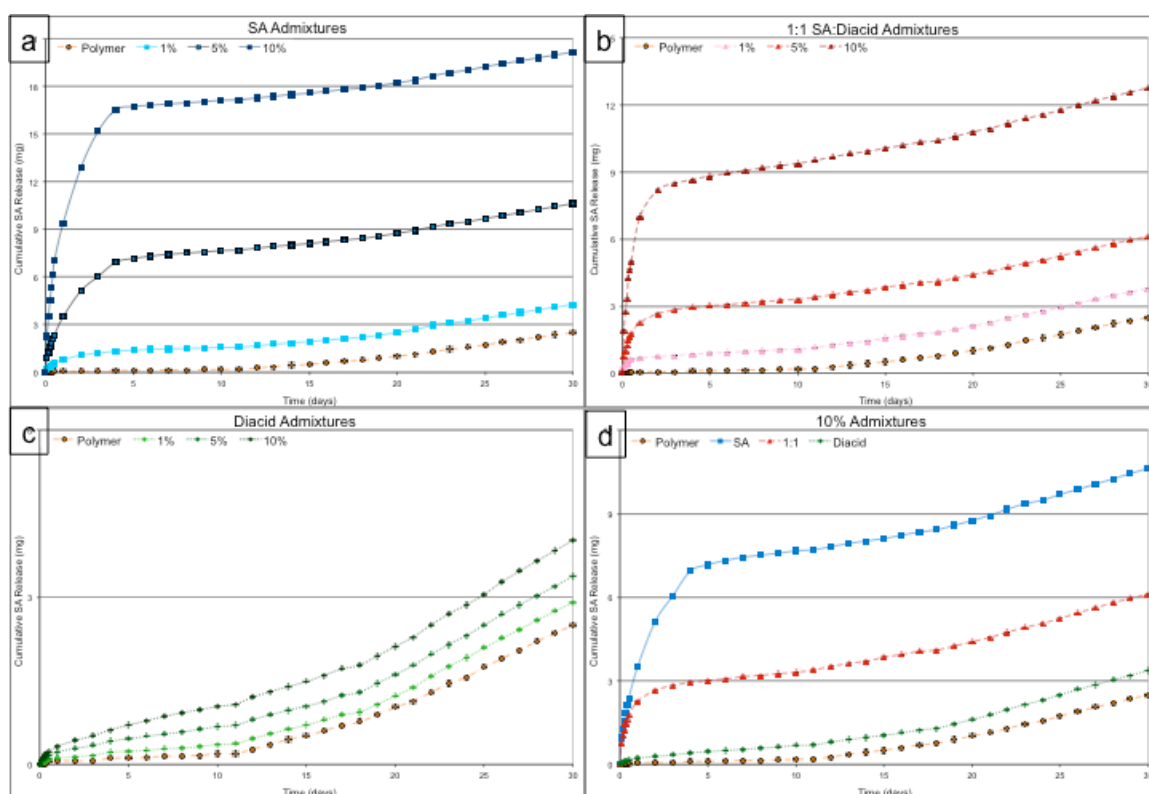


Figure 5.3. Cumulative release profiles of polymer and 1 %, 5 %, and 10 % (w/w) admixtures of SA (a), SA:diacid combination (b), and diacid (c) over 30 days. A comparison of the three different admixtures at the same weight percentage (10% w/w) is also shown (d).

The effect of the various small molecules on early SA release was well defined. Changes in weight percentage had the greatest effect on SA-loaded samples and the least on diacid samples (Figure 5.3a-c) as determined by SA released during the lag period. In addition, each admixture sample exhibited distinct profiles of increased drug release. When SA was incorporated, SA release was increased for 4 days at all weight percentages, while 1:1 SA:diacid mixtures exhibit increased SA over 2 days, with diacid samples exhibiting slightly increased SA for less than a day before the rates decrease and stabilize. The differences in time frame were likely due to the additional hydrolysis steps needed to obtain SA from the diacid. After these initial periods, all admixtures maintained near zero-order profiles (Figure 5.3d), with a post-lag period average of 0.11 ± 0.03 % SA released per day from the polymer alone and 0.13 ± 0.04 % SA per day combined average for all admixtures.

It is important to note that the samples in this study were compression-molded into discs. If these systems were formulated into fibers or microspheres, for example, the release profiles would likely differ as the geometry affects the erosion characteristics of the polyanhydride matrix.^{39, 40} *In vivo* results may also differ as the degradation media does not contain enzymes or other proteins.

5.3.2 Admixture effect on glass transition temperature

The incorporation of small molecules into a polymer matrix often alters the thermal properties.⁴¹ DSC measurements indicate a T_g of 88 °C for the polymer.

A characteristic lowering of the T_g was noted as the weight percentage of additive increased (Figure 5.4). This observation is consistent with previously reported results on diffusion-controlled drug release from polymers, where the admixed small molecules act as plasticizers.⁴¹ This aspect constrains the maximum weight percent for some SAPAEs as the device may not retain its shape *in vivo* if the T_g of a polymeric device is near or below physiological temperature (37 °C). Deformation after implantation could alter the surface area, resulting in unpredictable drug release since these PAEs are primarily surface-eroding.⁴²

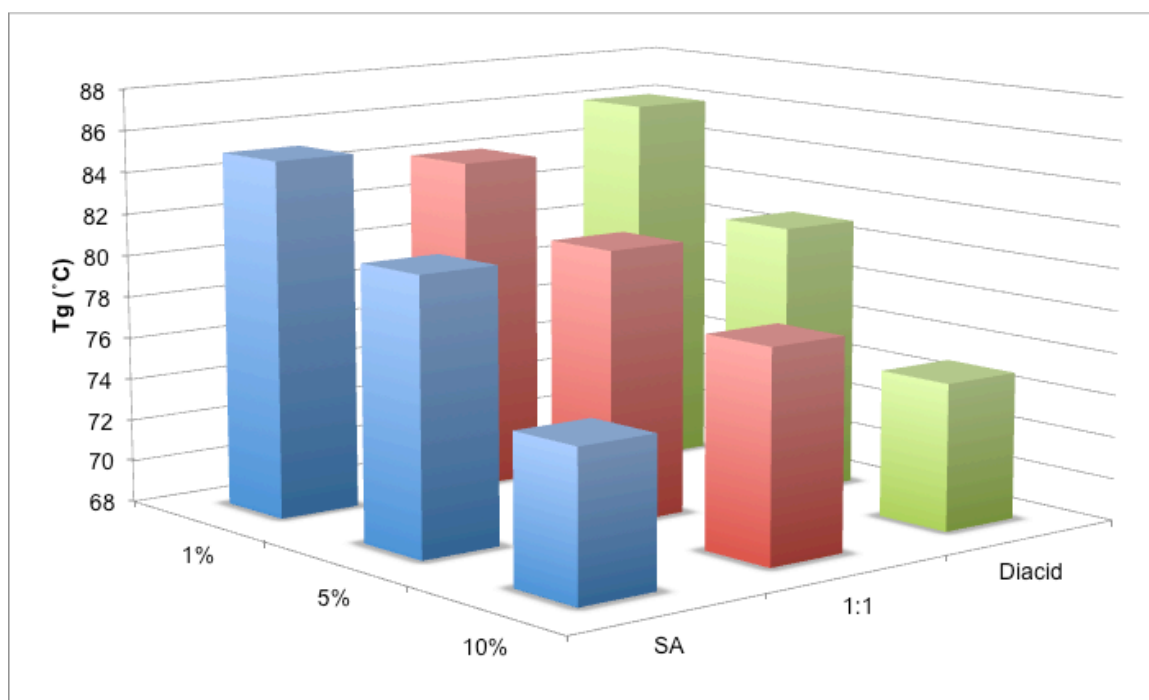


Figure 5.4. Glass transition temperatures measured for all samples. The highest point on the y-axis corresponds with the T_g of polymer alone.

5.4 Conclusions

As an anti-inflammatory drug, SA can be useful for the treatment of many diseases. Furthermore, localized, sustained SA release can both minimize side effects and improve patient compliance. To develop a polymeric device that would ensure the desired amount of SA is being released at any given time, SA and diacids were used as channeling agents to alter the polymer release profile and overcome the lag period. The duration as well as the amount of SA at early and late time points was controlled by adjusting multiple factors: polymer composition via the linker molecule, weight ratio of admixed molecules, and ratios of those molecules. With this ability to fine-tune the amount of SA present at various times over sustained periods, devices can be prepared that fit the specific needs of many different applications.

5.5 References

1. Wu KK. Aspirin and salicylate: An old remedy with a new twist. *Circulation*. 2000;102(17):2022-3.
2. Roseborough IE, Grevious MA, Lee RC. Prevention and treatment of excessive dermal scarring. *J Natl Med Assoc*. 2004;96(1):108-16.
3. Rumore MM, Kim KS. Potential role of salicylates in type 2 diabetes. *Ann Pharmacother*. 2010;44(7-8):1207-21.
4. Yamazaki R, Kusunoki N, Matsuzaki T, Hashimoto S, Kawai S. Aspirin and sodium salicylate inhibit proliferation and induce apoptosis in rheumatoid synovial cells. *J Pharm Pharmacol*. 2002;54(12):1675-9.
5. Perugini RA, McDade TP, Vittimberga FJ, Jr., Duffy AJ, Callery MP. Sodium salicylate inhibits proliferation and induces G1 cell cycle arrest in human pancreatic cancer cell lines. *J Gastrointest Surg*. 2000;4(1):24-32.

6. Spitz GA, Furtado CM, Sola-Penna M, Zancan P. Acetylsalicylic acid and salicylic acid decrease tumor cell viability and glucose metabolism modulating 6-phosphofructo-1-kinase structure and activity. *Biochem Pharmacol.* 2009;77(1):46-53.
7. Uhrich KE, Cannizzaro SM, Langer RS, Shakesheff KM. Polymeric systems for controlled drug release. *Chemical reviews.* 1999;99(11):3181-98.
8. Amann R, Peskar BA. Anti-inflammatory effects of aspirin and sodium salicylate. *Eur J Pharmacol.* 2002;447(1):1-9.
9. Domb AJ. Polymeric carriers for regional drug therapy. *Molecular medicine today.* 1995;1(3):134-9.
10. Jain JP, Modi S, Domb AJ, Kumar N. Role of polyanhydrides as localized drug carriers. *Journal of Controlled Release.* 2005;103(3):541-63.
11. Tang Y, Singh J. Controlled delivery of aspirin: effect of aspirin on polymer degradation and in vitro release from PLGA based phase sensitive systems. *Int J Pharm.* 2008;357(1-2):119-25.
12. Tada D, Tanabe T, Tachibana A, Yamauchi K. Drug release from hydrogel containing albumin as crosslinker. *Journal of Bioscience and Bioengineering.* 2005;100(5):551-5.
13. Hu Y, Zhou X, Lu Y, Hu C, Hu X. Novel biodegradable hydrogels based on pachyman and its derivatives for drug delivery. *Int J Pharm.* 2009;371(1-2):89-98.
14. Wenk E, Wandrey AJ, Merkle HP, Meinel L. Silk fibroin spheres as a platform for controlled drug delivery. *J Control Release.* 2008;132(1):26-34.
15. Wang Q, Zhang N, Hu X, Yang J, Du Y. Chitosan/polyethylene glycol blend fibers and their properties for drug controlled release. *Journal of biomedical materials research Part A.* 2008;85(4):881-7.
16. Huang X, Brazel CS. On the importance and mechanisms of burst release in matrix-controlled drug delivery systems. *Journal of Controlled Release.* 2001;73(2-3):121-36.

17. Schmeltzer RC, Johnson M, Griffin J, Uhrich K. Comparison of salicylate-based poly(anhydride-esters) formed via melt-condensation versus solution polymerization. *Journal of biomaterials science Polymer edition*. 2008;19(10):1295-306.
18. Griffin J, Delgado-Rivera R, Meiners S, Uhrich KE. Salicylic acid-derived poly(anhydride-ester) electrospun fibers designed for regenerating the peripheral nervous system. *Journal of Biomedical Materials Research Part A*. 2011;97A(3):230-42.
19. Erdmann L, Macedo B, Uhrich KE. Degradable poly(anhydride ester) implants: effects of localized salicylic acid release on bone. *Biomaterials*. 2000;21(24):2507-12.
20. Harten RD, Svach DJ, Schmeltzer R, Uhrich KE. Salicylic acid-derived poly(anhydride-esters) inhibit bone resorption and formation in vivo. *Journal of biomedical materials research Part A*. 2005;72(4):354-62.
21. Reynolds MA, Prudencio A, Aichelmann-Reidy ME, Woodward K, Uhrich KE. Non-steroidal anti-inflammatory drug (NSAID)-derived poly(anhydride-esters) in bone and periodontal regeneration. *Current drug delivery*. 2007;4(3):233-9.
22. Carbone AL, Uhrich KE. Design and Synthesis of Fast-Degrading Poly(anhydride-esters). *Macromolecular rapid communications*. 2009;30(12):1021.
23. Prudencio A, Schmeltzer RC, Uhrich KE. Effect of Linker Structure on Salicylic Acid-Derived Poly(anhydride-esters). *Macromolecules*. 2005;38(16):6895-901.
24. Johnson ML, Uhrich KE. Concurrent release of admixed antimicrobials and salicylic acid from salicylate-based poly(anhydride-esters). *Journal of biomedical materials research Part A*. 2009;91(3):671-8.
25. Vogel B, Mallapragada S. Synthesis of novel biodegradable polyanhydrides containing aromatic and glycol functionality for tailoring of hydrophilicity in controlled drug delivery devices. *Biomaterials*. 2005;26(7):721-8.

26. Torres MP, Vogel BM, Narasimhan B, Mallapragada SK. Synthesis and characterization of novel polyanhydrides with tailored erosion mechanisms. *Journal of Biomedical Materials Research Part A*. 2006;76A(1):102-10.
27. Prudencio A, Schmeltzer RC, Uhrich KE. Effect of linker structure on salicylic acid-derived poly(anhydride-esters). *Macromolecules*. 2005;38(16):6895-901.
28. Mountziaris PM, Mikos AG. Modulation of the Inflammatory Response for Enhanced Bone Tissue Regeneration. *Tissue Engineering Part B: Reviews*. 2008;14(2):179-86.
29. Simon AM, O'Connor JP. Dose and Time-Dependent Effects of Cyclooxygenase-2 Inhibition on Fracture-Healing. *The Journal of Bone and Joint Surgery*. 2007;89(3):500-11.
30. Gonzalez-Rodriguez ML, Perez-Martinez JI, Merino S, Fini A, Rabasco AM. Channeling agent and drug release from a central core matrix tablet. *Drug Dev Ind Pharm*. 2001;27(5):439-46.
31. Shen E, Kipper MJ, Dziadul B, Lim MK, Narasimhan B. Mechanistic relationships between polymer microstructure and drug release kinetics in bioerodible polyanhydrides. *J Control Release*. 2002;82(1):115-25.
32. Sibambo SR, Pillay V, Choonara YE, Penny C. A Novel Salted-out and Subsequently Crosslinked Poly(Lactic-co-Glycolic Acid) Polymeric Scaffold Applied to Monolithic Drug Delivery. *Journal of Bioactive and Compatible Polymers*. 2008;23(2):132-53.
33. Kishida A, Goto H, Murakami K, Kakinoki K, Akashi M, Endo T. Polymer Drugs and Polymeric Drugs IX. Synthesis and 5-Fluorouracil Release Profiles of Biodegradable Polymeric Prodrugs γ -Poly(α -Hydroxymethyl-5-Fluorouracil-Glutamate). *Journal of Bioactive and Compatible Polymers*. 1998;13(3):222-33.
34. Kim JM, Seo KS, Jeong YK, Lee HB, Kim YS, Khang G. Co-effect of aqueous solubility of drugs and glycolide monomer on in vitro release rates from poly(D,L-lactide-co-glycolide) discs and polymer degradation. *Journal of Biomaterials Science, Polymer Edition*. 2005;16(8):991-1007.

35. Yoo JY, Kim JM, Khang G, Kim MS, Cho SH, Lee HB, et al. Effect of lactide/glycolide monomers on release behaviors of gentamicin sulfate-loaded PLGA discs. *International Journal of Pharmaceutics*. 2004;276(1-2):1-9.
36. Ouimet MA, Snyder SS, Uhrich KE. Tunable drug release profiles from salicylate-based poly(anhydride-ester) matrices using small molecule admixtures. *Journal of Bioactive and Compatible Polymers*. 2012;27(6):540-9.
37. Erdmann L, Uhrich KE. Synthesis and degradation characteristics of salicylic acid-derived poly(anhydride-esters). *Biomaterials*. 2000;21(19):1941-6.
38. Schmeltzer RC, Schmalenberg KE, Uhrich KE. Synthesis and cytotoxicity of salicylate-based poly(anhydride esters). *Biomacromolecules*. 2005;6(1):359-67.
39. Göpferich A, Tessmar J. Polyanhydride degradation and erosion. *Advanced Drug Delivery Reviews*. 2002;54(7):911-31.
40. Akbari H, D'Emanuele A, Attwood D. Effect of geometry on the erosion characteristics of polyanhydride matrices. *International Journal of Pharmaceutics*. 1998;160(1):83-9.
41. Siepmann F, Le Brun V, Siepmann J. Drugs acting as plasticizers in polymeric systems: a quantitative treatment. *J Control Release*. 2006;115(3):298-306.
42. Whitaker-Brothers K, Uhrich K. Investigation into the erosion mechanism of salicylate-based poly(anhydride-esters). *Journal of Biomedical Materials Research Part A*. 2006;76A(3):470-9.

6. APPENDIX: IN VITRO DEGRADATION OF AN AROMATIC POLYANHYDRIDE WITH ENHANCED THERMAL PROPERTIES

6.1 Introduction

Polyanhydrides have successfully been utilized as drug delivery systems due to their excellent biocompatibility, controlled erosion, and ability to encapsulate sensitive bioactives.¹⁻³ Polyanhydride use as polymer matrices for the drugs delivery has been widely studied because polyanhydrides typically exhibit surface erosion, thereby resulting in more stable drug release than other polymer classes, such as polyesters, which exhibit bulk degradation.^{1, 4}

The two most commonly studied polyanhydrides studied are the linear aliphatic poly(sebacic acid) (SA) and the aromatic poly[1,3-bis-(*para*-carboxyphenoxy)propane] (*p*CPP).¹⁻³ Although *p*CPP fully degrades over three years, it is insoluble in common organic solvents and has high glass transition (T_g) and melting (T_m) temperatures, leading to difficulty in device fabrication.^{1, 3} SA has greater solubility and a lower T_g and T_m , but it degrades completely in a matter of days.⁵

Gliadel[®], an implantable device to control chemotherapeutic drugs delivery to treat brain cancer, is a *p*CPP:SA (20:80) copolymer.⁶ This *p*CPP:SA combination is commonly used to adjust the solubility, thermal properties, and polymer degradation rates.¹ However, this technique does not provide polymers with optimal properties as *p*CPP:SA copolymers with a high SA content still degrade within a few days, and copolymers with a high *p*CPP content have T_g s

below physiologic temperature. These low temperatures are advantageous for processing, but can be a problem if the polymer is to be used as a biomaterial as they deform when placed in the body. For drug delivery devices, the inability to retain a shape over time does not allow for accurate drug release rate calculations.⁷ Hence, polymers with T_g s above physiological temperature are desired for their ability to retain their mechanical integrity *in vivo*.

An aromatic polyanhydride, poly[α,α' -bis(*ortho*-carboxyphenoxy)-*para*-xylene] (oCPX), was previously synthesized by melt-condensation polymerization methods.⁸ This polymer is being studied as a potential biomaterial and drug delivery matrix because it is soluble in organic solvents and the T_g value falls within a practical range for thermal processability, approximately 68 °C, while still being above physiological temperatures.⁸ It is these solubility and thermal characteristics that permit the facile fabrication of geometries such as microspheres, fibers, or films that can be of use in biomedical applications.

Because poly(oCPX) is an aromatic polyanhydride, it is expected to have a slower degradation rate than linear aliphatic polyanhydrides.³ This study reports the changes that occur during hydrolytic degradation of oCPX. The polymers and their degradation products were evaluated via several methods: polymer matrix mass loss after *in vitro* degradation, high pressure liquid chromatography (HPLC) analysis of polymer degradation products, UV analysis of polymer degradation concentration, and scanning electron microscopy (SEM) analysis of the degraded polymer discs. The polymer was also tested for stability

to common sterilization techniques and polymer degradation products were tested for cytotoxicity.

6.2 Materials and Methods

6.2.1 Materials

Acetic anhydride used to synthesize the polymer was purchased from Fischer (Fair Lawn, NJ). All other chemicals and reagents were purchased from Sigma-Aldrich (Milwaukee, WI) and used as received.

6.2.2 Polymer synthesis and characterization

The polymer was synthesized by methods previously reported (summarized in Figure 6.1 below),⁸ resulting in a polymer with a weight averaged molecular weight = 5600 Da, a polydispersity = 2.1, and a T_g = 68 °C. The melting temperature (T_m) previously reported⁸ was found to be due to impurities, as the poly(oCPX) used in this study did not exhibit a T_m . The originally reported T_m = 114 °C for poly(oCPX) is near the oCPX methyl ester precursor T_m = 120-122 °C.

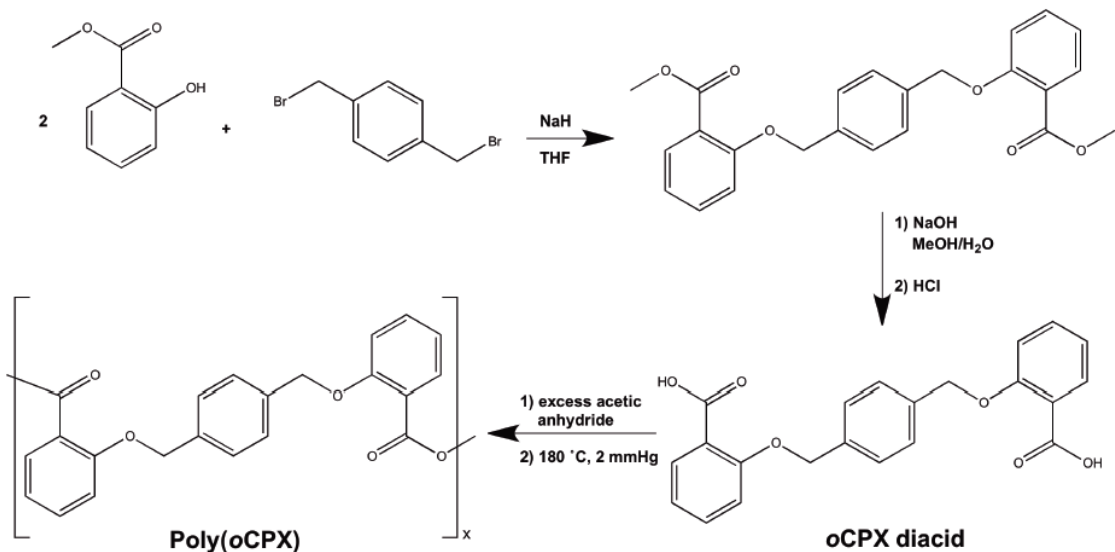


Figure 6.1. Poly(oCPX) synthesis.⁸

6.2.3 Polymer *in vitro* degradation

Polymer discs were prepared by compressing finely ground polymer (~150 mg) into discs (13 mm diameter x ~1 mm thick) using a hydraulic press (Carver (Model M), Garfield, NJ). A 10,000 psi force was applied for 10 minutes at room temperature. Degradation media consisted of phosphate buffered saline (PBS) at pH 7.4 prepared from Sigma-Aldrich PBS tablets. Hydrolytic degradation was conducted in triplicate by placing polymer discs in 10 mL PBS in glass scintillation vials. Samples were placed in an incubator shaker (37°C, 60 rpm). Every 5 days the media was replaced with fresh PBS. Collected media was analyzed for degradation products and their concentrations. After 90 days, the polymer disc remains were collected, rinsed with deionized water, dried under vacuum, and analyzed for mass loss and molecular weight. The 90-day cutoff was chosen because, by that point in time, the polymer had shown stable release

rates of the monitored degradation product, such that further degradation could be determined from earlier trends.

6.2.4 Degradation product analysis via HPLC

To determine what degradation products were being released into solution and if UV spectroscopy would be a viable method to quantify degradation product concentration, analysis of polymer degradation media was performed on the spent degradation media from one sample at each time point using a Waters system consisting of a 2695 Separations Module with a 2487 dual λ absorbance detector. Empower software was used for data collection and processing. Samples were resolved at room temperature on an Xterra reversed phase RP18 5 μ m column (4.6 x 150 mm). UV detection of eluted components was performed at $\lambda_{\text{max}} = 278$ nm. Mobile phase consisted of acetonitrile:water (95:5) with ~1% phosphoric acid and brought to pH =2.5 with hydrochloric acid at 1 mL/min. Samples were filtered through 0.22 μ m PVDF filters (Fisher) prior to injection.

6.2.5 Diacid concentration determination via UV absorbance

oCPX diacid concentration in spent media was analyzed by UV spectrophotometry using a Perkin Elmer Lambda XLS spectrophotometer (Waltham, MA) at $\lambda_{\text{max}} = 278$ nm to specifically monitor diacid release. Data were calculated against a calibration curve of absorbance values from standard solutions of known diacid concentrations in PBS. The UV absorbance values of the degradation media were then fit to the calibration curve to determine diacid

concentration in the samples. A saturated diacid solution in PBS was also made and evaluated by UV absorbance to determine if the degradation media samples had reached saturation.

6.2.6 Molecular weight analysis

Molecular weight analyses of the polymers samples were taken both before and after the 90 day *in vitro* degradation study. After the 90 days, the remains of the polymer discs were dried in a vacuum desiccator overnight then ground with mortar and pestle and the resulting powder was used for final molecular weight determination. Polymer disc weight average molecular weights (M_w) and polydispersity indices (PDIs) were determined by gel permeation chromatography (GPC) on a Perkin-Elmer (PE) LC system consisting of a Series 200 refractive index detector, a Series 200 pump, and an ISS 200 autosampler. A DEC Celebris 466 computer running PE TurboChrom 4 software was used for data collection and processing, and to automate the analysis via PE-Nelson 900 Interface and 600 Link. Samples were dissolved in dichloromethane and filtered through 0.45 μm PTFE syringe filters then resolved on a Jordi divinyl benzene mixed-bed GPC column (7.8 x 300 mm) at 1 mL/min. Molecular weights were calibrated relative to narrow molecular weight polystyrene standards (Polysciences, Dorval, Canada).

6.2.7 Scanning electron microscopy

Polymer discs were prepared and subjected to 30 days *in vitro* degradation as described in section 6.2.3. At day 30, the discs were rinsed with deionized water then dried under vacuum. Once dried, the discs were cut down the middle using a razor. Images of the discs were obtained using an AMRAY-1830I microscope (AMRAY Inc.) after coating the samples with Au/Pd using a sputter coater (SCD 004, Blazers Union Limited).

6.2.8 Radiation exposure

BD Falcon 5 mL polystyrene round-bottom tubes (12 x 75 mm; BD Bioscience Discovery Labware, Bedford, MA) were used to ship 6 samples of polymer powder (1 g each) to Sterile Process Technology (Johnson & Johnson) for radiation exposure. At ambient temperatures, samples were exposed to either a MDS Nordion Gamma Cell 220 Research Irradiator (Cobalt 60 source) or a Mevex 5 MeV, 2 kW electron beam linear accelerator. Samples were exposed to either 25 kGy (normal sterilizing dose) or 50 kGy (maximum sterilizing dose). Additional samples were sent which were not exposed to radiation to account for any changes to the polymer that were due to factors other than sterilization (such as shipping conditions), these are denoted as traveller samples.

6.2.9 *In vitro* cytotoxicity evaluation

Polymer cytocompatibility was performed by culturing NCTC clone 929 (strain L) mouse areolar fibroblast cells (ATCC, Manassas, VA) in medium

containing the dissolved diacid, as polymer solubility in aqueous mediums is negligible. These L929 fibroblast cells are a standard cell type for cytocompatibility testing as recommended by the ASTM.⁹ The cell culture medium consisted of Dulbecco's modified Eagle's medium (DMEM) (Sigma-Aldrich, St Louis, MO), 10 % (v/v) fetal bovine serum (Atlanta Biologicals, Lawrenceville, GA), 1 % L-glutamate (Sigma), and 1 % penicillin/streptomycin (Sigma). Diacid was dissolved at 100 mg/mL dimethyl sulfoxide (DMSO) (Sigma, St Louis, MO) as a stock solution and serially diluted with DMSO and then cell culture medium to obtain cell culture medium with 1% DMSO and 1, 0.5, 0.1, 0.05, and 0.01 mg diacid /mL. The polymer-containing medium was distributed in a 96-well plate at 200 μ L/well and seeded at an initial concentration of 2000 cells/well. Concentrations were tested in triplicate. Cell viability was determined using a CellTiter 96 Aqueous One Solution Cell Proliferation Assay (Promega, Madison, WI). Following a 90 min incubation time with 20 μ L MTS reagent in the culture medium, the absorbance was recorded with a micro-plate reader at λ = 490 nm. Cell viability was normalized to cells grown in cell medium with 1% DMSO and 0 mg diacid/mL at 24 hr. A one-way ANOVA followed by Bonferroni's all pairs comparison was used to determine significance (KaleidaGraph 4.1, Synergy Software, Reading, PA).

6.3 Results and Discussion

6.3.1 *In vitro* degradation

Poly(oCPX) is being studied for its potential use as a biodegradable biomaterial. Its degradation behavior was studied under conditions that mimic the physiological environment (pH 7.4, 37 °C, 60 rpm). The degradation media was analyzed by HPLC. Notably, degradation products other than the diacid (e.g., dimers or trimers) were not observed in the degradation media, as determined by the single peak detected in the HPLC spectra with a retention time (1.77 min) that corresponds to solubilized diacid (Figure 6.2). The lack of other degradation products in the media is likely due to their poor solubility in aqueous solvents.

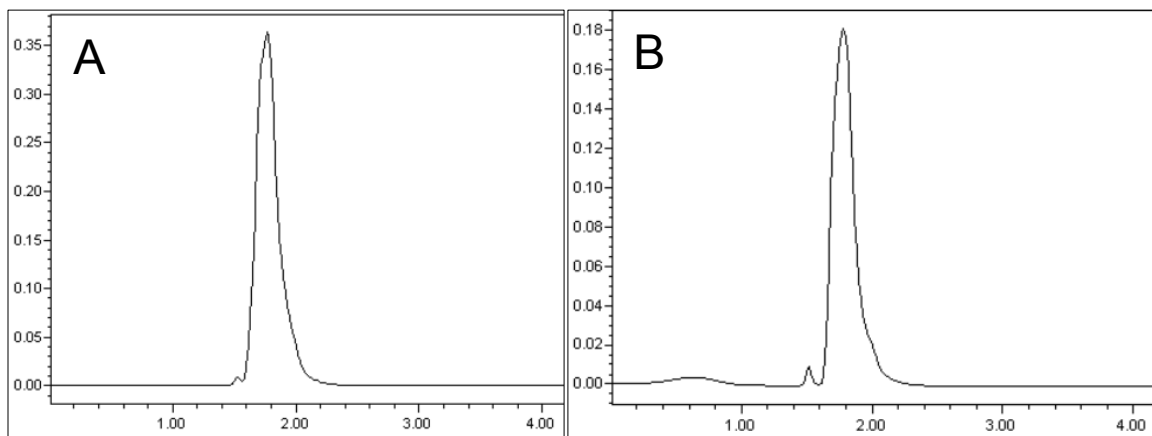


Figure 6.2. HPLC spectra of a diacid standard (A) and the degradation media (B) both exhibit retention times of 1.77 min.

The diacid dissolution rate can affect polymer degradation; if the degradation media were saturated with diacid, subsequent degradation products

would remain on the disc surface and impede water penetration into the matrix, thus, slowing degradation.¹⁰ Therefore, the diacid solubility in PBS was monitored to ensure that its concentration in the degradation media was sufficiently low, so as not to affect degradation rates. The maximum diacid solubility in the buffered media (PBS, pH 7.4) is 1.34 mg/mL. The highest diacid concentration detected in the media samples was 1.02 mg/mL. The samples experienced sink-like conditions that might be expected in a dynamic system such as the human body.

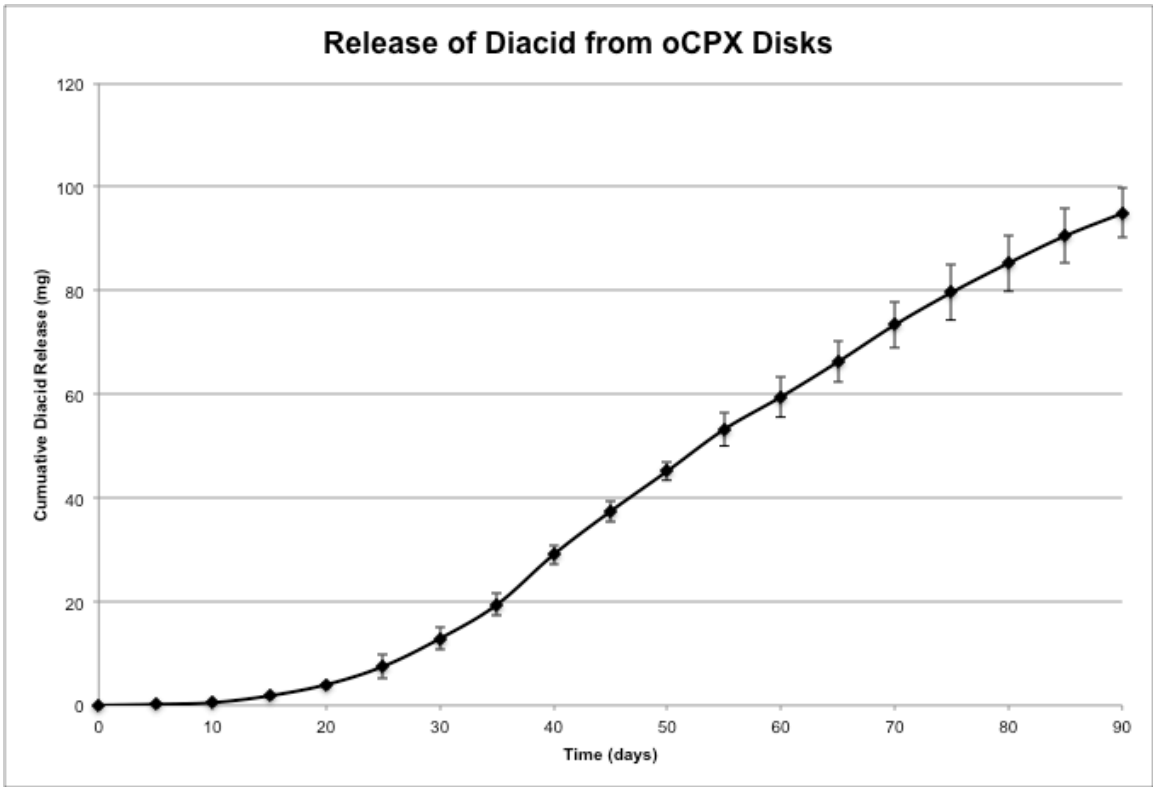


Figure 6.3. Cumulative diacid release (mg) into degradation media from 150 mg poly(oCPX) discs in PBS.

The diacid concentration in the degradation media was used to monitor the polymer disc erosion. Figure 6.3 shows cumulative diacid release from the polymer discs (in mg) from the 150 mg discs. During the first 10 days, minimal diacid was detected in the PBS media. This profile indicates a lag period during which polymer degradation products are at concentrations below the detectable limit. This lag period is often observed with polyanhydrides, where polymer chains on the matrix surface are hydrolyzed, but not to the extent that diacid is released and solubilized into the media.¹¹ After this lag period, diacid was released into the media at a constant rate (~ 1.36 mg/day) as indicated by the linear release profile ($R^2 = 0.99$). At this rate, these polymer discs would be expected to be fully degraded at ~ 6 months (calculated by extrapolating the linear release trend to 150 mg). This six-month degradation time is longer than that typically seen with many polyanhydrides with similar T_g s.^{3, 4, 10}

Due to the linear trend and the expected length of the total degradation time, the *in vitro* degradation study was stopped at 90 days and the remainders of the discs were collected for further analysis. The average mass loss at 90 days was 72.3%. This amount is a slightly higher mass loss than would be expected based on the amount of diacid monitored in the degradation media. This additional mass loss may have occurred during the rinsing procedure used to remove salts from the discs before the mass loss measurements were taken.

6.3.2 Morphological changes

Polymer discs were monitored by SEM before degradation and after 30 days in PBS for morphological changes. The undegraded disc has a uniformly smooth cross section (Figure 6.4A). The degraded disc exhibits a porous structure (area a, Figure 6.4B) on the exterior surface, while farther from the disc surface, the polymer remains uniform (area b, Figure 6.4B). This porous structure, known as an erosion zone, is indicative of water penetration into the disc. This feature is typical in surface-eroding polymers such as polyanhydrides and is responsible for the zero-order release profile observed in the diacid release profile (Figure 6.3).^{10, 12}

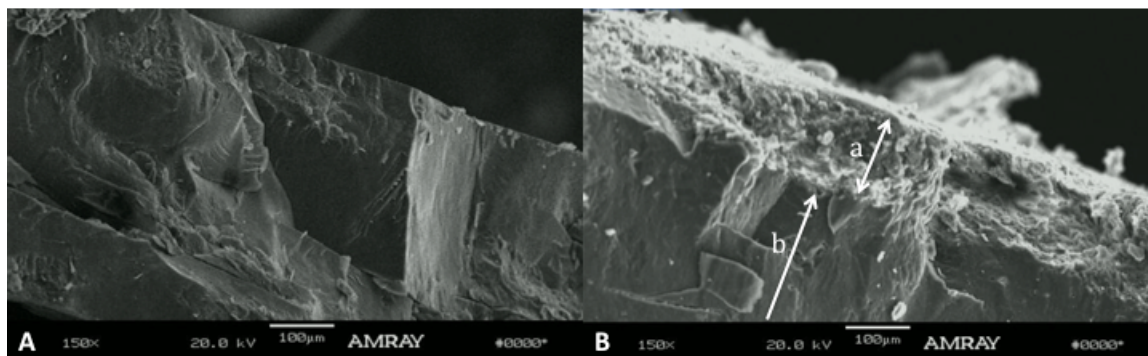


Figure 6.4. SEM images of disc cross sections at day 0 (A) and day 30 (B). Note the porous structure on the disc surface (area a) which indicative of water penetration with the more uniform section (area b) below.

6.3.3 Molecular weight change due to *in vitro* degradation

The polymer molecular weight was analyzed before and after 90 days hydrolytic degradation. The M_w of the entire polymer disc decreased over 90 days from 5600 Da (PDI: 2.1) to 1900 Da (PDI: 3.1). Before degradation, the

GPC spectra for the polymer samples contained only one peak with a maximum peak at 4200 Da (Figure 6.5A). After 90 days, the GPC spectra for all samples were trimodal (Figure 6.5B). The first peak with a maximum at 3800 Da, corresponding to mostly undegraded polymer, the second peak corresponded to a M_w of 600 Da, indicating the presence of dimers, and the third peak at 300 Da, corresponding to the presence of diacid.

Figure 6.5. Representative poly(oCPX)GPC spectra (A) before and (B) after 90 day degradation with peak molecular weights labeled.

This multimodal molecular weight distribution supports the SEM findings that poly(oCPX) discs are primarily surface-eroding,¹³ as significant portions of the polymer matrix did not experience changes in molecular weight. If the polymer were exhibiting bulk-eroding behavior, the molecular weight would have dropped throughout the matrix. Surface-eroding behavior is beneficial for controlled, zero-order release of encapsulated molecules,⁴ suggesting that poly(oCPX) is an appropriate polymer candidate for controlled, sustained drug delivery.

6.3.4 Ionizing radiation

As poly(oCPX) is being investigated as a potential biomaterial, its stability to common sterilizing procedures was tested. Electron beam and gamma irradiation were the methods chosen as other common sterilizing methods involve heat and/or moisture (e.g., dry heat, autoclaving, and ethylene oxide), which cause polyanhydride degradation.¹⁴ Polymer samples were subjected to 0, 25, or 50 kGy (untreated, standard sterilizing dose, and maximum sterilizing dose, respectively) electron beam or gamma radiation doses.¹⁵ The irradiated polymers were then analyzed for changes in molecular weight or degradation rates. No significant differences were observed between irradiated and non-irradiated samples (Figure 6.6).

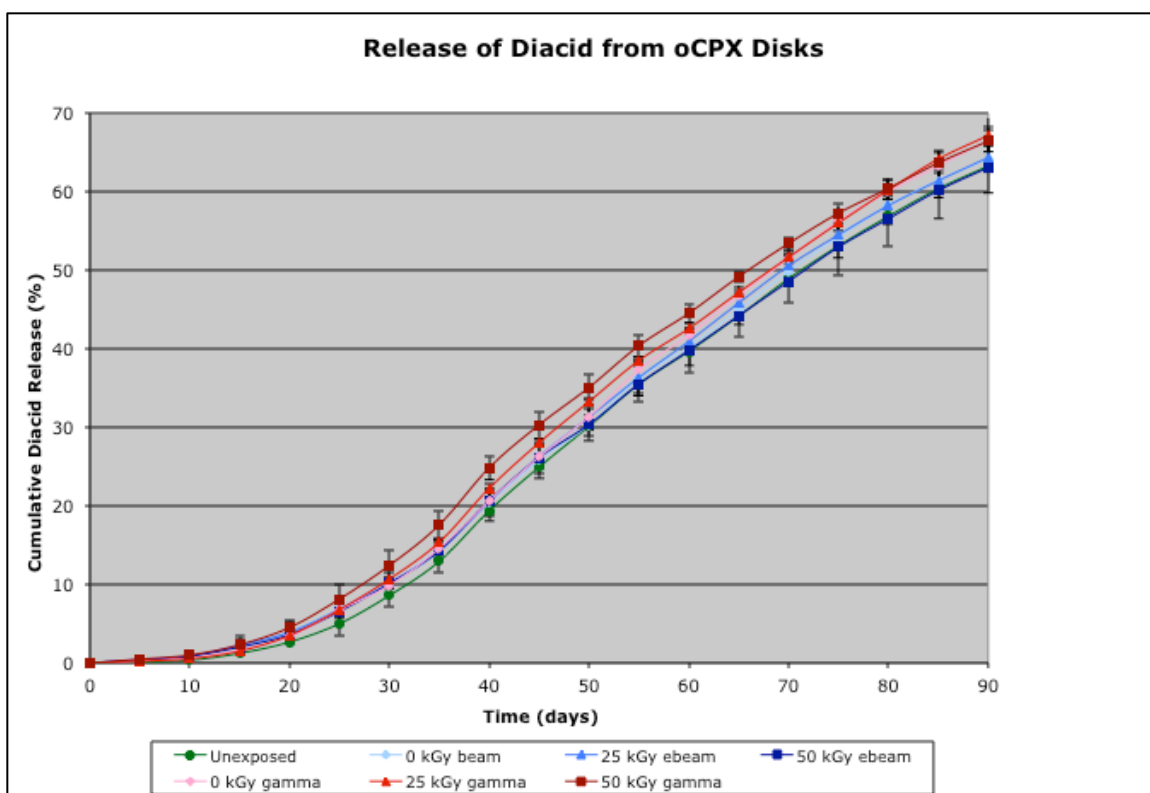


Figure 6.6. Cumulative diacid release into degradation media from 150 mg irradiated poly(oCPX) discs in PBS.

6.3.5 Cytotoxicity

L929 fibroblasts were exposed to increasing oCPX diacid concentrations for 72 hr to evaluate its effect on cell viability and proliferation. The only significant difference in cell viability seen between the samples and the DMSO control was the 1 mg/mL sample at 72 hr (Figure 6.7). In the *in vitro* studies, this diacid concentration was only reached when the discs had been in the same 10 mL of media for 5 days. *In vivo*, the turnover rate for the surrounding liquid would be expected to be greater than this in most circumstances, indicating that

poly(oCPX) would be expected to be biocompatible. This data is supported by the minimal inflammation observed when a poly(oCPX) blend was implanted in a rat model.¹⁶

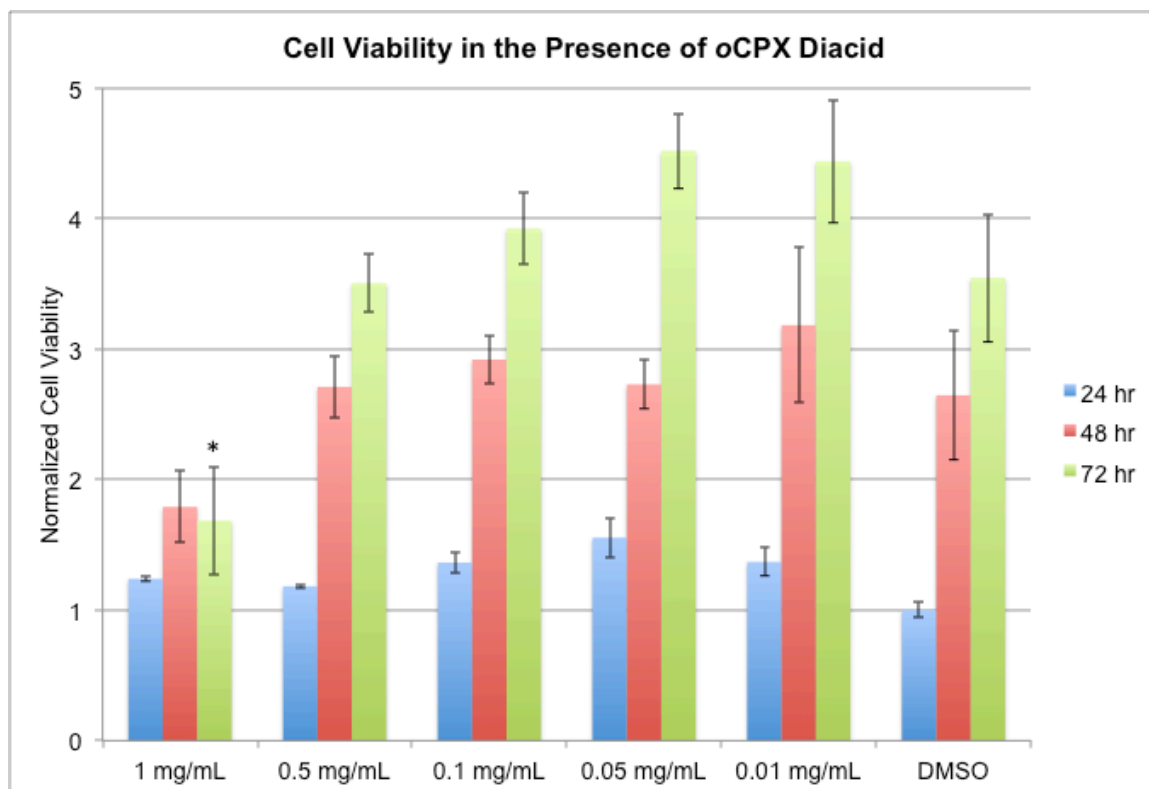


Figure 6.7. oCPX diacid did not significantly affect cell viability at 0.5 mg/mL and lower (* indicates a significant difference ($p < 0.05$) in cell viability from the DMSO control). Data are normalized to control viability at 24 hours.

6.4 Conclusions

Poly(oCPX), an aromatic polyanhydride, was investigated for its potential as a drug delivery matrix since it has desirable thermal and solubility properties. Its degradation, radiation stability, and biocompatibility were investigated. The

polymer degraded to release only its biocompatible diacid precursor into solution. Polymer discs exhibited a 10-day lag period before releasing the diacid in a linear fashion. At this steady degradation rate, the polymer discs would be expected to degrade in ~ 6 months. SEM imaging and M_w changes indicate that the polymer is primarily surface-eroding. The combination of its thermal properties, solubility, degradation time, and erosion mechanism indicate that poly(oCPX) would be a suitable candidate for long term controlled drug delivery. Poly(oCPX) stability to ionizing radiation is advantageous if it is to be used as a biomaterial.

6.5 References

1. Kumar N, Langer RS, Domb AJ. Polyanhydrides: an overview. *Advanced drug delivery reviews*. 2002;54(7):889-910.
2. Gopferich A, Tessmar J. Polyanhydride degradation and erosion. *Advanced drug delivery reviews*. 2002;54(7):911-31.
3. Domb A, Jain JP, Kumar N. Polyanhydrides. In: Lendlein A, Sisson A, editors. *Handbook of Biodegradable Polymers: Synthesis, Characterization and Applications*: Wiley-VHC Verlag GmbH & Co.; 2011.
4. von Burkersroda F, Schedl L, Gopferich A. Why degradable polymers undergo surface erosion or bulk erosion. *Biomaterials*. 2002;23(21):4221-31.
5. Ron E, Mathiowitz E, Mathiowitz G, Domb A, Langer R. NMR characterization of erodible copolymers. *Macromolecules*. 1991;24(9):2278-82.
6. Wang PP, Frazier J, Brem H. Local drug delivery to the brain. *Advanced drug delivery reviews*. 2002;54(7):987-1013.
7. Uhrich KE, Cannizzaro SM, Langer RS, Shakesheff KM. Polymeric systems for controlled drug release. *Chemical reviews*. 1999;99(11):3181-98.

8. Anastasiou TJ, Uhrich KE. Novel polyanhydrides with enhanced thermal and solubility properties. *Macromolecules*. 2000;33(17):6217-21.
9. International A. Standard Practice for Direct Contact Cell Culture Evaluation of Materials for Medical Devices. ASTM F813. West Conshohocken, PA2012.
10. Gopferich A. Mechanisms of polymer degradation and erosion. *Biomaterials*. 1996;17(2):103-14.
11. D'Emanuele A, Hill J, Tamada JA, Domb AJ, Langer R. Molecular weight changes in polymer erosion. *Pharmaceutical research*. 1992;9(10):1279-83.
12. Whitaker-Brothers K, Uhrich K. Investigation into the erosion mechanism of salicylate-based poly(anhydride-esters). *Journal of biomedical materials research Part A*. 2006;76(3):470-9.
13. Akbari H, D'Emanuele A, Attwood D. Effect of geometry on the erosion characteristics of polyanhydride matrices. *International Journal of Pharmaceutics*. 1998;160:83-9.
14. Rosario-Melendez R, Lavelle L, Bodnar S, Halperin F, Harper I, Griffin J, et al. Stability of a salicylate-based poly(anhydride-ester) to electron beam and gamma radiation. *Polymer degradation and stability*. 2011;96(9):1625-30.
15. Yagoubi N, Peron R, Legendre B, Grossiord JL, Ferrier D. Gamma and electron beam radiation induced physico-chemical modifications of poly(propylene). *Nuclear Instruments and Methods in Physics Research Section B: Beam Interactions with Materials and Atoms*. 1999;151(1-4):247-54.
16. Griffin J, Carbone A, Delgado-Rivera R, Meiners S, Uhrich KE. Design and evaluation of novel polyanhydride blends as nerve guidance conduits. *Acta Biomaterialia*. 2010;6(6):1917-24.

7 CONCLUSIONS AND FUTURE WORK

The research described herein involves the design and evaluation of salicylic acid-based poly(anhydride-esters) (SAPAEs) devices for wound healing and tissue engineering. SAPAEs can provide localized, controlled release of salicylic acid (SA), an anti-inflammatory drug, to modulate the inflammatory responses that direct wound healing.

The administered drug amount and the timing of anti-inflammatory therapy are crucial to permit optimal wound healing. SA release from SAPAEs was controlled by changing the polymer linker molecules used to synthesize the diacids (Sections 2 and 3) and by creating copolymers (Sections 2 and 4). Additionally, polymer matrix geometry controlled drug release with increased porosity from channeling agents resulting in diminished lag periods (Section 5). In addition to releasing SA, SAPAE physical properties can be advantageous in directing tissue regeneration (Sections 2, 3, and 4).

7.1 Guided bone regeneration device using salicylic acid-based poly(anhydride-esters) and osteoconductive scaffolds

SAPAE caps were developed for guided bone regeneration (GBR) purposes, in addition to their anti-inflammatory effects. The SAPAEs did not significantly improve bone formation over other GBR barriers, and although they induced less inflammation than the non-bioactive polymer control, so did the ceramic GBR caps.

Ongoing studies are investigating the effect of combining the two SAPAEs evaluated in this study into one device to achieve the early anti-inflammatory effects from the fast-degrading SAPAE with the sustained barrier properties from the slow-degrading SAPAE. These studies are also evaluating the caps combined with scaffolds containing BMP-2 to increase osteogenesis. In these studies, the SAPAEs may have similar effects as described in Section 3 wherein the SAPAE was able to decrease ectopic bone caused by BMP-2 therapy.

One aspect of this study that may have affected the results is that the scaffolds were designed with straight caps that did not fit the skull curvature well, resulting in diminished barrier efficacy. The polymer caps appeared to swell to provide a better fit than the ceramic caps. This aspect of the SAPAE caps is an advantage over the ceramic caps in this study; however, the solid ceramic caps appeared to increase osteoconductivity near the caps compared to all polymer groups. If the caps were designed to better match the defect curvature, the ceramic caps might be expected to result in increased bone growth, compared to polymer caps. Future work could combine a thin (one layer is 250 μm) solid ceramic layer for osteoconductive properties with an SAPAE cap above that to create a tighter seal and provide anti-inflammatory and analgesic therapy to the overlying tissue.

7.2 Polymeric bone wraps to prevent heterotopic ossification

In initial studies, the 40 % SAA bone wraps inhibited both heterotopic ossification as well as bone growth within the defect space (Section 3). Ongoing

studies are investigating 100 % PCL wraps to determine to what extent this decrease in bone formation is due to SA release versus how much is due to the presence of a physical barrier around the site. While SA is known to inhibit bone formation at high concentrations, the wrap could be affecting BMP-2 diffusion out of the defect site, as well as inhibiting oxygen, nutrient, and waste diffusion in the area. SAPAE wraps with slower SA release are also being investigated to determine if delayed SA release would permit more bone growth within the defect, while still preventing bone growth elsewhere.

It may be that high SA concentrations immediately after surgery are the primary reason for diminished bone growth both in the defect as well as in the surrounding tissue. A way to address this problem would be to create a wrap with biphasic SAPAE loading (Figure 7.1). Mats could be electrospun such that the wrap portion that gets wrapped around the defect first would contain 100 % PCL while the outer wrap layer of the wrap would contain 40 % SAA. This design could decrease the SA concentration within the defect, as the inner wrap layer would not be releasing SA, while the outer layer could still release enough SA to prevent heterotopic ossification in the surrounding tissue.

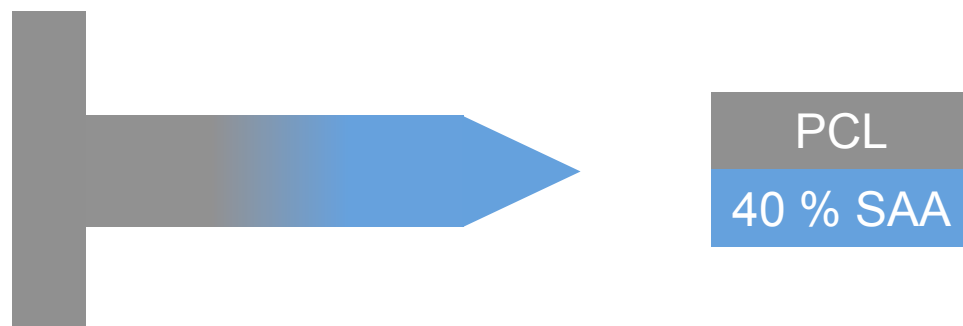


Figure 7.1. Bone wrap with biphasic SAPAE loading.

7.3 Flowable salicylic acid-based poly(anhydride-esters) for injectable barrier applications

The SAA:PEG copolymers described in Section 4 have been shown *in vitro* to have mechanical and pharmaceutical characteristics suitable for fibrous adhesion prevention applications, but the polymers have not yet been tested *in vivo*. The 1:1 copolymer would be the first barrier material tested as its drug release profile lasts throughout the critical time period, unlike the 1:2 copolymer, and its lower viscosity should make it easier to apply during surgery than the 2:1 copolymer.

A potential complication that might arise *in vivo* is that the polymer amount required to provide sufficient barrier capabilities might result in SA concentrations that could inhibit healing of surgical incisions. If this problem occurs, the optimal SA release rate will need to be determined. Additional non-pharmaceutical barriers could then be used in conjunction with the copolymers to provide an additional physical means of preventing adhesions.

7.4 Tunable drug release profiles from salicylate-based poly(anhydride-ester) matrices using small molecule admixtures

Physical admixtures allowed for SA release during the typical SAPAE lag period, with the diacid admixtures resulting in near constant SA release rates over all times from the polymer systems described in Section 5. This ability to overcome the lag time is overcomes a large problem associated with

polyanhydrides and is advantageous for applications where immediate drug release is desired.

7.5 Summary

SAPAEs can provide localized control of inflammation over long periods of time to modulate wound healing. Additionally, SAPAE mechanical characteristics allow them to physically direct tissue regeneration. This research describes the development manipulation of SAPAE properties for various wound healing applications.